NRL Memorandum Report 3429

A Survey of Background Noise from Acoustic Frequencies to Optic Frequencies

HENRY N. HO

Space Environment Branch
Space Systems Division

December 1976

NAVAL RESEARCH LABORATORY
Washington, D.C.

SECURITY CLASSIFICATION OF THIS PAGE (When Data Entered)

REPORT DOCUMENTATION PAGE

READ INSTRUCTIONS BEFORE COMPLETING FORM

1 REPORT NUMBER: NRL Memorandum Report 3429	2 GOVT ACCESSION NO.
3 RECIPIENT'S CATALOG NUMBER	
4 TITLE (and Subtitle): A SURVEY OF BACKGROUND NOISE FROM ACOUSTIC FREQUENCIES TO OPTIC FREQUENCIES	5 TYPE OF REPORT & PERIOD COVERED: Interim report on a continuing NRL problem.
	6 PERFORMING ORG REPORT NUMBER
7 AUTHOR(s): Henry N. Ho	8 CONTRACT OR GRANT NUMBER(s)
9 PERFORMING ORGANIZATION NAME AND ADDRESS: Naval Research Laboratory, Washington, D.C. 20375	10 PROGRAM ELEMENT PROJECT, TASK AREA & WORK UNIT NUMBERS: NRL Problem R01-85A
11 CONTROLLING OFFICE NAME AND ADDRESS: Naval Electronic Systems Command (PME 108), Washington, D.C. 20360	12 REPORT DATE: December 1976
	13 NUMBER OF PAGES: 143
14 MONITORING AGENCY NAME & ADDRESS (if different from Controlling Office)	15 SECURITY CLASS. (of this report): UNCLASSIFIED
	15a DECLASSIFICATION/DOWNGRADING SCHEDULE

16 DISTRIBUTION STATEMENT (of this Report)

Approved for public release; distribution unlimited.

17 DISTRIBUTION STATEMENT (of the abstract entered in Block 20, if different from Report)

18 SUPPLEMENTARY NOTES

19 KEY WORDS (Continue on reverse side if necessary and identify by block number)

Acoustic noise	Environmental noise	Radio noise
Ambient noise	Galactic noise	
Atmospheric absorption noise	Noise spectrum	
Background noise	Noise statistics	
Black body radiation	Quantum noise	

20 ABSTRACT (Continue on reverse side if necessary and identify by block number)

This report presents a summary of background noise characteristics considered useful for the analysis and specification of performances of receiver systems. The frequency range of interest covers the region from acoustic frequencies to optic frequencies. Extensive data of measured noise characteristics are provided. These measured data show:

1. The acoustic noise in the deep ocean is largely determined by the sea state condition,
2. The radio frequency (RF) background noise between the ELF and HF bands is dominated by radiations from terrestrial lightenings,

(Continues)

DD FORM 1 JAN 73 1473 EDITION OF 1 NOV 65 IS OBSOLETE
S/N 0102-014-6601

SECURITY CLASSIFICATION OF THIS PAGE (When Data Entered)

25195

20. Abstract (Continued)

3. From VHF through optic frequencies galectic radiations and atmospheric absorption noises are the major sources of background noise.

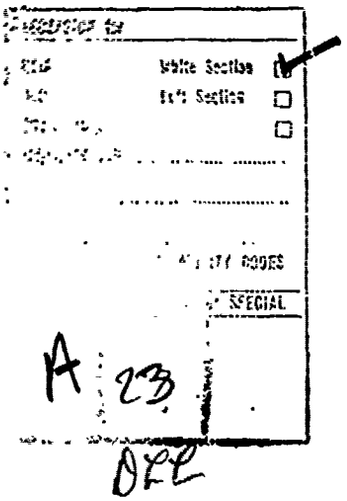

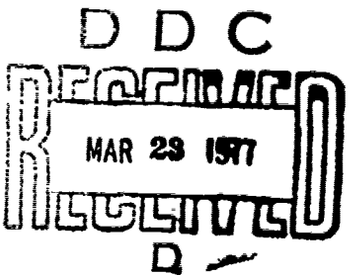

CONTENTS

1. ACOUSTICS 1

Introduction
Sources of Ambient Noise
Measured Ambient Spectrum Levels
Variability of Ambient Noise
Amplitude Distribution
Sample Calculation

2. EXTREMELY LOW FREQUENCY 11

Introduction
Measured ELF Data
Variability of ELF Data

3. VOICE FREQUENCY (VF), and Very Low Frequency (VLF) 20

Introduction
Characteristics of Lightening Discharge
VF and VLF Noise Measurements
Long Term and Mean Value
Short Term Statistics

4. LOW FREQUENCY (LF), MEDIUM FREQUENCY (MF), AND HIGH FREQUENCY (HF). 55

Introduction
Description of Noise
Noise Characteristics
Variation of Noise with Sunspot Activity
Short Term Statistics
Measured Median Values

5. VERY HIGH FREQUENCY (VHF), ULTRA-HIGH FREQUENCY (UHF), SUPER HIGH FREQUENCY (SHF) 117

Introduction
Atmospheric Noise
Man made Noise
Cosmic Noise
Atmospheric Absorption Noise
Sun, Moon, Radio Stars
Flux Density and Brightness Temperature

6. OPTICAL 127

Introduction
Background Noise
Direct Radiation
Reflected Background Noise

A SURVEY OF BACKGROUND NOISE FROM ACOUSTIC FREQUENCIES TO OPTIC FREQUENCIES

CHAPTER 1

ACOUSTICS

INTRODUCTION

Acoustic Noise is ever-present in the underwater medium, such as the ocean. This type of noise, called ambient noise, can interfer with the transmission and reception of sound signals.

The ambient-noise level is defined as the intensity, in decibels, of the ambient background measured with a nondirectional hydrophone and referred to the intensity of a plane wave having a rms pressure of 1 dyne/cm^2 per Hz bandwidth [1]. The ambient noise levels, plotted as a function of frequency, are called the "ambient spectrum levels".

Sources of Ambient Noise

Ambient noise levels have been measured extensively over the frequency range 1 hz to 100 khz. Over this relatively broad range of frequencies, studies have shown that in the deep ocean the noise spectrum can be related to many different sources. Figure 1 is an example of a typical deep water noise spectrum divided into 5 frequency bands. In Band I the source of acoustic energy below 1 hz is largely unknown, but is believed to originate from hydrostatics (tides and waves), or from seismic disturbances. Band II is characterized by a slope of -8 to -10 dB/octave, with only a slight dependence on windspeed, leading to the belief that the noise in this band is caused by oceanic turbulance. In Band III, a pronounced "flattening out" in the noise spectrum is noted. Non-

Note: Manuscript submitted November 30, 1976.

dependence on wind speed and other evidences indicate that the noise is dominated by distant shipping traffic. Band IV contains the Knudsen spectra [2], having a slope of -5 to -6 dB/octave and the noise originates mainly from sea surface wave effects. Band V is due to thermal noise arising from the molecular motion of the sea and has a positive slope of approximately 6 dB/octave.

Other sources of underwater noise are also often encountered. Among these are precipitation noise due to rain and hail above 100 hz and biological noise caused by marine animals such as snapping shrimps and croakers.

Measured Ambient Spectrum Levels

In the absence of sounds from ships and marine life, measurements have shown that underwater ambient noise levels are dependent on wind forces and sea state in the frequency range 100 hz to 25 khz. For this reason, ambient noise spectrum in the main frequency band of interest (100 hz to 25 khz) is classified in terms of wind velocity and sea states, and a related parameter called Beauforte Scale (wind force). Table 1 [3] below shows the approximate relation between wind speed, wave height and sea state.

A composite of ambient noise spectra due to many different component sources in the frequency band 1 hz to 100 khz is shown in Figure 2. To estimate the ambient noise in a particular situation the combined effects of the component spectra must be summed.

The curves in Figure 2 are averages over both deep and shallow water data. For deep water applications the values in Fig. 2 should be lowered by 2 or 3 dB. For shallow water the values should be raised by 2 or 3 db. Notice that the reference pressure intensity is 0.0002 dyne/cm^2. To relate the spectrum levels in Fig. 2 to a

reference of 1 dyne/cm^2, a factor of 74 dB should be subtracted from the former. Figure 3 shows the expected ambient noise level for three frequently encountered conditions.

Variability of Ambient Noise

Ambient noise level measurements is characterized by a great deal of variability. To a large extent, this variability is due to the constant changing conditions in wind speed, ocean tides, shipping, and sound transmission paths. The values of noise levels shown in Fig. 2 represent average values and serve as a good guide to expected levels. However, a residual variability remains that creates an uncertainty of 5 to 10 dB between an estimate based on average values and an amount that might be measured at a given location over a short period of time.

Daily and seasonal variations in ambient noise levels, have also been observed. One cause for seasonal variations is the change in propagation characteristics. Over a 4-year period of observation with a bottom mounted hydrophones at Bermuda and at Bahama Islands, Walkinshaw [5] has observed that the average signal strength was 7 dB higher in winter than in summer for a long distance transmission link. In another study, a peculiar periodic variation of 12 to 24 hours was noted by Wenz [6] in the frequency band 20 to 100 hz. The analysis of data collected at six locations spaced over 45° of longitude in the Pacific Ocean indicated a maximum noise level at midnight and noon, local time, and appear to be independent of longitude. The cause of this periodic variations in noise level is not known.

Amplitude Distribution

Not a great deal of information exist on the amplitude probability distribution of ambient noise. At moderate depth Calderon [4] has performed a probability density analysis of ambient noise and conclude the amplitude distribution is approximately Gaussian. Near the sea surface however hydrophone measurements made a few feet under the surface indicate that the ambient noise is more impulsive than Gaussian.

Sample Calculation [1,7]

We give a sample calculation of the voltage output of a hydrophone suspended underwater with an ambient noise level L. Assume the hydrophone is omni-directional and has a sensitivity of H (db/v)/(dyne/cm^2-Hz). Assume the ambient noise level is L dB/(dyne/cm^2-Hz), at a particular frequency f_o. Then the hydrophone output at the frequency is

$$V=H+L \tag{1}$$

where V = Hydrophone output (dB/volt) per Hz
H = Hydrophone sensitivity (dB/v)/(dyne/cm^2) per Hz
L = Spectrum level dB/(dyne/cm^2) per Hz

If we are interested in the same hydrophone output for a frequency band $\Delta f = f_2 - f_1$, where $f_2 > f_1$, than the hydrophone output voltage will be due to the total noise energy in Δf. Suppose the noise intensity level is frequency dependent, and can be expressed as L(f) (dyne/cm^2 - Hz), then there exist an average noise level $\bar{L}$ (dyne/cm^2 - Hz) such that

$$\bar{L}\,\Delta f = \int_{f_1}^{f_2} L(f)\,df \tag{2}$$

from which

$$\bar{L} = \frac{1}{\Delta f} \int_{f_1}^{f_2} L(f)\,df \qquad (3)$$

Now the hydrophone output voltage due to the noise in the band Δf will be

$$V = H + 10 \log_{10} \bar{L} + 10 \log_{10} \Delta f \qquad (4)$$

where

V - hydrophone output dB/v
H = hydrophone sensitivity (dB/v) / (dyne/cm^2)
Δf = bandwidth
$\bar{L}$ = mean noise level (dyne/cm^2 - hz)

REFERENCES

1. Urick, R. J., Principles of Underwater Sound for Engineers McGraw-Hill Book Co., New York, 1967.

2. Knudsen, V. O., R. S. Alford, and J. W. Emiling, Underwater Ambient Noise, Journal of Marine Research, Vol. 7 1948, pp 410.

3. Wenz, G. M., Acoustic Ambient Noise in the Ocean: Spectra and Sources, The Journal of the Acoustic Society of America, Vol. 34, no. 12, December, 1962, pp 1936-1956.

4. Calderon, M. A., Probability Density Analysis of Ocean Ambient and Ship Noise, NEL Report 1248, November, 1964,

5. Wilkinshaw, H. M., Low Frequency Spectrum of Deep Ocean Ambient Noise (Abstract), Journal of Acoustic Society of America, Vol 32, 1960, pg. 1497.

6. Wenz, G. M., Some Periodic Variations in Low-Frequency Acoustic Ambient Noise Levels in the Ocean, Journal of Acoustic Society of America, Vol. 33, 1961, pg. 64.

7. Albers, V. A., Underwater Acoustics Handbook - 11, Pennsylvania State University Press, Penn., 1965.

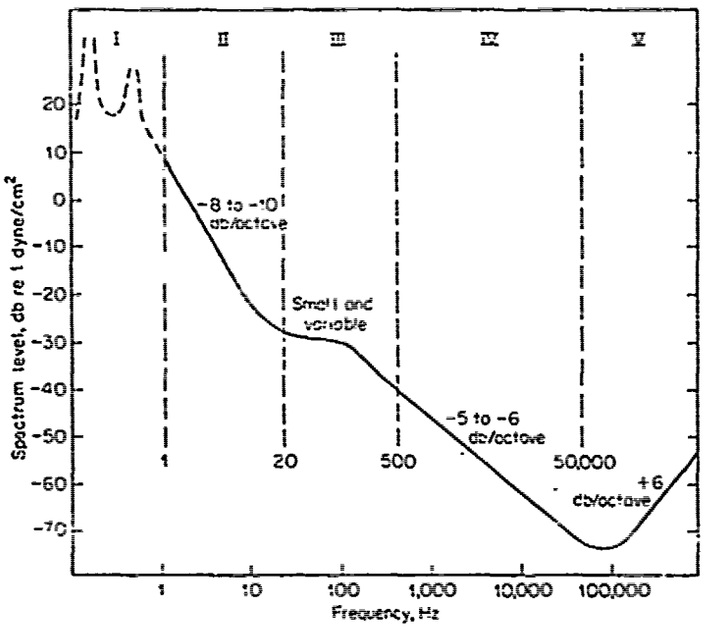

Fig. 1 — Sample spectrum of deep-sea noise showing five frequency bands of differing spectral slopes. The slopes are given in decibels per octave of frequency.

TABLE I. Approximate relation between scales of wind speed, wave height, and sea state.

Sea criteria	Wind speed: Beaufort scale	Wind speed: Range knots (m/sec)	Wind speed: Mean knots (m/sec)	12-h wind: Wave height[a,b] ft (m)	Fully arisen sea: Wave height[a,b] ft (m)	Fully arisen sea: Duration[b,c] h	Fully arisen sea: Fetch[b,c] naut. miles (km)	Sea-state scale
Mirror-like	*0*	<1 (<0.5)						*0*
Ripples	1	1–3 (0.5–1.7)	2 (1.1)					½
Small wavelets	2	4–6 (1.8–3.3)	5 (2.5)	<1 (<0.30)	<1 (<0.30)			1
Large wavelets, scattered whitecaps	3	7–10 (3.4–5.4)	8½ (4.4)	1–2 (0.30–0.61)	1–2 (0.30–0.61)	<2.5	<10 (<19)	2
Small waves, frequent whitecaps	4	11–16 (5.5–8.4)	13½ (6.9)	2–5 (0.61–1.5)	2–6 (0.61–1.8)	2.5–6.5	10–40 (19–74)	3
Moderate waves, many whitecaps	5	17–21 (8.5–11.1)	19 (9.8)	5–8 (1.5–2.4)	6–10 (1.8–3.0)	6.5–11	40–100 (74–185)	4
Large waves, whitecaps everywhere, spray	6	22–27 (11.2–14.1)	24½ (12.6)	8–12 (2.4–3.7)	10–17 (3.0–5.2)	11–18	100–200 (185–370)	5
Heaped-up sea, blown spray, streaks	7	28–33 (14.2–17.2)	30½ (15.7)	12–17 (3.7–5.2)	17–26 (5.2–7.9)	18–29	200–400 (370–740)	6
Moderately high, long waves, spindrift	8	34–40 (17.3–20.8)	37 (19.0)	17–24 (5.2–7.3)	26–39 (7.9–11.9)	29–42	400–700 (740–1300)	7

[a] The average height of the highest one-third of the waves (significant wave height).
[b] Estimated from data given in U. S. Navy Hydrographic Office (Washington, D. C.) publications HO 604 (1951) and HO 603 (1955).
[c] The minimum fetch and duration of the wind needed to generate a fully arisen sea.

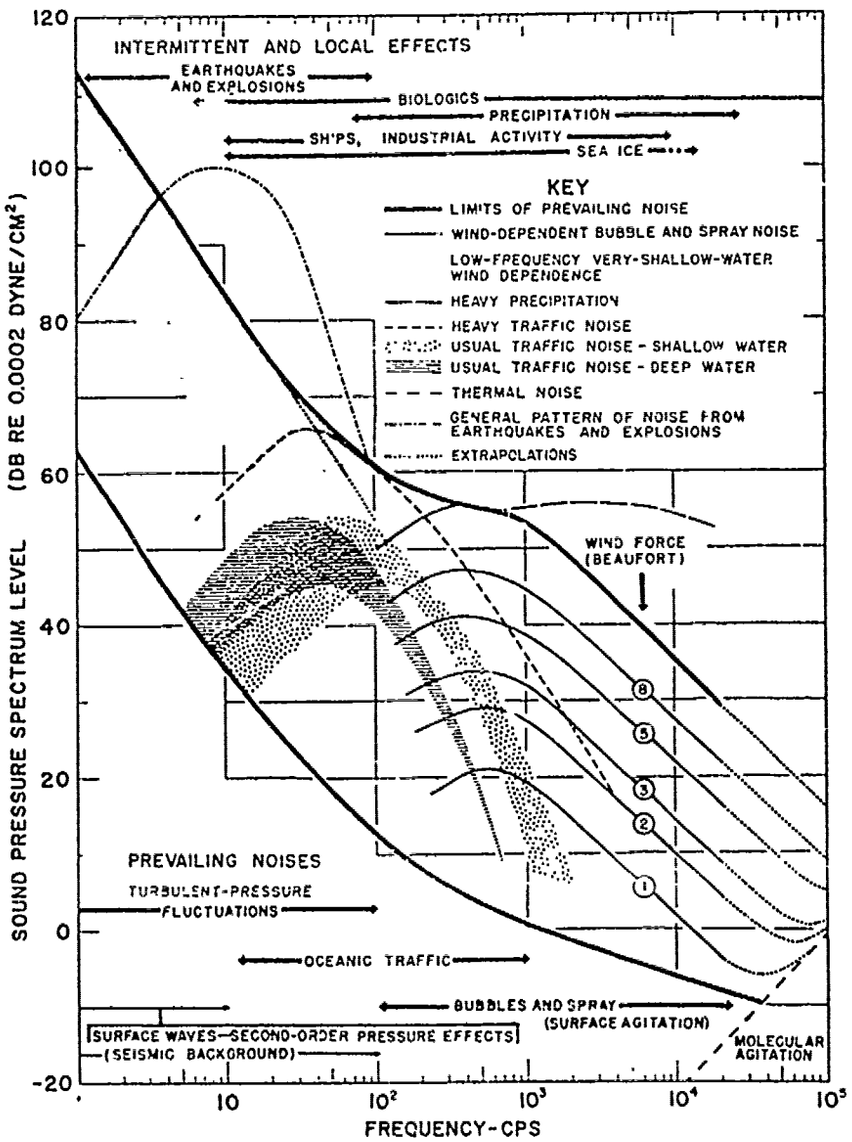

Fig. 2 — A composite of ambient-noise spectra, summarizing results and conclusions concerning spectrum shape and level and probable sources and mechanisms of the ambient noise in various parts of the spectrum between 1 cps and 100 kc. The key identifies component spectra. Horizontal arrows show the approximate frequency band of infulence of the various sources. An estimate of the ambient noise to be expected in a particular situation can be made by selecting and combining the pertinent component spectra.

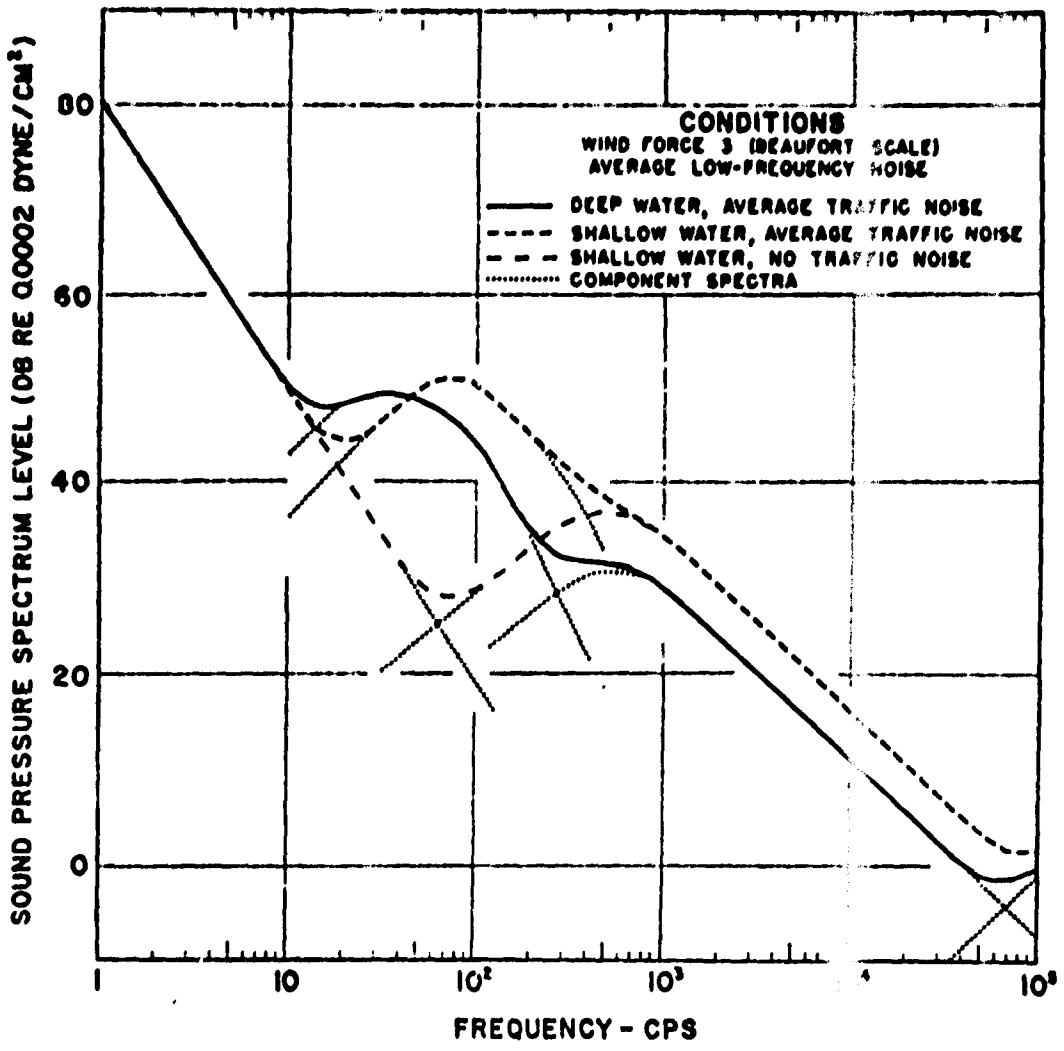

Fig. 3 — Ambient-noise spectra estimated for three frequently encountered situations. The dotted-line extensions indicate, in the regions of overlap, the individual component spectra from which the estimated spectra were derived.

CHAPTER 2

EXTREMELY LOW FREQUENCY (ELF) (30-300 hz)

INTRODUCTION

Noise in the ELF band result from a number of different sources. Among these sources are: atmospheric (lightening discharges), power line radiations and other man-made sources such as mechinery and ignition systems.

At locations free from man-made sources, ELF noise is dominated by the radiations from lightening discharges, which occur on a world wide basis. A substantial amount of ELF noise measurements has been made at various geographical locations around the world in support of the SANGUINE program [1,2 and 3]. Recorded ELF noise data has been analyzed to determine its amplitude statistics. The results of these analysis indicate that the ELF noise waveforms contain frequent spikes and the amplitude statistic is not Gaussian.

In references [1,2 and 3] the analysis indicate that the log-normal statistics provides a better approximation of ELF noise amplitude statistics.

Measured ELF Data

As previously mentioned, ELF noise waveforms are characterized by frequent large amplitude spikes. Fig. 1 shows some typical waveforms measured at Malta using a receiver with a bandwidth 5-320 hz. The large dynamic range of the noise amplitude can be seen.

Figure 2 shows the amplitude probability distribution of some ELF noise recorded at Saipan, Norway and Malta [4]. In this figure the noise amplitude relative to its rms valuse, is plotted in terms of decibels. For each of the three locations shown in Fig. 2, the non-Gaussian behavior

of amplitude statistics at higher amplitude levels is evident.

Additional ELF noise measurements have been made and analyzed by Ginsberg [3] at Malta and Guam for the time period July 1969 through April 30,1970. These measurements were made using a "Portable Atmospheric Noise Data Acquisition" (PANDA) system. Atmospheric Noise were recorded at 33, 41, 83 and 180 hz. A 2-meter monopole antenna was used to measure the verticle electric and horizontal magnetic fields. A core antenna with a turn area product of 830 M^2 was used to measure the magnetic intensity. The recorded data was analyzed and the cumulative probability distributions for H_x (X component of magnetic field) and H_y (y component of magnetic field) are shown as Figs. 3 and 4, respecively. In Fig. 3A the magnetic field intensity (H_x) measure at Malta during the fall at 33,41 and 88 hz has a distribution which is approximately log-normal about the 95 exceedance level (the value exceeded 95% of the time) to the 10% exceedance level. Fig. 3B shows the measured magnetic intensity statistic (Hx) in spring at Malta. In this case, except for the 41 hz noise, the magnetic intensity statistics of Hx is approximately log-normal from the 99% to the 1% exceedance levels.

For Guam, the contribution of local thunderstorms to the high noise exceedance levels stand out. Fig. 4A shows the statistics of magnetic intensity H_y for fall at Guam. The 1% exceedance level for this case is 13-18dB greater than the median level, compared to a 1% exceedance level of 12-14dB greater than the median level for Malta (Fig. 3A). The larger 1% exceedance levels (relative to the median level) at Guam are attributed to the more frequent occurrance of thunderstorms in the vicinity of Guam.

The long term probability distribution for the spring season at Guam is shown in Fig. 4B. When compared with

the data in Figs. 3A, 3B, and 4A, Fig. 4B gives the best fit to a log-normal distribution. This data correlates with minimum local thunderstorm conditions. No local thunderstorms were recorded during the measurement period of Fig. 3B data.

Variability of ELF Data

Since ELF noise levels is dependent upon local and worldwide thunderstorm activities, a relation between noise intensity with seasons is noted. In general, thunderstorm activities are more frequent during fall and summer than during winter and spring.

Figure 5 gives the spectral density of H_x for the median and 1% noise exceedance levels for each season at Malta. The highest 1% exceedance levels were in the fall. The lowest 1% exceedance levels were in the spring. The electric field intensity scale (right-side of Fig. 5) is obtained by E=377H, where E is the electric field intensity and H is the magnetic field intensity.

Similarly, amplitude statistics of the total magnetic intensity at Guam has been computed for the four seasons for the 1% and the 50% exceedance levels. This is shown in Fig. 6.

REFERENCES

1. Atmospheric Noise Measurements at Malta and Guam, for the winter season 1969-1970, Special Topic Memorandum No. 34, Project Sanguine, RCA Lab., Princeton, New Jersey, May 31, 1970.

2. Atmospheric Noise Measurements at Malta and Guam, for the Autumn Season 1969, Special Topic Memorandum No. 33, Project Sanguine, RCA Lab., New Jersey, 31 March 1970.

3. Ginsberg, L. H., Extremely Low Frequency (ELF) Atmospheric Noise Level Statistics for Project Sanguine, IEEE Transactions on Communications, Vol. Com-22 No. 4, April 1974, pgs. 555-561.

4. Evans, J. E., and A. S. Griffiths, Design of a Sanguine Noise Processor based upon World-Wide Extremely Low Frequency (ELF) Recordings, IEEE Transactions on Communications Vol. Com-22, No. 4, April 1974, pgs. 528-539

5. Griffiths, A. S., Measurements of ELF Noise Processing, Technical Note 1975-33, Lincoln Laboratory, 2 Sep 1975.

6. IEEE Transactions on Communications, Vol. Com-22 No. 4, April 1974.

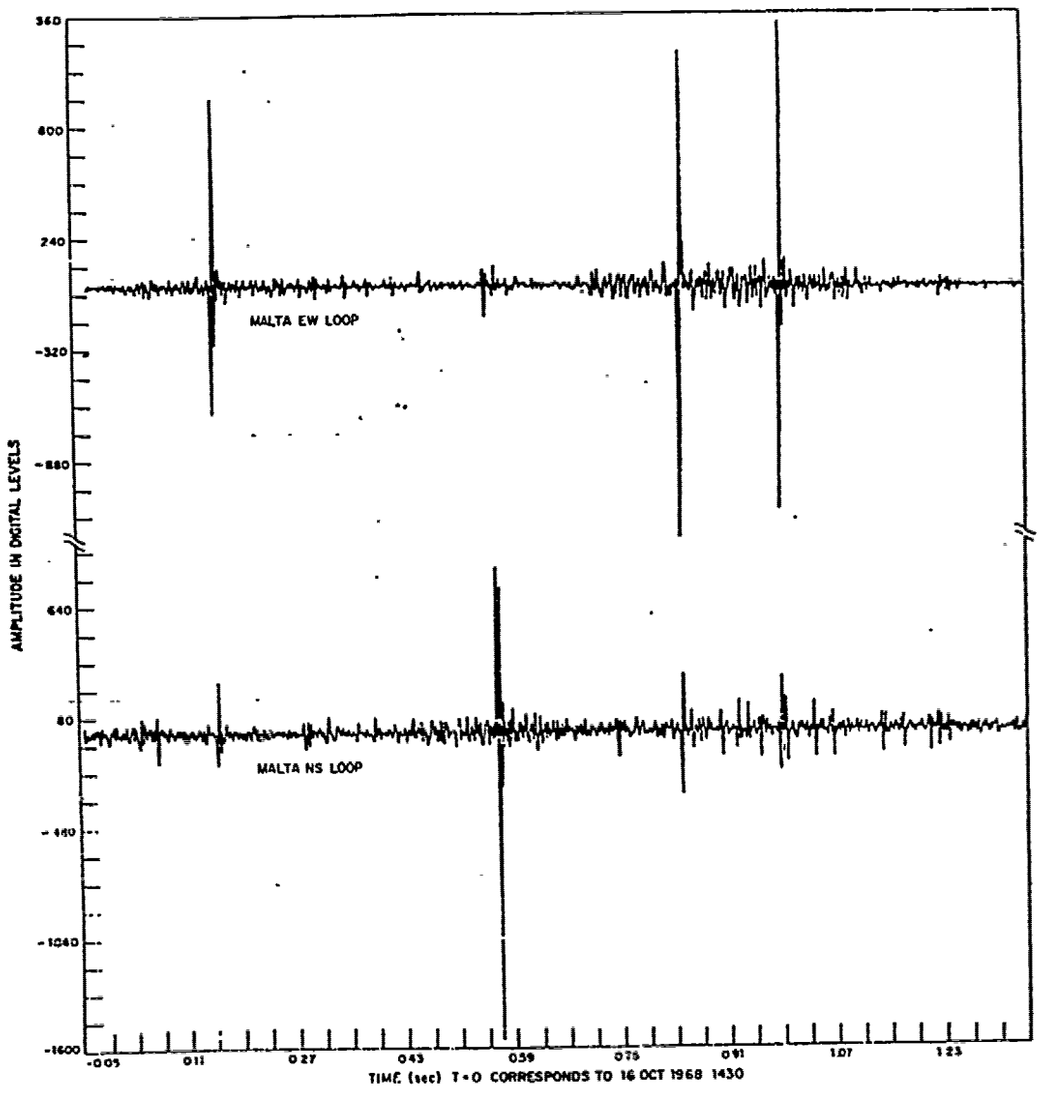

Fig. 1 — ELF waveforms recorded in Malta (Oct. 1968)

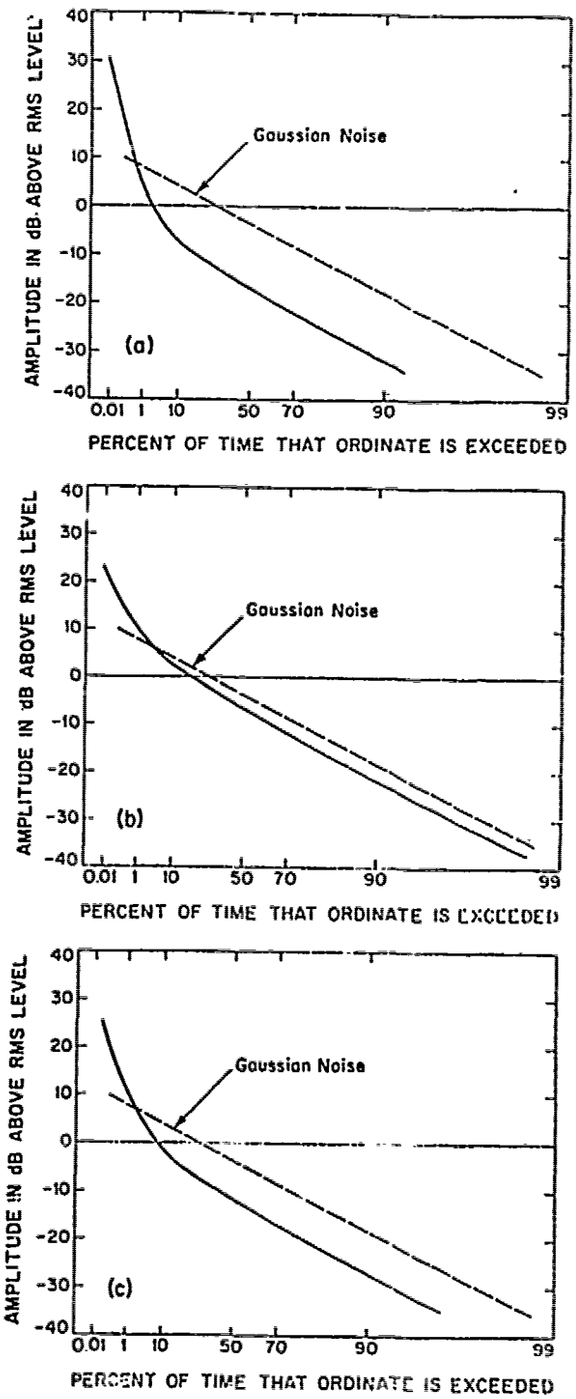

Fig. 2 — Amplitude probability distribution of (a) high-level Saipan (b) typical Norway, and (c) moderate level Malta ELF noise

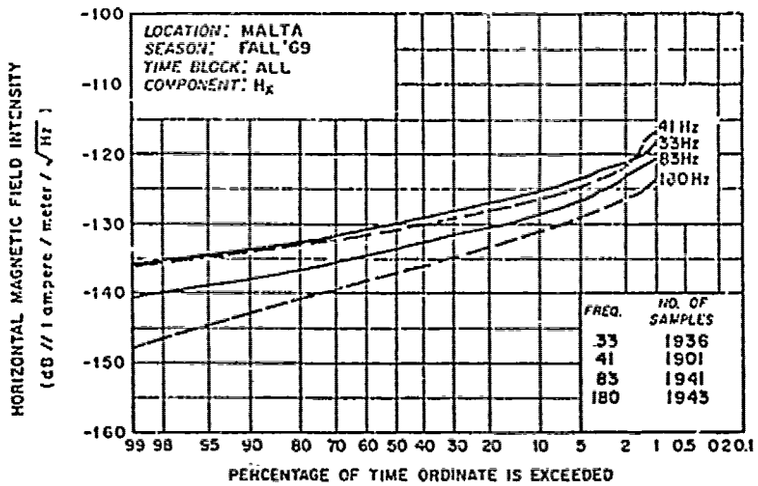

(a)

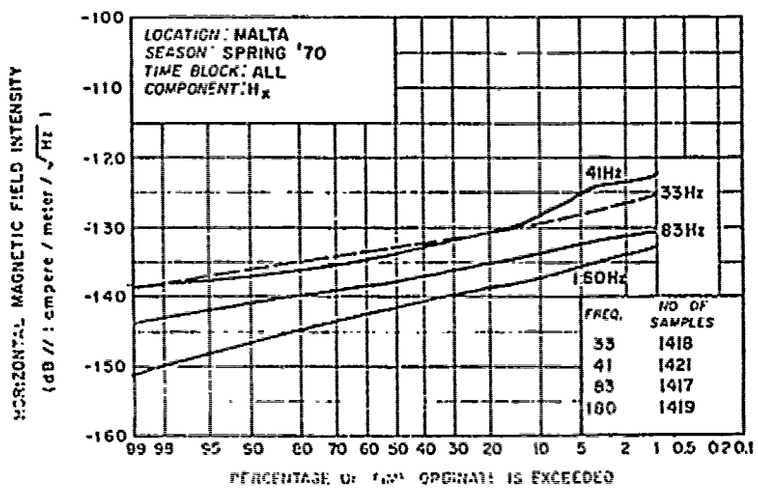

(b)

Fig. 3 — (a) ELF atmospheric noise, cumulative probability distribution for H_z, Malta, fall, and (b) ELF atmospheric noise, cumulative probability distribution for H_z, Malta, spring

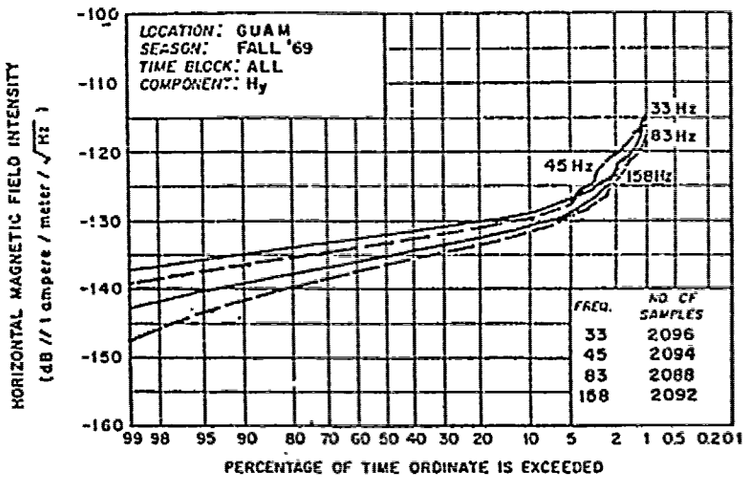

(a)

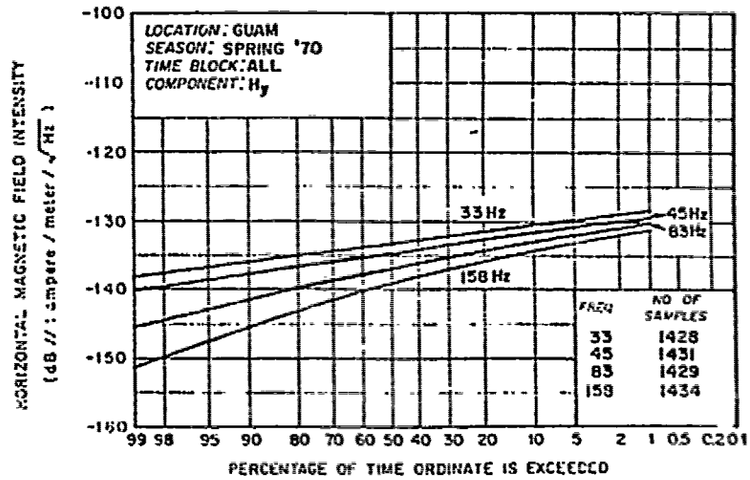

(b)

Fig. 4 — (a) ELF atmospheric noise, cumulative probability distribution for H_v, Guam, fall, and (b) ELF atmospheric noise, cumulative probability distribution for H_v, Guam, spring

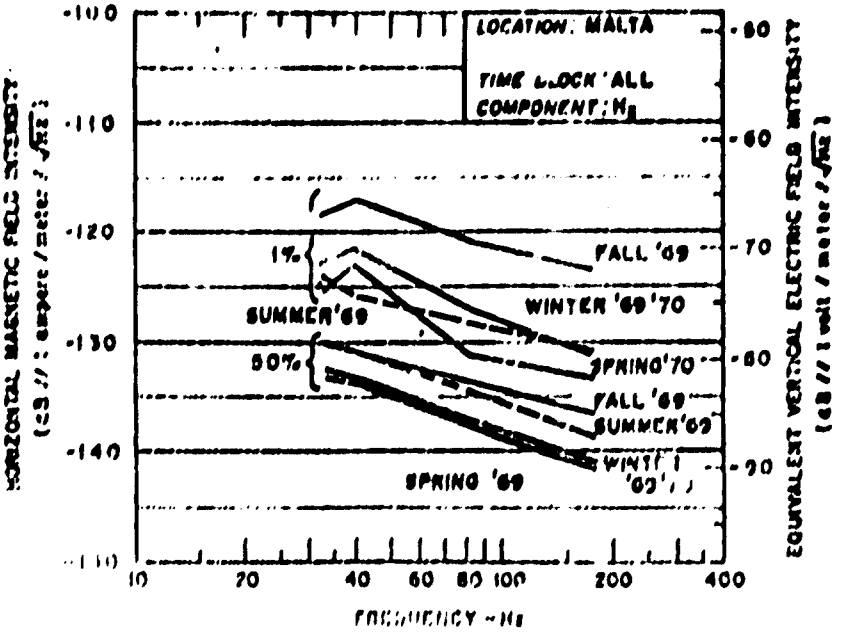

Fig. 5 — Spectra of 1 percent and 50 percent exceedance levels for H_z, Malta, for each season

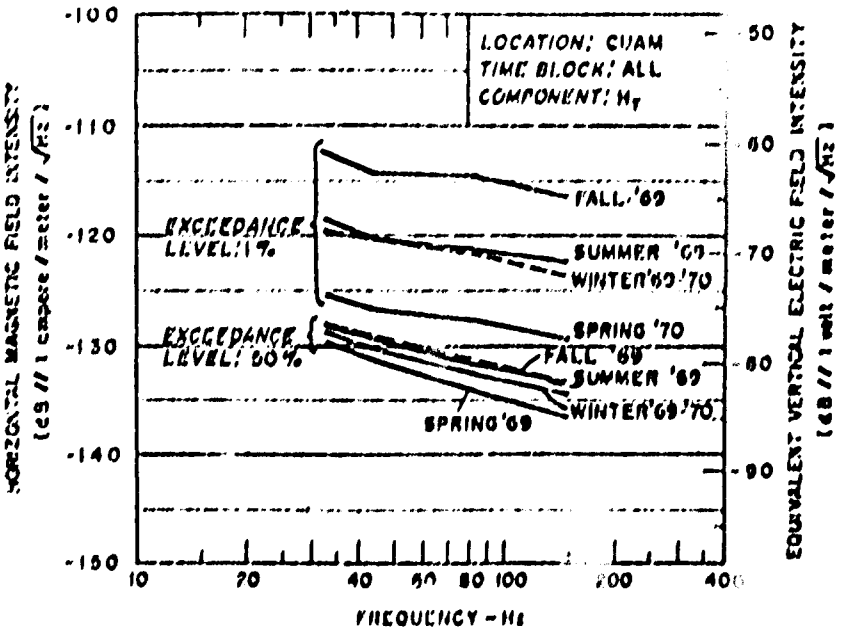

Fig. 6 — Spectra of 1 percent and 50 percent exceedance levels for H_T, Guam, where H_T is the $(H_{z(0.01)^2} + H_{y(0.01)^2})^{1/2}$ or $(H_{z(0.5)^2} + H_{y(0.5)^2})^{1/2}$

CHAPTER 3

VOICE FREQUENCY (VF) AND VERY-LOW FREQUENCY (VLF) (300-3000 hertz, 3-30 kilohertz)

INTRODUCTION

Radio frequency noise in the VF and VLF bands results mainly from the electromagnetic radiations caused by terrestial lightning. The noise waveforms observed in these frequency bands are characterized by large impulses which are associated with local and world-wide thunder storms.

Since lightning is the main cause of VF and VLF noise, the phenomena of lightning discharge has been throughly investigated and the process is relatively well-understood. Among the investigators of the lightning discharge phenomena are Watt [1], Norinder [2], Taylor and Jean [3], Robertson [4], McCann [5], and Pierce [6].

CHARACTERISTICS OF LIGHTNING DISCHARGE

Studies of lightning discharge characteristics have shown that the process can be considered as consisting of five stages [1] : (1) build-up of charge centers in clouds, (2) predischarge or leader formation, (3) main discharge or return stroke, (4) follow-on multiple strokes, and in some cases, (5) a continuing small current (500-1000 amps) flow which may flow between strokes and can follow the last stroke for a large fraction of a second. It has been estimated that on the average there are 100 lightning discharges that

occur per second, worldwide. The total noise field produced at an antenna is the integrated effects of all lightning stroke fields which arrive at the antenna within a time interval comparable to the reciprocal of the observation bandwidth.

VF AND VLF NOISE MEASUREMENTS

Noise in the VF and VLF bands have been measured by several investigators. Crichlow [7] described the efforts made at the National Bureau of Standards (NBS) toward atmospheric noise measurements, which were later adaped by the VIII Plenary Assembly of the International Radio Consultative Committee (CCIR) in Warsaw, Poland in September, 1956. Watt [8, 9] measured the amplitude distribution of atmospheric noise envelopes at several locations (Point Barrow, Alaska; Kenai, Alaska; Boulder, Colorado; and Balboa, Canal Zone). The measurements made by Crichlow and Watt indicate that over a short time period of several minutes to an hour the atmospheric noise statistic remain essentially constant and the typical amplitude-time distribution can be represented by Fig. 1. The scales of Fig. 1 were chosen so that the Rayleigh distribution would plot as a straight line with a slope of $-\frac{1}{2}$. In Fig. 1 we note that the lower portion of the curve approaches a Rayleigh distribution while the upper portion has a much steeper slope. This is a characteristic behavior of noise amplitude statistics when the dominant cause is terrestial lightning discharge.

We now present some measured noise values in the VF and VLF bands. Measured noise data will be classified as: (1) long term (average values) and (2) short term (statistical values). Short term noise data has

been of concern recently for communication system design. See, for example, Omura and Shaft [10] and Watt [11].

LONG TERM OR MEAN VALUES

The mean atmospheric noise spectrum at Malta was measured by Maxwell and Stone [12] during 1963 for three seasons (Spring, Summer, and Winter) at 2000-0400, local time and the result is shown in Fig. 2. In addition, the mean noise levels observed at three different locations (Colorado, Malta and Alaska) are compared in Fig. 3. In Figure 2 we notice that the mean noise level is greatest during the summer and lowest in winter. Also, we note a deep notch in noise levels exist at 3-4 kilohertz, which corresponds to high attenuation occurring at this frequency region. In Fig. 3, we can see the dependence of mean noise level upon location. The difference between the mean electric field spectrum levels measured at Malta and Alaska can be more than 20 dB.

More extensive world-wide measurements of the expected atmospheric noise levels in the frequency band 10 khz to 100 khz are tabulated in CCIR Report 322 [13]. Watt [1] has extrapolated the expected noise levels at 10 khz from CCIR Report 322. The expected atmospheric noise at 10 khz are divided into twenty-four (24) different time blocks and are plotted as Fig. 4 through Fig. 27. The 24 time blocks represent 4 season blocks, with each season block divided into 6 time blocks of 4 hours each. We point out that Figs. 4-27 represent the expected noise levels obtained by averaging data over 4-hour time blocks. The actual hourly average noise levels measured at a given location can differ from the expected noise levels. The amount of variation of the hourly average noise levels about the expected levels can be expressed by a quantity

D_u, which is defined as the upper decile value. The upper decile is a value which is exceeded 10% of the time. Figs. 28-30 give the best estimate of D_u in the VLF range obtained by Watt [1] based upon data contained in CCIR Report 322.

SHORT TERM STATISTICS

During a time span of several minutes to an hour the average value of atmospheric noise is relatively constant (± 2dB) and statistical measurements have been made for the amplitude probability distribution of atmospheric noise in the VF and VLF bands. Fig. 31 shows an amplitude probability distribution of atmospheric radio noise at 13.3 khz measured by Crichlow et al [14] . The data for Fig. 31 was taken at Boulder, Colorado and the curve represents noise levels over a time span of approximately 30 minutes. We note that at lower amplitudes the noise envelope is approximately Rayleigh while at higher amplitudes the slope is much steeper and non-Rayleigh. Some efforts to determine whether the amplitude statistics fits a log-normal distribution have been made. The results indicate that VF/VLF noise does not fit the log-normal distribution, except over a restricted region of amplitude probabilities.

Additional measured amplitude distribution of VLF noise were made by Watt and Maxwell [8] at Point Barrow, Alaska and Boulder, Colorado at 21 khz. This is shown by Fig. 32. Clarke et al [15] measured composite amplitude probability distributions at Singapore and Slough, England and the results are shown in Fig. 33.

LIST OF REFERENCES

1. Watt, A. D., VLF Radio Engineering, Pergamon Press, New York, 1967

2. Norinder, H., The Waveforms of the Electric Field in Atmospherics Recorded Simultaneously by Two Distant Stations, ARKIV for Geofysik, Band 2, n r 9, November 1954, page 161.

3. Taylor, W. L. and A. G. Jean, Very-Low-Frequency Radiation Spectra of Lightning Discharges, J. Res. NBS, 63D, 1959, pages 199-204.

4. Robertson, L. M., W. W. Lewis, and C. N. Faust, Lightning Investigation at High Altitudes in Colorado, Trans AIEE, Vol. 61, 1942, pages 201-208.

5. McCann, G. D., The Measurement of Lightning Current in Direct Strokes, Trans, AIEE, Vol. 63, 1944, pages 1157-1164.

6. Pierce, E. T., Some Topics in Atmospheric Electricity, Recent Advances in Atmospheric Electricity, Pergamon Press, New York, 1958, pages 5-16.

7. Crichlow, W. Q., Noise Investigation at VLF by the National Bureau of Standards, Proceedings of IRE, June, 1957, pages 778-782.

8. Watt, A. D. and E. L. Maxwell, Measured Statistical Characteristics of VLF Atmospheric Radio Noise, Proceedings of IRE, January, 1957, pages 55-62.

9. Watt, A. D. and E. L. Maxwell, Characteristics of Atmospheric Noise from 1 to 100 KC, Proceedings of the IRE, June, 1957, pages 787-794.

10. Omura, J. K., and P. D. Shaft, Modem Performance in VLF Atmospheric Noise, IEEE Transaction on Communication Technology, Vol. Com-19, No. 5, October 1971.

11. Watt, A. D., R. M. Coon, E. L. Maxwell, and R. W. Plush Performance of Some Radio Systems in the Presence of Thermal and Atmospheric Noise, Proceedings of the IRE, December, 1958, pages 1914-1917.

LIST OF REFERENCES (Cont.)

12. Maxwell, E. L. and D. L. Stone, Natural Noise Fields from 1 CPS to 100kc, IEEE Transaction on Antennas and Propagation, AP-11, No. 3, May 1963.

13. CCIR Report 322, World Distribution and Characteristics of Atmospheric Radio Noise, published by International Telecommunication Union, Genva, 1964.

14. Crichlow, W. Q., C. J. Roubique, A. D. Spaulding, and W. M. Beery, Determination of the Amplitude-Probability Distribution of Atmospheric Radio Noise from Statistical Moments, J. of Res. of NBS-D, Radio Propagation, Vol. 64D, No. 1, Jan-Feb., 1960, pages 49-56.

15. Clarke, C., P. A. Bradley, and D. E. Mortimer, Characteristics of Atmospheric Radio Noise Observed at Singapore, Proc. IEE (British) Vol. 112, No. 5, May 1965, pages 849-860.

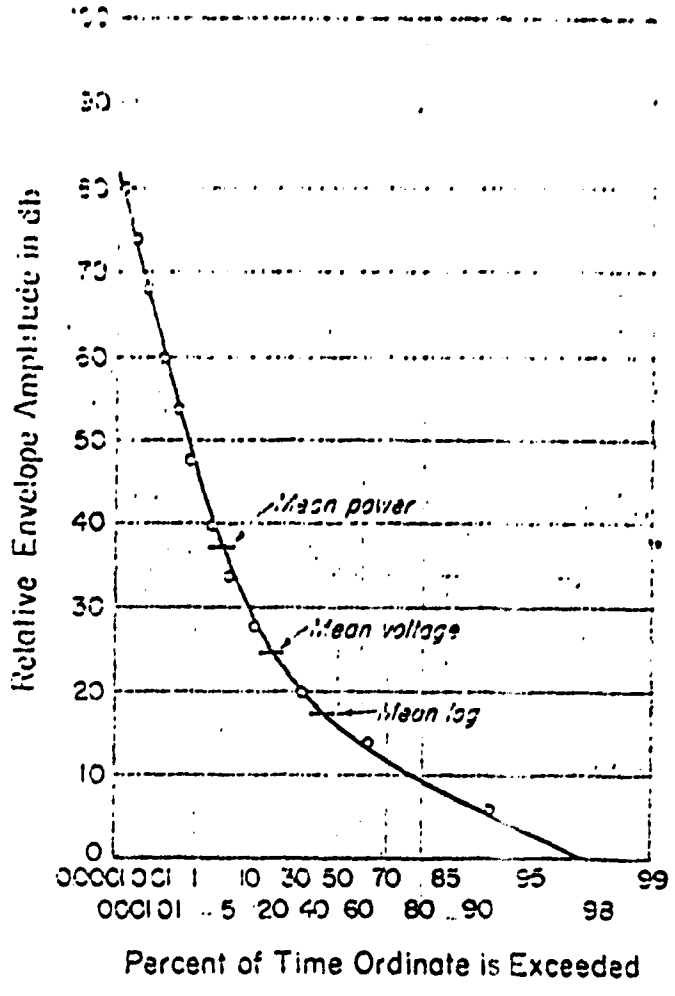

Fig. 1 — Typical amplitude-time distribution of short-term variations

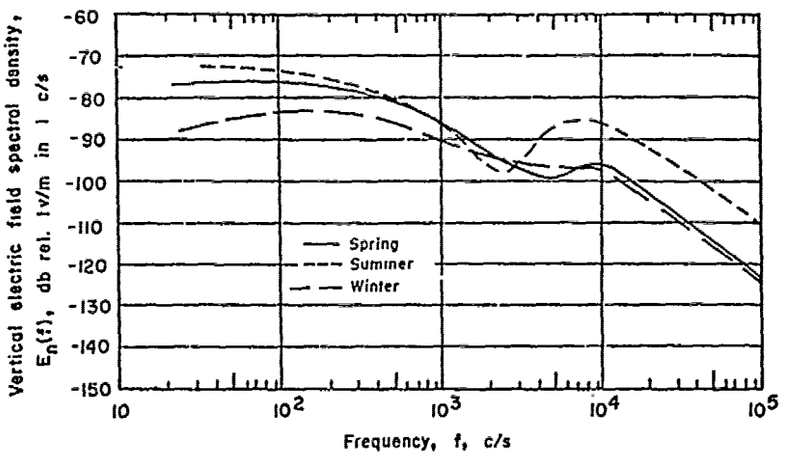

Fig. 2 — Mean atmospheric noise spectrum observed at Malta during 1963, 2000-0400 local time (data from Maxwell and Stone)

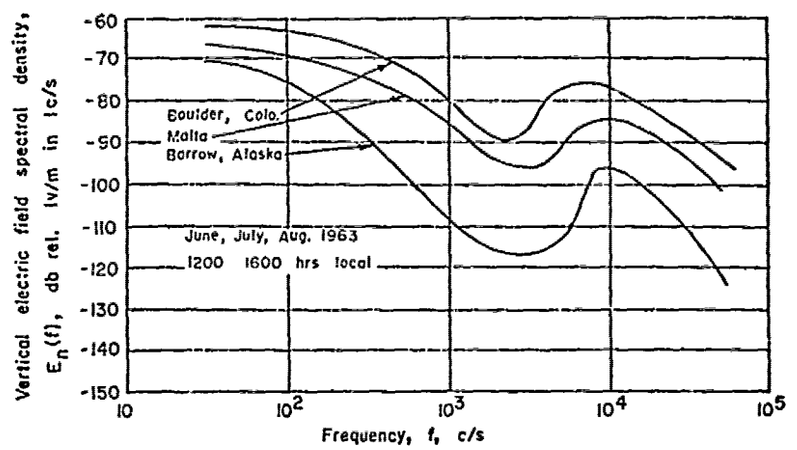

Fig. 3 — Mean atmospheric spectrum observed at Colorado, Malta, and Alaska, 1200-1600 hours local time (data from Maxwell and Stone)

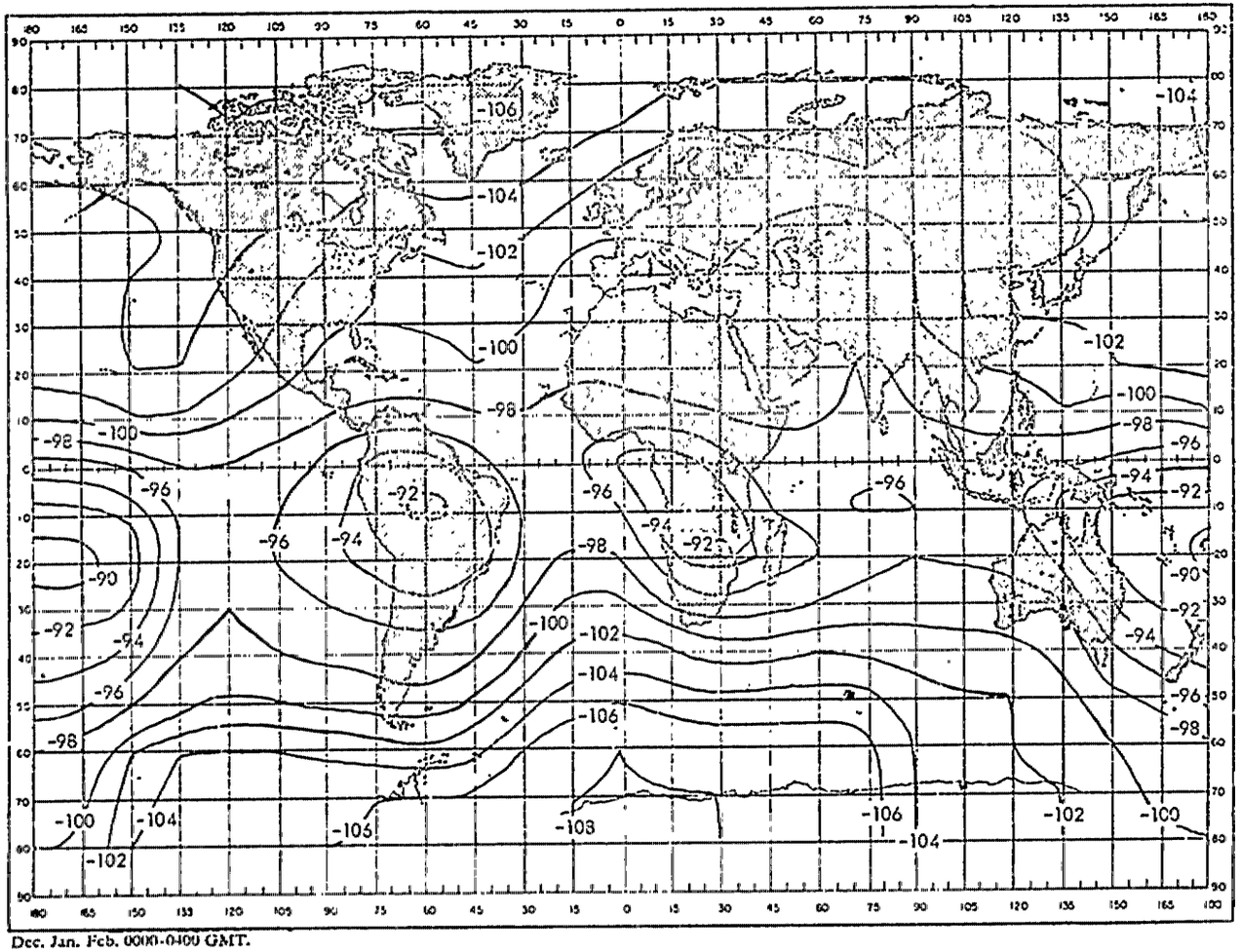

Dec. Jan. Feb. 0000-0400 GMT.

Fig. 4 — Expected atmospheric noise at 10 kc/s in decibels relative to 1 v/m$\sqrt{c/s}$ (data from CCIR 322)

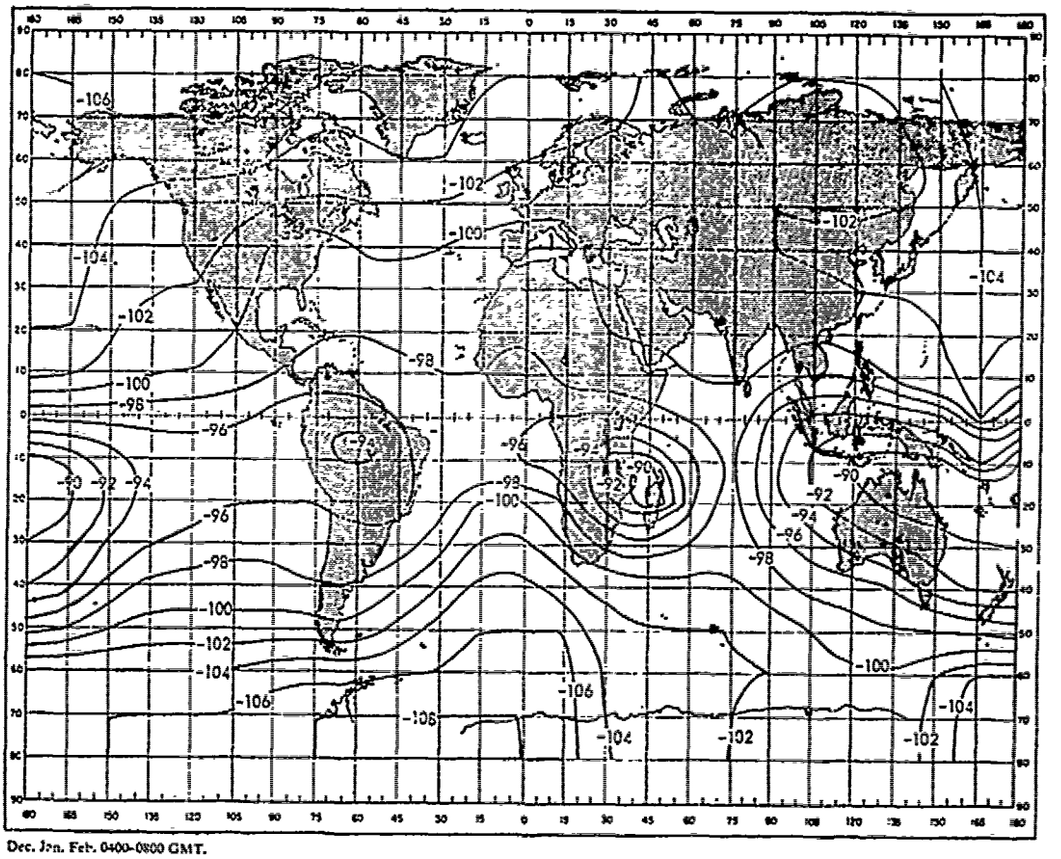

Dec. Jan. Feb. 0400-0800 GMT.

Fig. 5 — Expected atmospheric noise at 10 kc/s in decibels relative to $1/m/\sqrt{c/s}$ (data from CCIR 322)

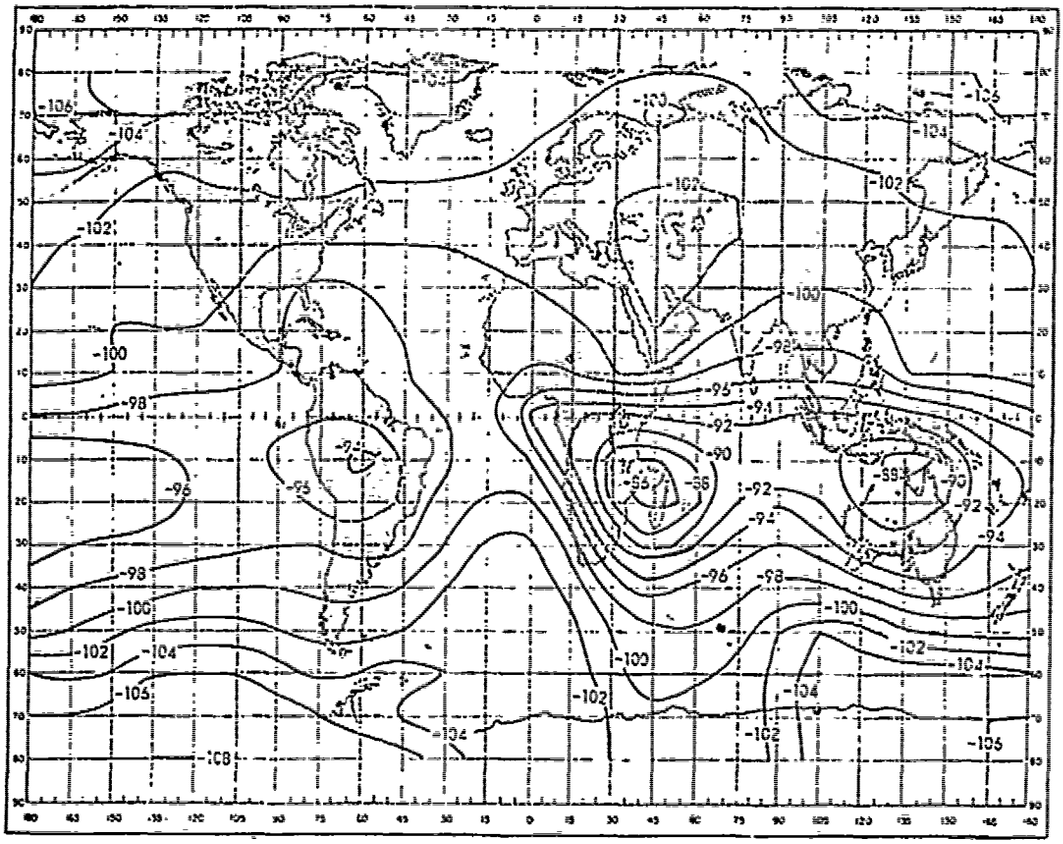

Dec. Jan. Feb. 0800–1200 GMT.

Fig. 6 — Expected atmospheric noise at 10 kc/s in decibels relative to 1 v/m/$\sqrt{}$c/s (data from CCIR 322)

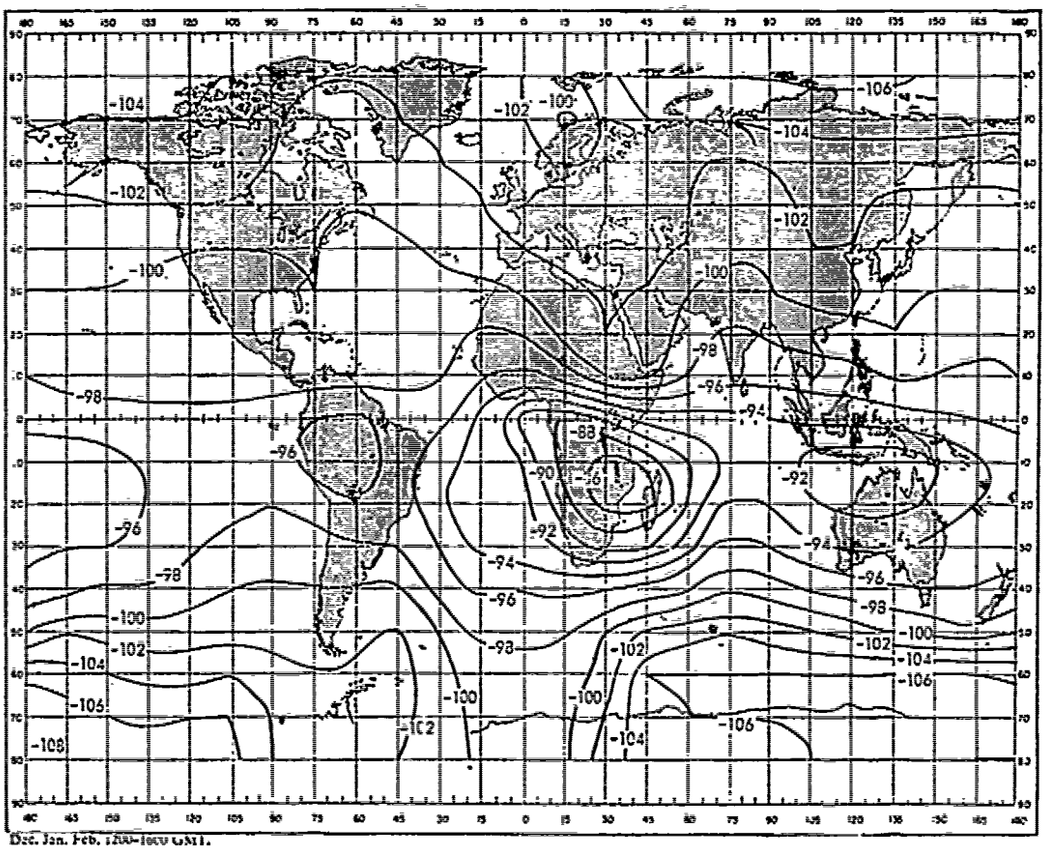

Fig. 7 — Expected atmospheric noise at 10 kc/s in decibels relative to 1 v/m/√c/s (data from CCIR 322)

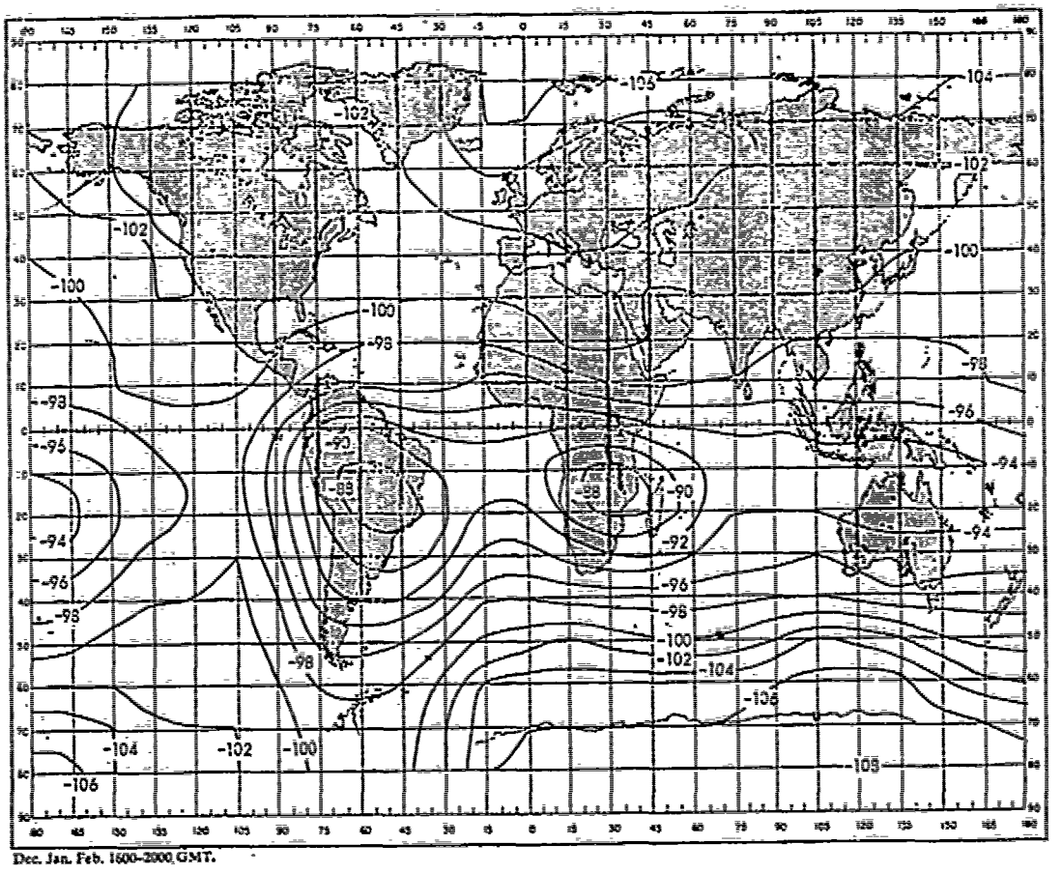

Fig. 8 — Expected atmospheric noise at 10 kc/s in decibels relative to 1 v/m/$\sqrt{c/s}$ (data from CCIR 322)

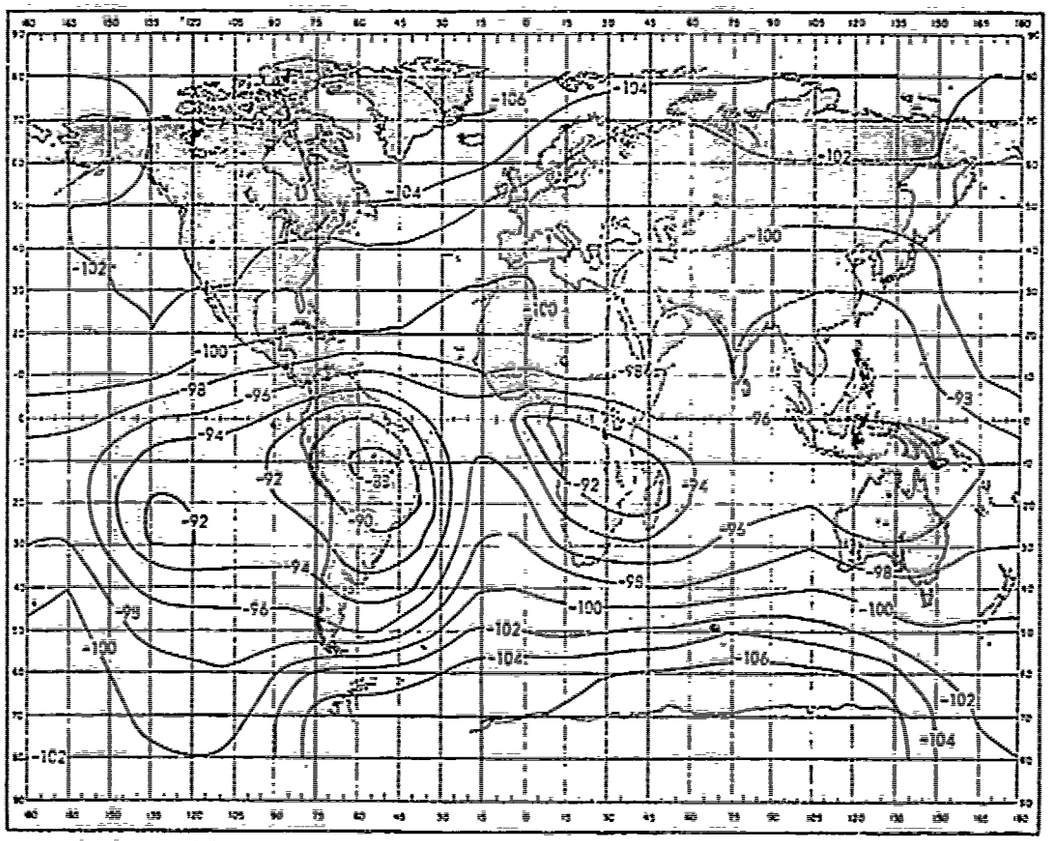

Dec. Jan. Feb. 2000-2400 GMT.

Fig. 9 — Expected atmospheric noise at 10 kc/s in decibels relative to 1 v/m/$\sqrt{c/s}$ (data from CCIR 322)

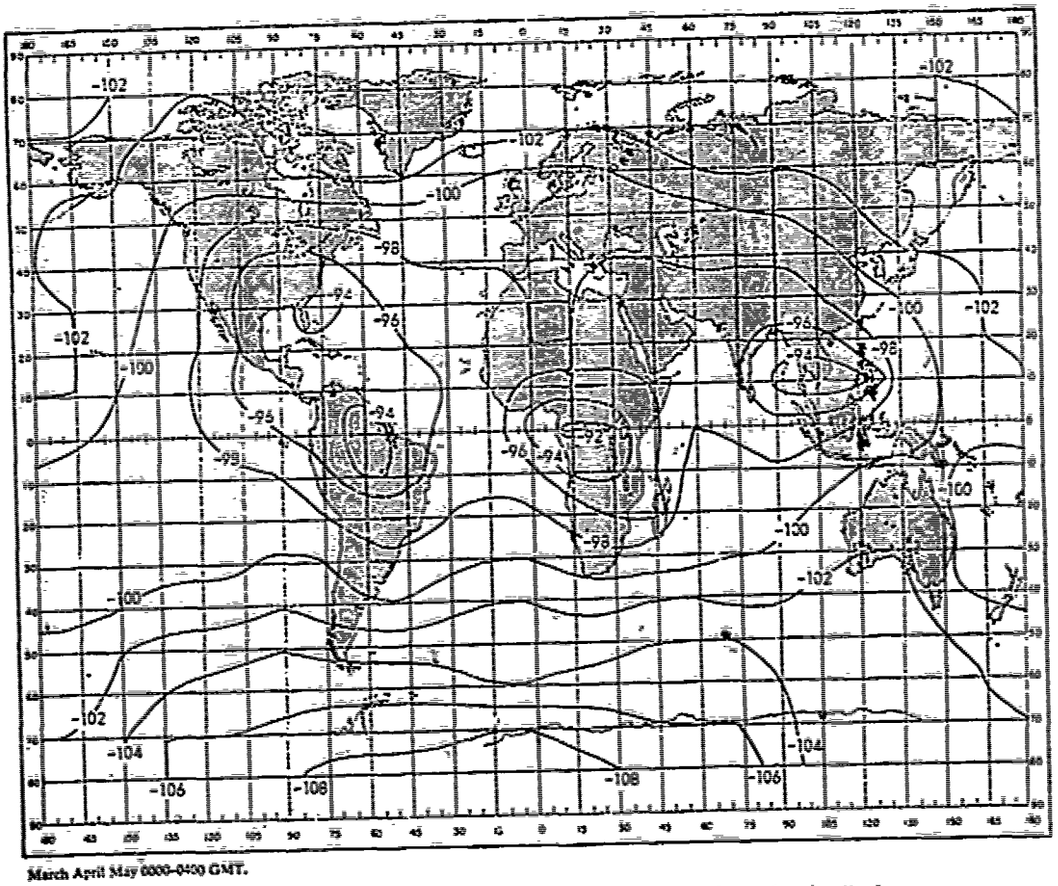

Fig. 10 — Expected atmospheric noise at 10 kc/s in decibels relative to 1 v/m/√c/s (data from CCIR 322)

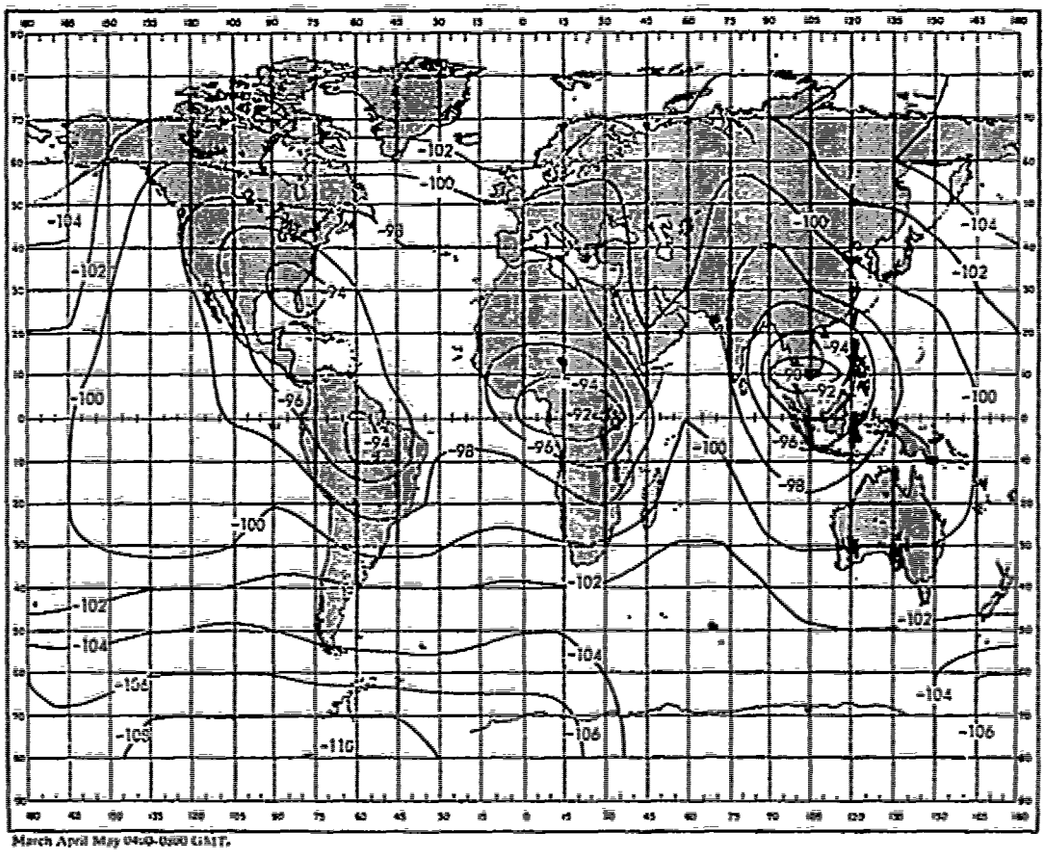

Fig. 11 — Expected atmospheric noise at 10 kc/s in decibels relative to 1 v/m/$\sqrt{c/s}$ (data from CCIR 322)

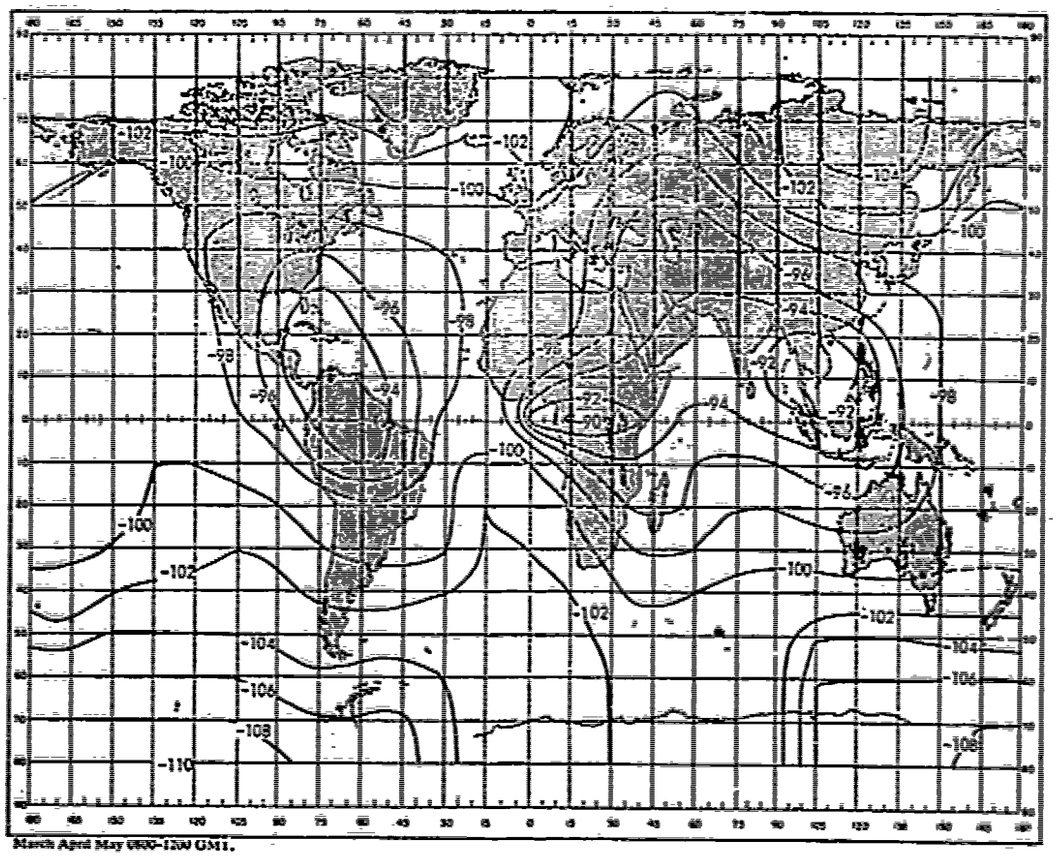

Fig. 12 — Expected atmospheric noise at 10 kc/s in decibels relative to 1 v/m/$\sqrt{c/s}$ (data from CCIR 322)

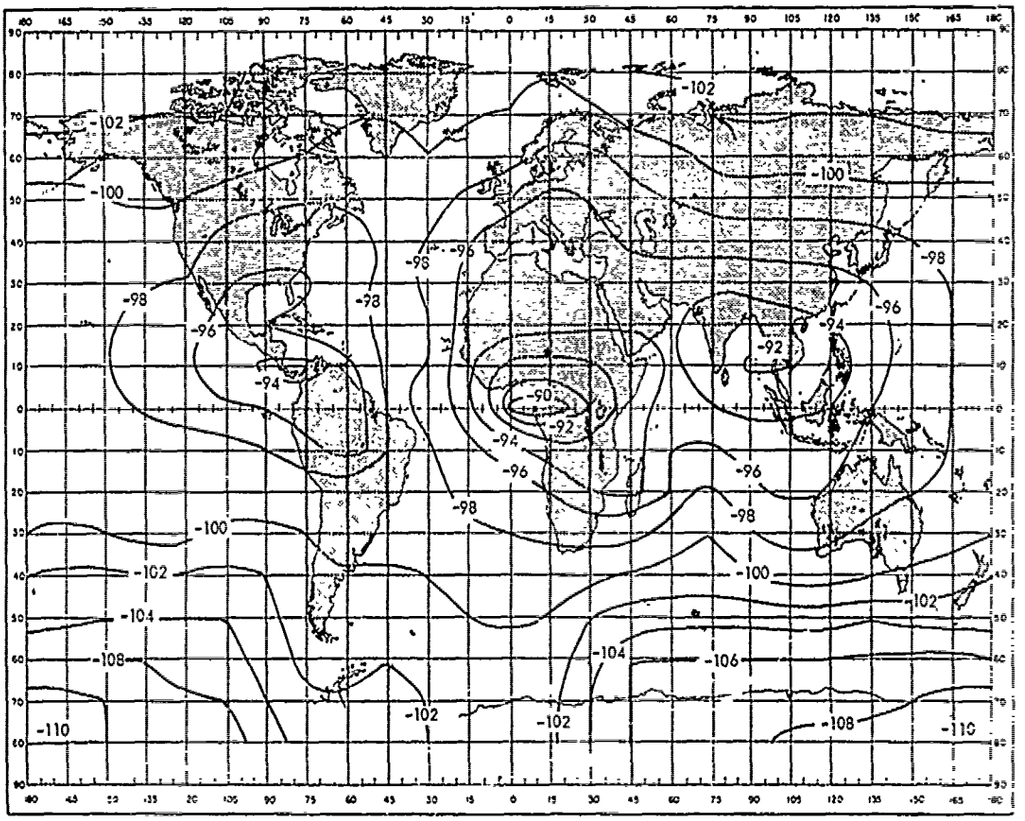

March April May 1200-1600 GMT.

Fig. 13 — Expected atmospheric noise at 10 kc/s in decibels relative to 1 v/m/$\sqrt{c/s}$ (data from CCIR 322)

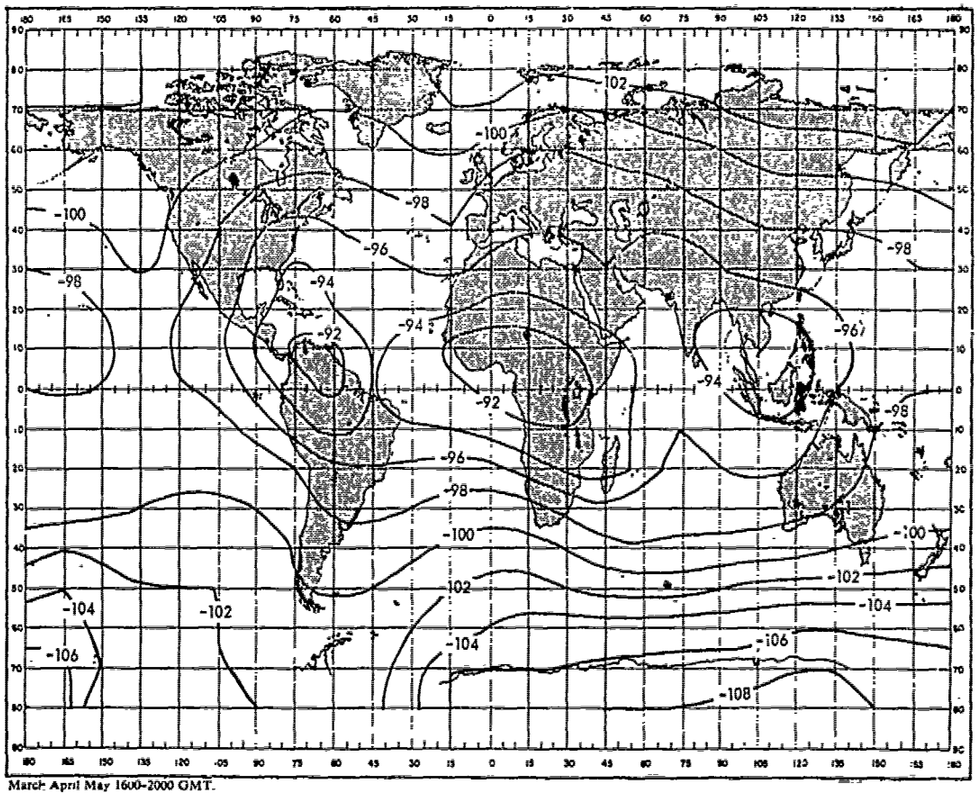

Fig. 14 — Expected atmospheric noise at 10 kc/s in decibels relative to 1 v/m/$\sqrt{c/s}$ (data from CCIR 322)

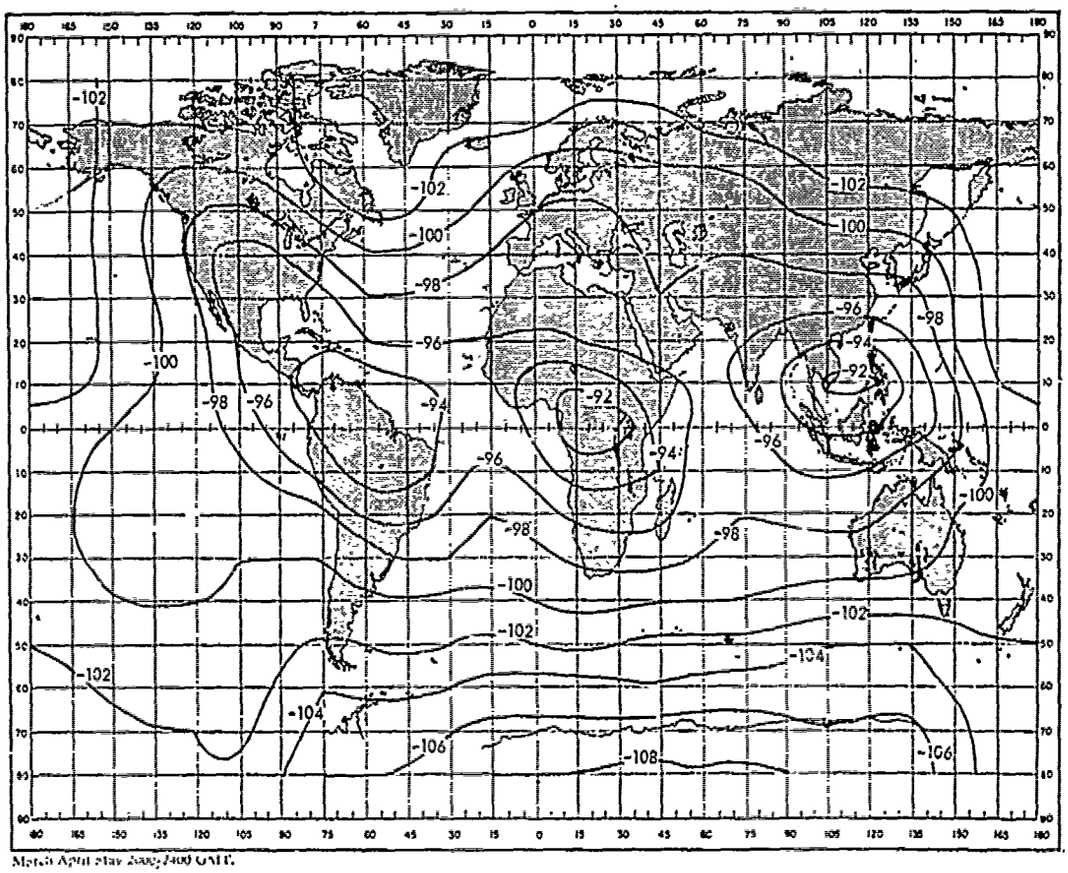

Fig. 15 — Expected atmospheric noise at 10 kc/s in decibels relative to 1 v/m/$\sqrt{c/s}$ (data from CCIR 322)

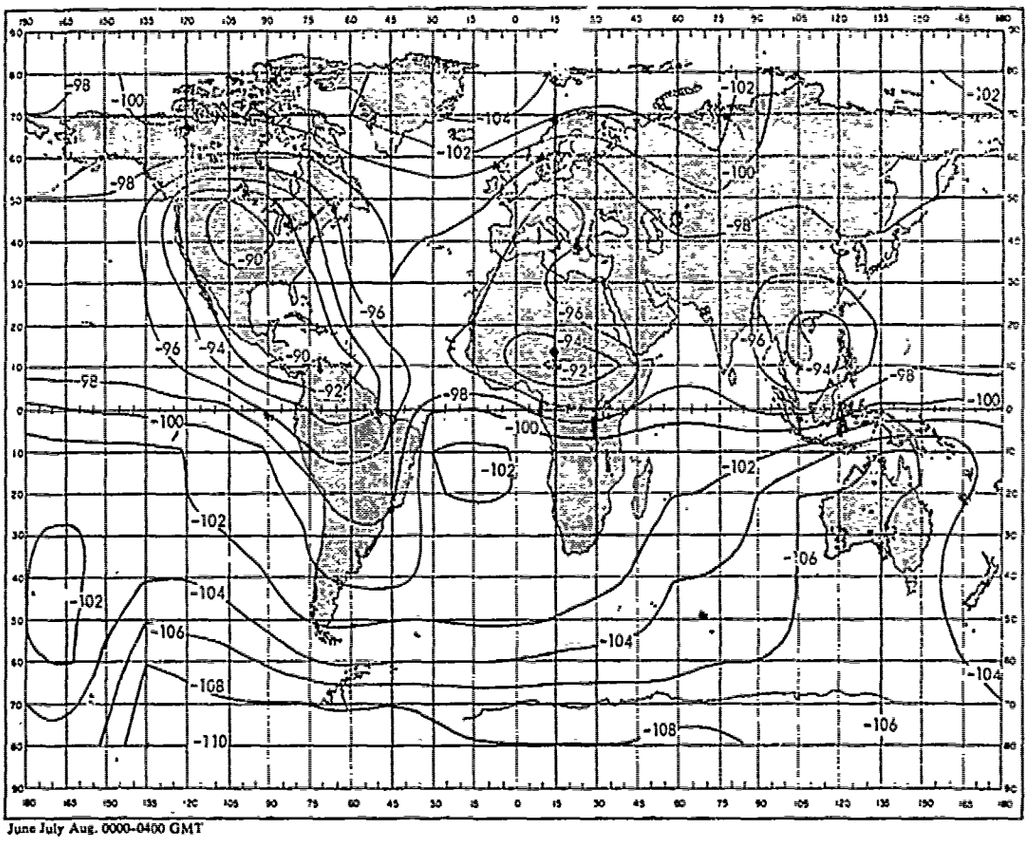

Fig. 16 — Expected atmospheric noise at 10 kc/s in decibels relative to 1 v/m/$\sqrt{c/s}$ (data from CCIR 322)

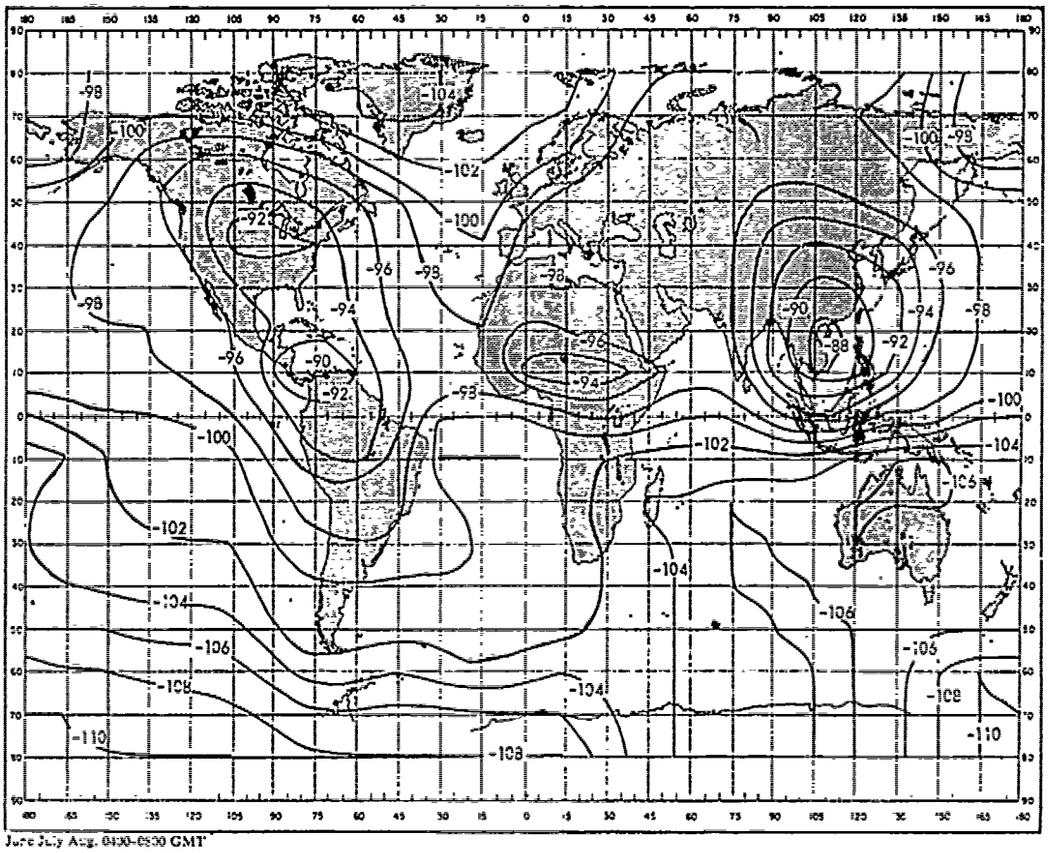

Fig. 17 — Expected atmospheric noise in 10 kc/s in decibels relative to 1 v/m/$\sqrt{c/s}$ (data from CCIR 322)

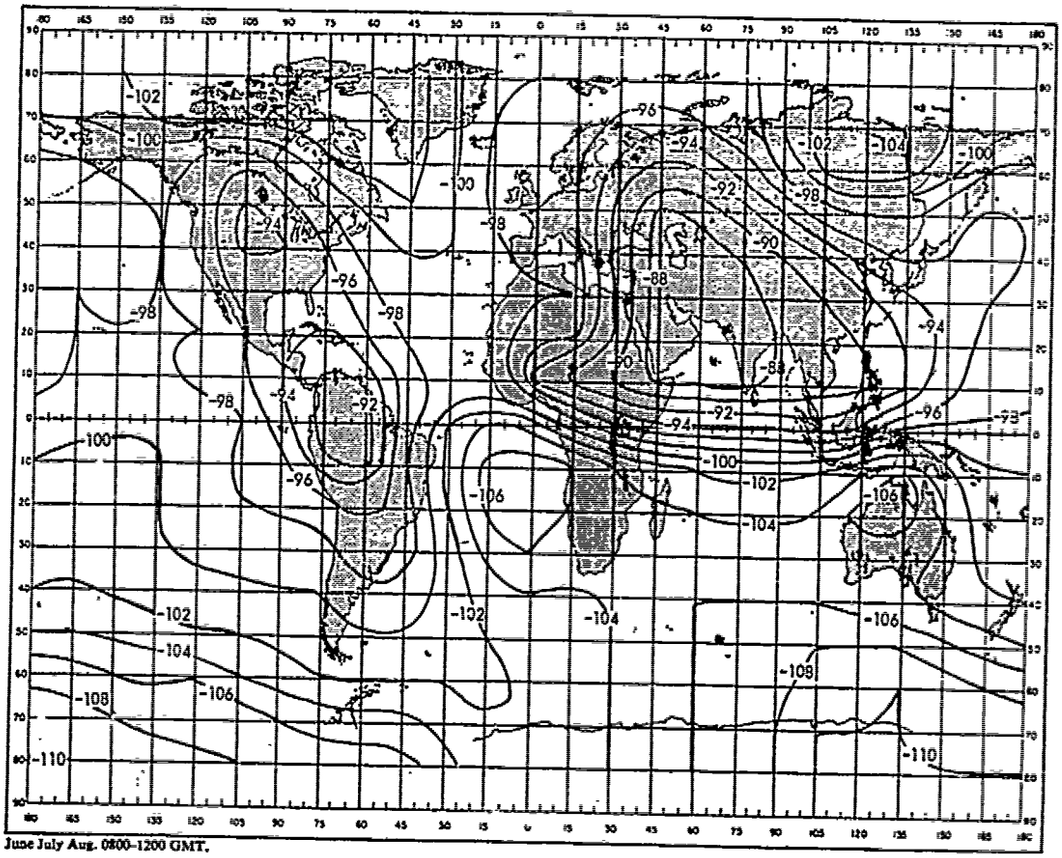

Fig. 18 — Expected atmospheric noise at 10 kc/s in decibels relative to 1 v/m/$\sqrt{c/s}$ (data from CCIR 322)

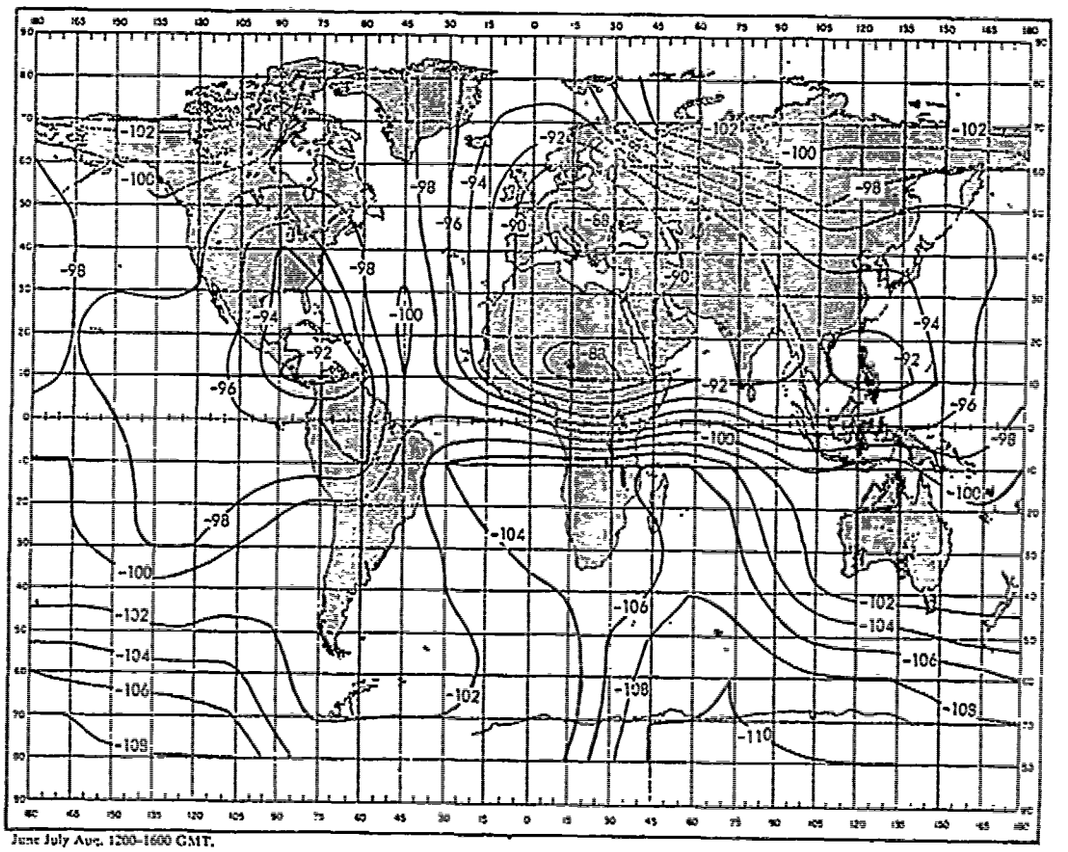

Fig. 19 — Expected atmospheric noise at 10 kc/s in decibels relative to 1 v/m/$\sqrt{c/s}$ (data from CCIR 322)

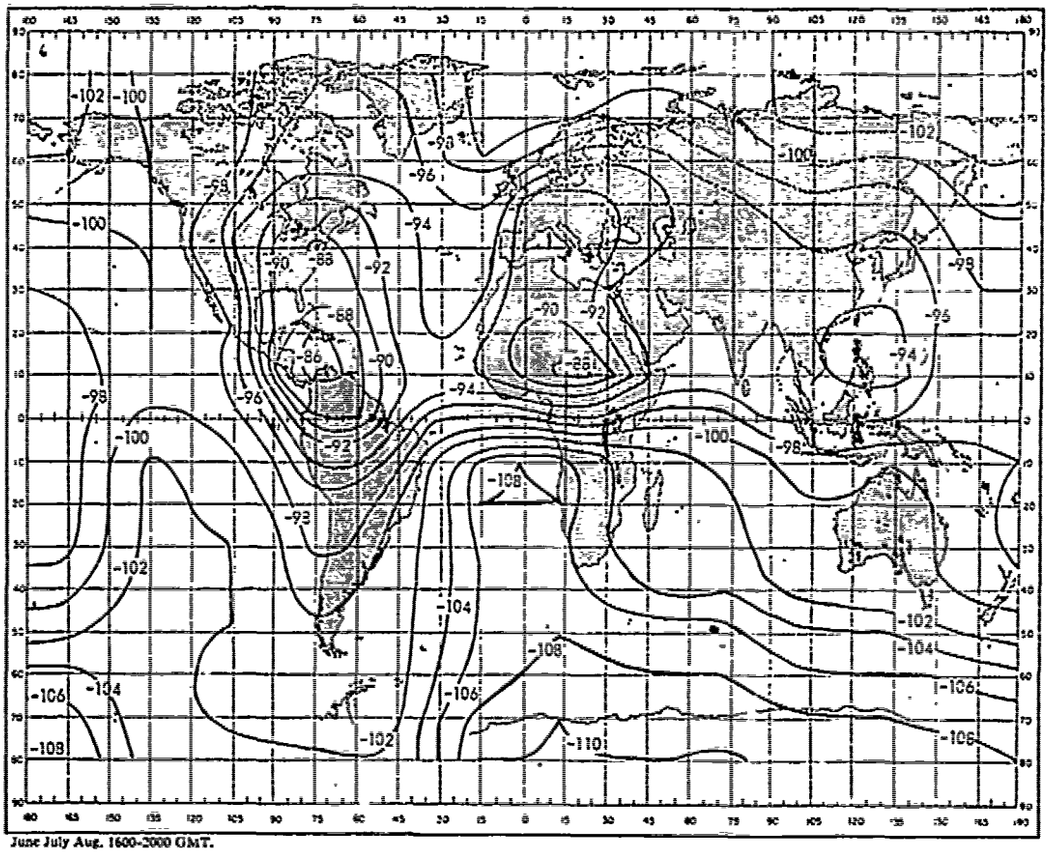

Fig. 20 — Expected atmospheric noise at 10 kc/s in decibels relative to 1 v/m/$\sqrt{c/s}$ (data from CCIR 322)

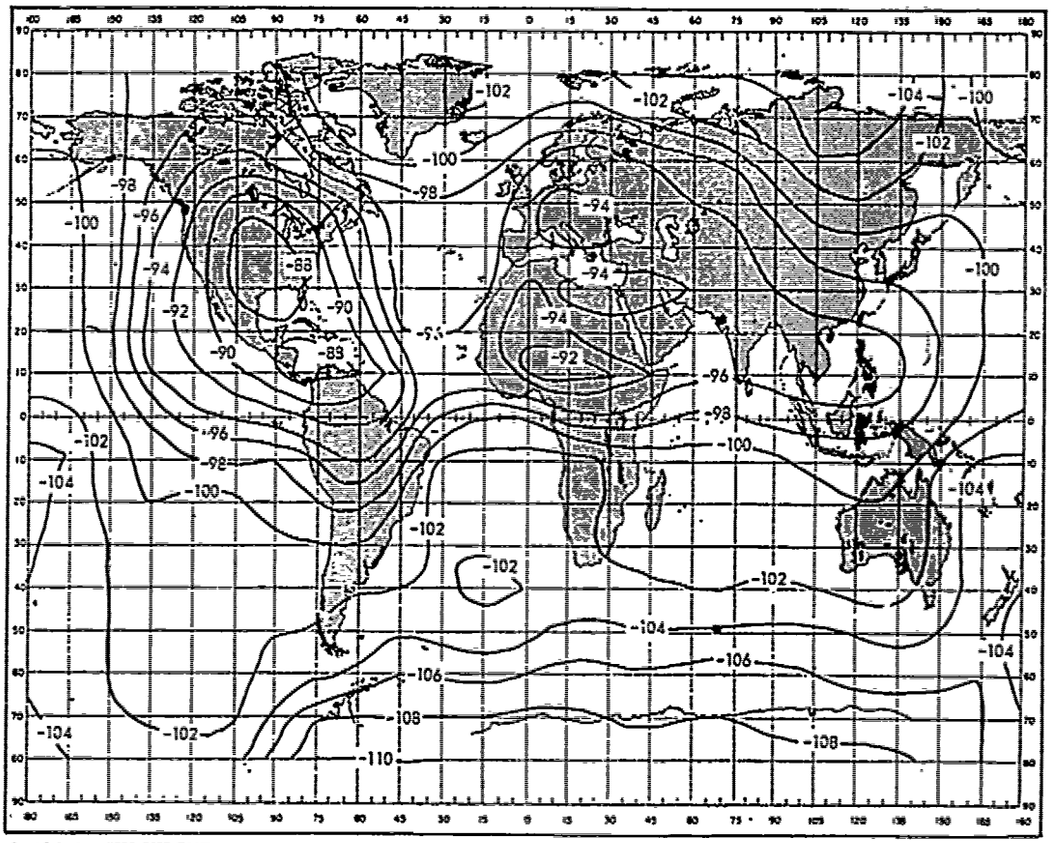

June July Aug. 2000-2400 GMT.

Fig. 21 — Expected atmospheric noise at 10 kc/s in decibels relative to 1 v/m/$\sqrt{c/s}$ (data from CCIR 322)

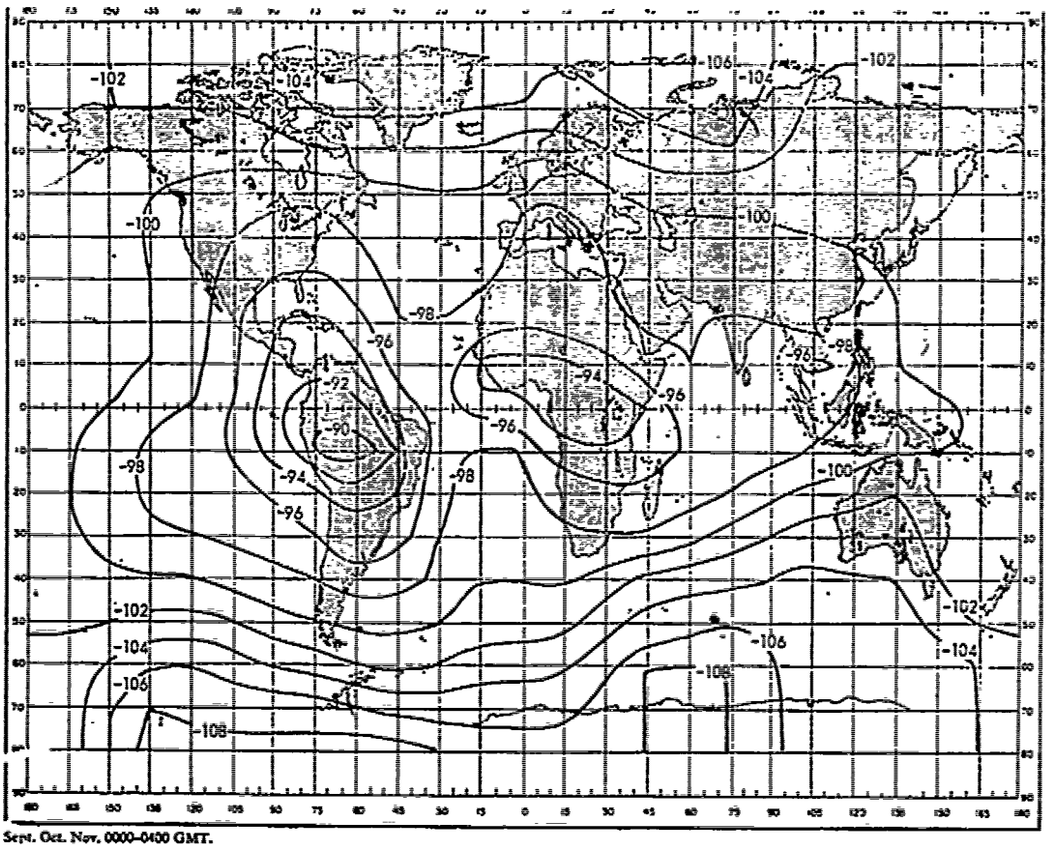

Fig. 22 — Expected atmospheric noise at 10 kc/s in decibels relative to 1 v/m/$\sqrt{c/s}$ (data from CCIR 322)

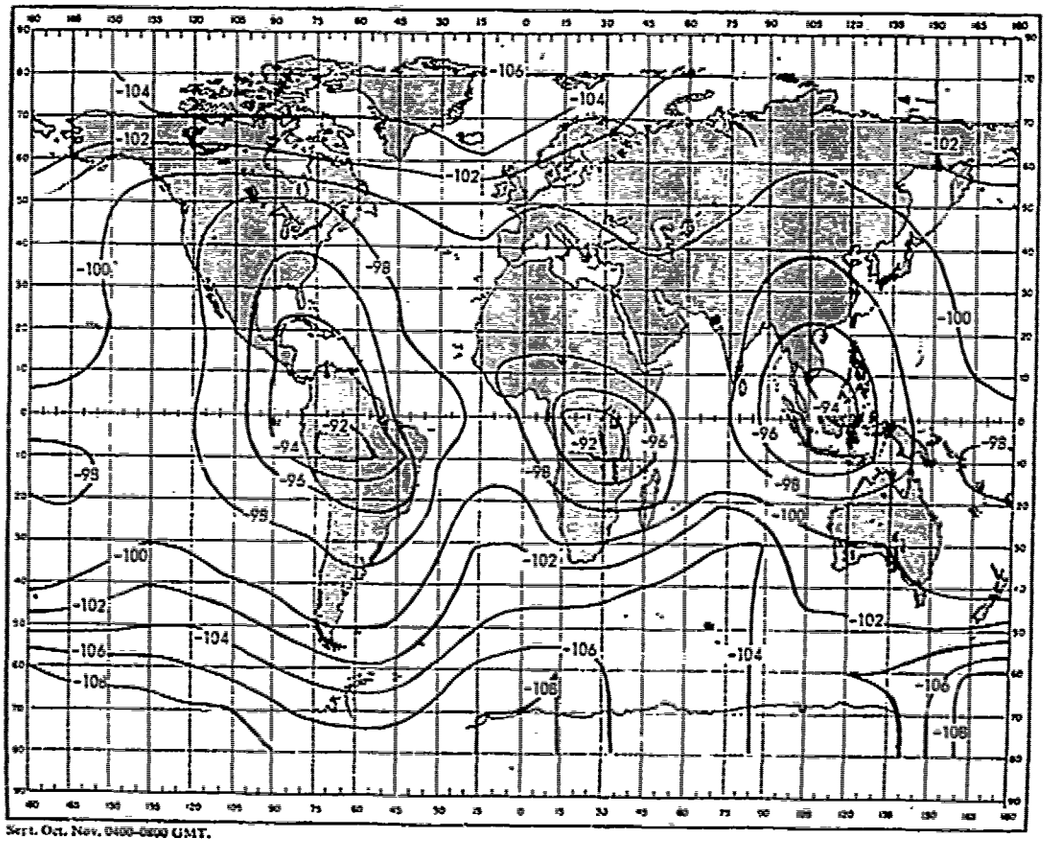

Fig. 23 — Expected atmospheric noise at 10 kc/s in decibels relative to 1 v/m/$\sqrt{c/s}$ (data from CCIR 322)

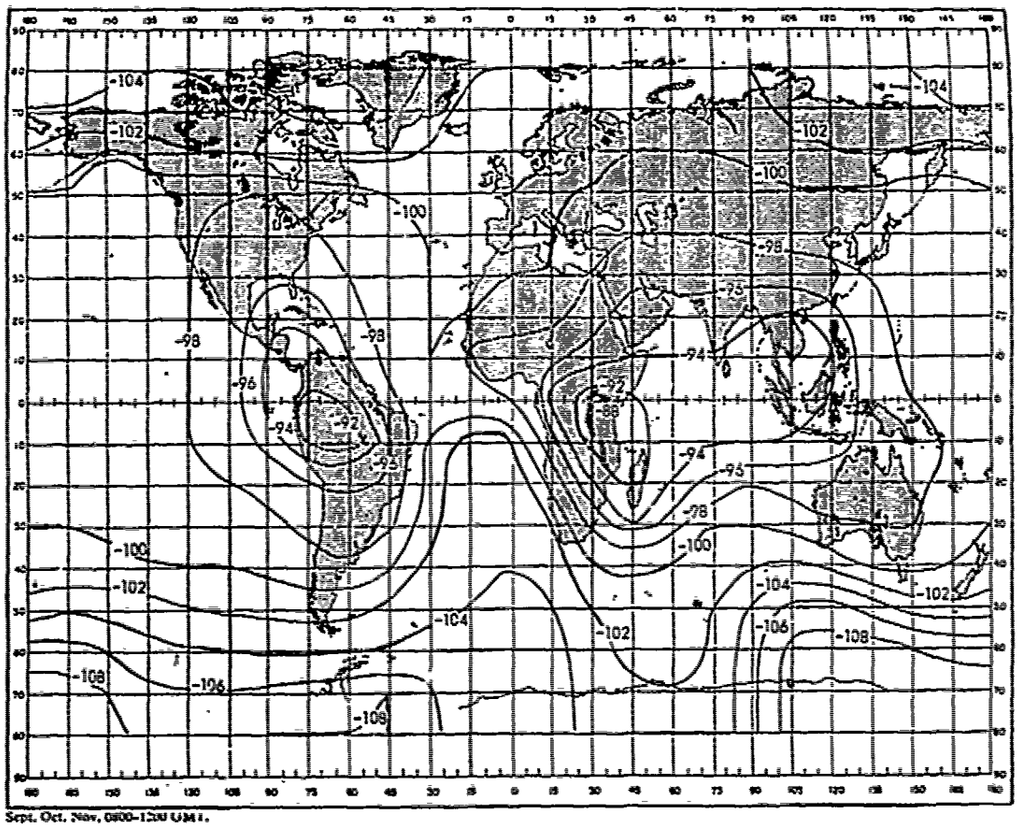

Fig. 24 — Expected atmospheric noise at 10 kc/s in decibels relative to 1 v/m/$\sqrt{c/s}$ (data from CCIR 322)

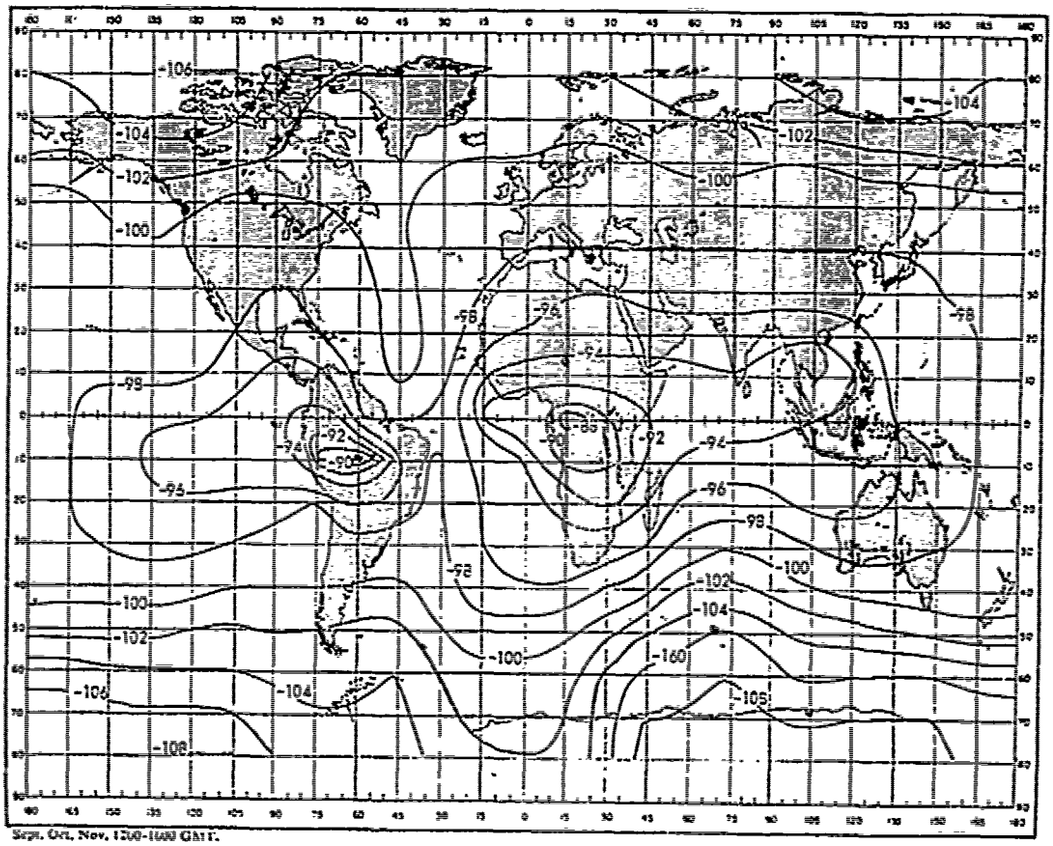

Fig. 25 — Expected atmospheric noise at 10 kc/s in decibels relative to 1 v/m/$\sqrt{c/s}$ (data from CCIR 322)

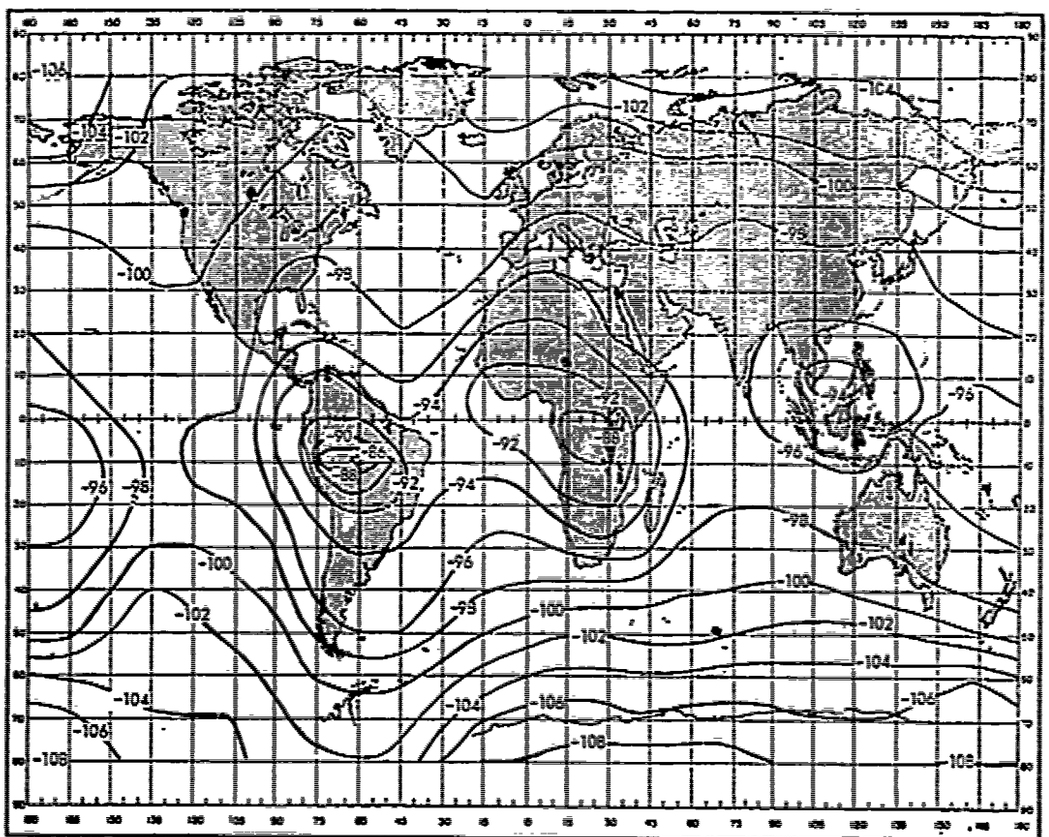

Fig. 26 — Expected atmospheric noise at 10 kc/s in decibels relative to 1 v/m/√c/s (data from CCIR 322)

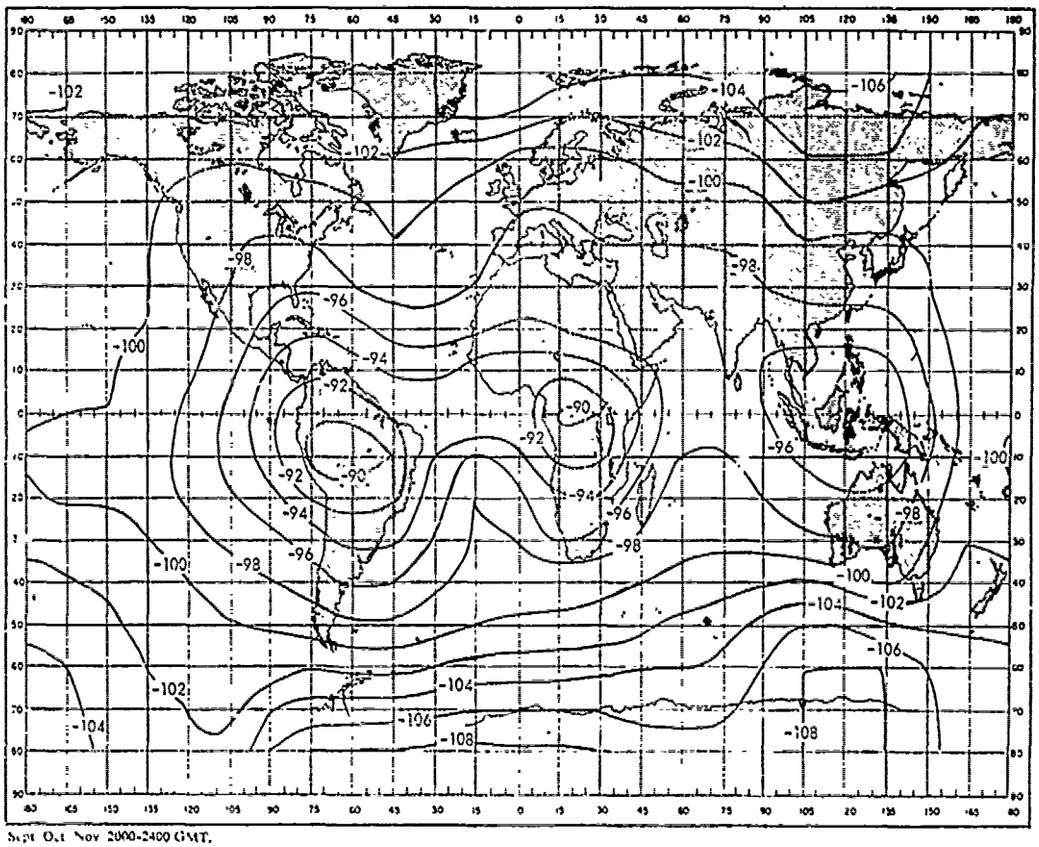

Fig. 27 — Expected atmospheric noise at 10 kc/s in decibels relative to 1 v/m/$\sqrt{c/s}$ (data from CCIR 322)

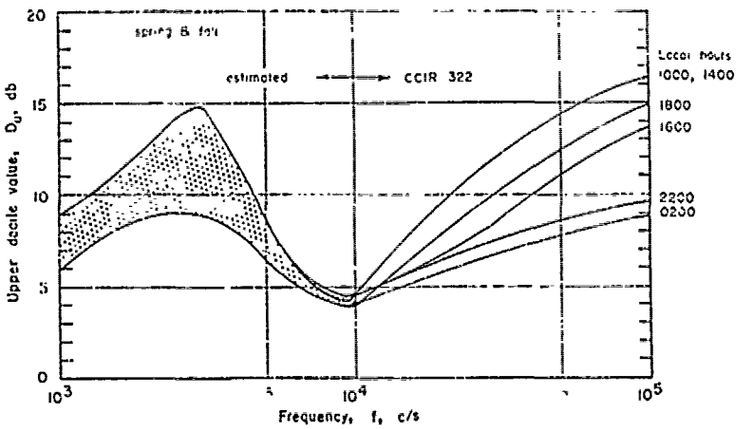

Fig. 28 — Upper decile value vs. frequency

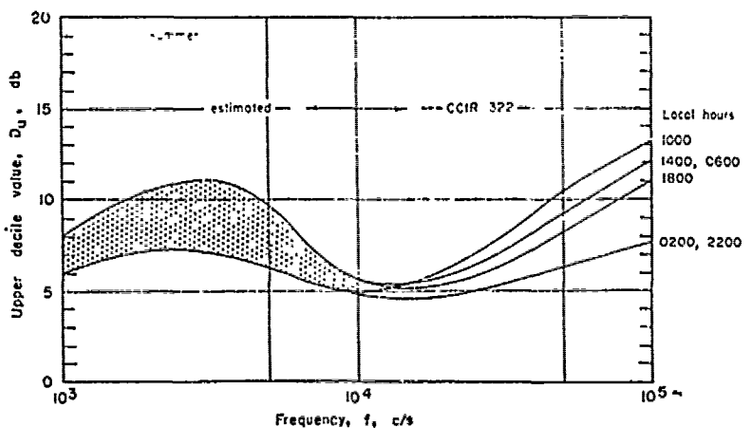

Fig. 29 — Upper decile value vs. frequency

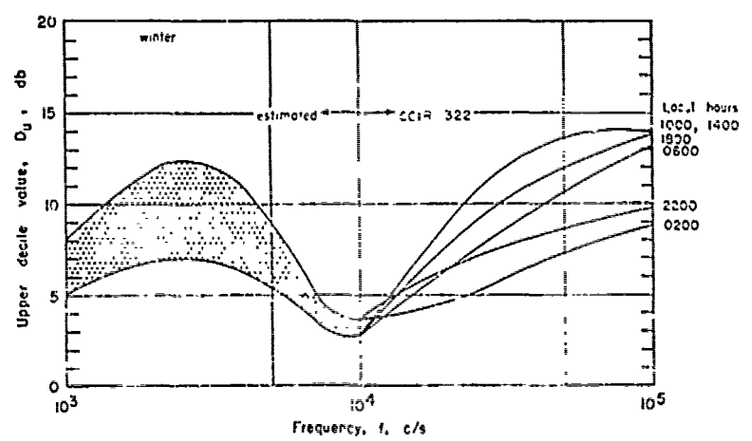

Fig. 30 — Upper decile value vs. frequency

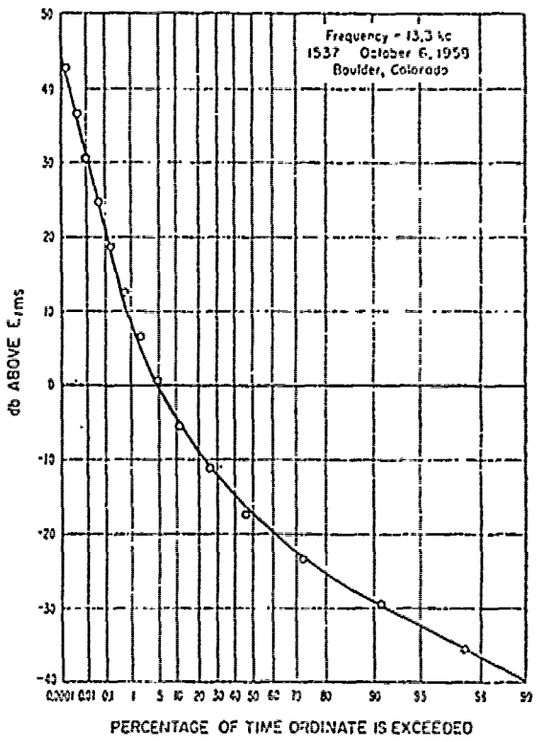

Fig. 31 — Measured amplitude-probability distribution of atmospheric radio noise

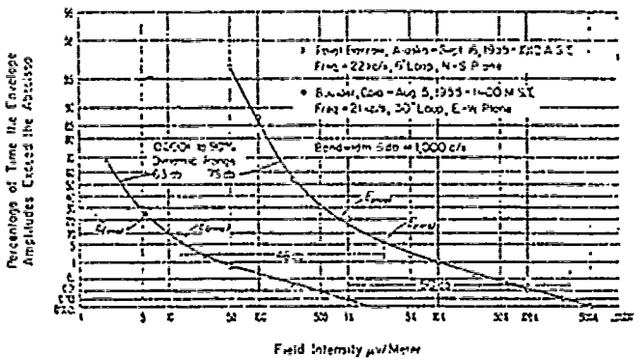

Fig. 32 — Amplitude distributions of atmospheric noise envelopes showing maximum range of amplitude level observed at all five stations

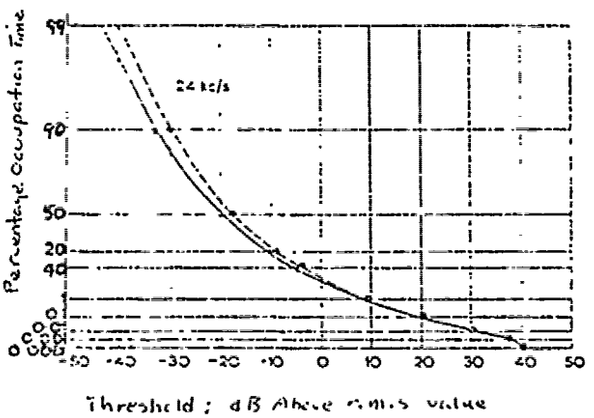

Threshold ; dB Above r.m.s. Value

Fig. 33 — Composite amplitude probability distribution at Singapore (—) and Slough (---)

CHAPTER 4

LOW FREQUENCY (LF), MEDIUM FREQUENCY (MF), AND HIGH FREQUENCY (HF)

(30 to 300 Kilohertz, 300-3000 kilohertz, and 3-30 megahertz)

INTRODUCTION

In the LF, MF, and HF bands the noise at a receiver generally result from two sources: (1) external to the antenna, called external noise and (2) within the antenna and receiver system, called internal noise. In this section we shall be concerned primarily with the external noise.

The external noise in the three above frequency bands arise from three main sources: (1) atmospheric, (2) galactic and (3) man-made. For frequencies below about 30 megahertz and in the absence of man-made noise, the dominate noise sources is due to atmospheric noise, or noise that result from lightening discharges.

In a previous section, on VF and VLF noise bands, we have given a brief discussion on the mechanism of lightening discharges. The general behavior of atmospheric noise is that the levels gets lower as the frequency increases. Oh [1] has compiled a summary of atmospheric noise spectrum that shows in general the atmospheric noise in the region of present interest decreases at the rate of 1/f, where f is the frequency (Fig. 1).

As before, we will present some measured noise data for long term average values and for short term statistics.

The most comprehensive measured data is that contained in the CCIR report 322 [2] which attempts to show world-wide distribution of atmospheric noise.

The data is based upon world-wide measurements made in the frequency range 10 khz to 100 mgz. The measured data was grouped into four seasons and six four-hour periods. Thus twenty-four time blocks were represented.

The division of a year into four seasons, of three months each, was made in the following way:

MONTHS	SEASON	
	NORTHERN HEMISPHERE	SOUTHERN HEMISPHERE
December,January,February	Winter	Summer
March, April, May	Spring	Autumn
June, July, August	Summer	Winter
September,October,November	Autumn	Spring

Data for each of the four seasons was grouped into six four-hour periods as follows:

LOCAL HOURS

0000 - 0400
0400 - 0800
0800 - 1200
1200 - 1600
1600 - 2000
2000 - 2400

The world-wide measurements were recorded mainly at sixteen stations shown in Fig. 2, using the standarized recording equipment ARN-2 Radio Noise Recorder. The data was collected from the stations during the period from 1957 to 1962.

DESCRIPTION OF NOISE

Since noise must be described quantitively using a measuring device, one may define a measure of noise power. The noise power received from sources external to the antenna can be expressed in terms of an effective antenna noise factor, f_a, which is defined as

$$f_a = \frac{P_n}{k T_o b} = \frac{T_a}{T_o} \qquad (1)$$

where

P_n: Noise power available from an equivalent loss free antenna

k : Boltzmann's constant, 1.38×10^{-23} jouls $/^{0}k$

T_o: $288^{o}k$, reference temperature

b : effective receiver noise bandwidth (hz)

T_a: effective antenna temperature in the presence of external noise.

From Eq. 1 we see two alternative methods of specifying noise power, by the effective noise factor, f_a, or the effectiver temperature, T_a, of the antenna. Both f_a and T_a are independent of bandwidth, because the amount of noise power is portional to bandwidth. In this section the effective antenna noise factor will be given for a short verticle antenna over a perfectly conducting ground-plane and are expressed in dB, (F_a). The parameter F_a is related to the r.m.s. noise field strength along the antenna (a third way of expressing the noise level) by:

$$E_n = F_a - 65.5 + 20 \log_{10} f_{mhz} \qquad (2)$$

where E_n: r.m.s. field strength for a 1 khz bandwidth (dB above 1 μv/m)

F_a: Noise factor

f_{mhz}: frequency (mhz)

The value of field strength for any bandwidth b Hz other than 1 kHz can be obtained by adding (10 $\lg_{10}$ b - 30) to E_n. Fig. 3 is a nomogram for the solution of Eq. 2. We should point out that E_n is the vertical component of the field at the antenna; and in general, the field may be complex so that the knowledge of E_n alone is not sufficient to describe the complex wave.

NOISE CHARACTERISTICS

The atmospheric noise in the three bands is characterized by large, rapid fluctuations and the statistics of noise is a nonstationary process. However, the value of noise power averaged over tens of minutes to an hour are found to be relatively constant; variations rarely exceed $\pm$ 2dB, except near sunrise and sunset, or when there are local thunderstorms. The CCIR Report 322 data was based upon measurements made at eight frequencies spaced over the frequency band and for fifteen minutes each hour. Thus, at each frequency, the value F_a is considered as the hourly average.

The noise level measurements are dependent upon many factors such as location, season, time of day, frequency. There are other variations of F_a which must be accounted for statistically. The value of F_a for a given hour of the day varies from day to day due to the changes in thunderstorm activities and propagation conditions. The medium of the hourly values within a time block (4-hour blocks) is called the time block median, F_{am}. Variations of the hourly values during the time blocks can be denoted by values exceeded 10% of the time (D_u) and values exceed-

ed 90% of the time (D_e). When plotted on normal probability graph (levels in dB), the amplitude of the deviations, D, above the median can be represented with reasonable accuracy by a straight line through the median and upper decile (D_u) values, and a corresponding line through the median and the lower decile (D_e), for variations below the median.

VARIATION OF NOISE WITH SUNSPOT ACTIVITY

It is reasonable to expect a dependence of noise level with a change in Sunspot activity, since it is known that sunspot activities affect propagation conditions. However, the expected correlation between sunspot activity and atmospheric noise levels are at present unknown. The increased level of galactic noise at these times tend to obscure variations in atmospheric noise.

SHORT TERM STATISTIC

While knowledge of F_a is useful for communications system design by providing a measure of average noise level to permit a specification of average SNR requirements, the short term noise statistic is required to permit realiability predictions and optimum receiver design. For this reason, short term noise statistics, such as the probability amplitude distribution of noise envelop (PAD) have been computed. The PAD curves provide an indication of the percentage of time in which the noise envelope exceed a certain level, so provide a amplitude-time statistics of the noise envelope.

The PAD of noise has been measured at many different areas, world-wide. The data from various locations are reasonably consistant. Analysis of noise data indicates that the PAD curves can be represented to a sufficient degree of accuracy by a family of idealized curves, one

may be chosen to fit a particular case. When the PAD curves are plotted in a coordinate system in which a Rayleight distribution has a slope of -0.5, the family of PAD curves has a slope which is approximately Rayleigh at small amplitude values and has a higher slope (negative) for higher amplitude values.

From data analysis, Crichlow et al [3] has shown that the PAD curves can be determined if the ratio of r.m.s. to average voltage, V_d (dB), is measured; and Spaulding et al [4] provides a method for the conversion of the PAD curves from one bandwidth to another.

MEASURED MEDIAN VALUES

Figures 4 through 27 show the median values of atmospheric noise on a world-wide basis for twenty-four time blocks from CCIR Report 322. In Fig. 4A the values of F_{am} represent median noise levels likely to be encountered at a location when man-made radio noise and unwanted signals are removed. Since the values of F_{am} in Fig. 4A is shown for 1 Megahertz, Fig. 4B is used to extrapolate F_{am} values at other frequencies by first finding a value on the 1 Megahertz curve of Fig. 4B and then follow the contour curve to another frequency to determine the corresponding value of F_{am}. Also plotted on Fig. 4B are the expected value of man-made noise and galactic noise. The man-made noise represent the minimum levels to be expected, while the galactic noise represents expected upper limits. Since both the man-made and galactic noise levels are representative values, caution should be exercised in their use. The actual value of man-made noise depends upon local conditions and can be much greater than the level indicated; while the galactic noise levels will depend upon the type of antenna used and its orientation.

Similarily, the values of F_{am} in a time block must be used with caution, because these represent long term average values.

Since the parameters F_{am}, D_u, D_e, V_{dm} (median value of V_d), are median values within a time block, there are variations to be expected for measured data about the median. Fig. 4C shows the expected value of the standard deviation of measured data about the mean values within a time block. In Fig. 4C the parameters $\sigma_{F_{am}}$, D_u, σ_{D_u}, D_e and σ_{D_e} are independent of bandwidth. V_d, however, is bandwidth dependent and was measured at 200 hertz. To compute the value of V_d at a different bandwidth, a method due to Spaulding [4] can be used. This computation can be made by using the curves of Fig. 28, in which V_{dn} and V_{dw} are the values of V_d corresponding to the narrower bandwidth, b_n, and the wider bandwidth, b_w, respectively. The corresponding values of V_{dn} and V_{dw} are read at the intersection of the lines defined by the bandwidth ratio, b_w/b_n, and the known value of V_d.

AMPLITUDE PROBABILITY DISTRIBUTION CURVES

PAD curves corresponding to various values of V_d are shown in Fig. 29, plotted as a function of $A = A - A_{rms}$, where A and A_{rms} are the instantaneous and r.m.s. envelop voltages, respectively.

REFERENCES

1. Oh, L. L., Measured and Calculated Spectral Amplitude Distribution of Lightening Sferics, IEEE Trans. on Electromagnetic Compatibility, Vol. EMC-11, No. 4, November 1969, pps. 123-130.

2. C. C. I. R. Report 322, World Distribution and Characteristics of Atmospheric Noise, Documents of the Xth Plenary Assembly, Geneva, 1963.

3. Crichlow, W. Q., C. J. Roubique, A. D. Spaulding, and W. M. Beery, Determination of the Amplitude - Probability Distribution of Atmospheric Radio Noise from Statistical Moments, Journal of Research of NBS-D., Radio Propagation, Vol. 64D, No. 1, January-February 1960, pps. 49-56.

4. Spaulding, A. D., C. J. Roubique, and W. Q. Crichlow, Conversion of the Amplitude - Probability Distribution Function for Atmospheric Radio Noise from One Bandwidth to Another, Journal of Research of NBS - D. Radio Propagation, Vol. 66D, No. 6, November - December 1962, pps. 713-720.

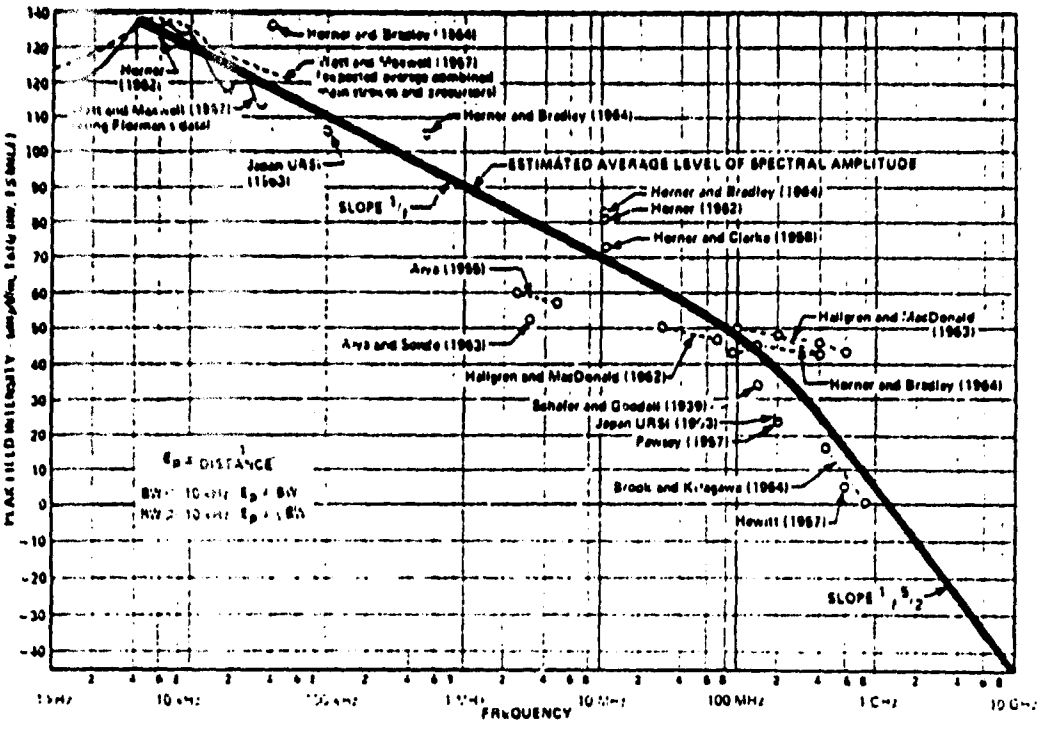

Fig. 1 — Spectral amplitude distribution of sferics

TABLE I
LITERATURE SURVEY: LIGHTNING RESEARCH

Investigators	Observation Frequency	Antenna Polarization	Receiver Bandwidth	Average Sferic Distance (miles)	Normalized Peak Field Strength, Median Value (dB above 1 μV/m, 1 kHz, 1 mi)
[illegible] and Maxwell (1957)*	1 kHz–10 kHz	—	—	20–30	See composite curves, Fig. 1
[illegible]er and Bradley (1964)	40 kHz	Vertical	250 Hz†	4–10	136
	550 kHz	Vertical	250 Hz†	4–10	105
	11 MHz	Vertical	250 Hz†	4–10	82
	200 MHz	Vertical	250 Hz†	4–10	48
	400 MHz	Vertical	250 Hz†	4–10	43
[illegible]ya (1958)	2.9 MHz	Vertical	6 kHz	300–2500	60
	4.7 MHz	Vertical	6 kHz	400–2500	58
[illegible]ya and Sonde (1963)	3 MHz	Vertical	6 kHz	1–15	52.4
[illegible]rner and Clarke (1958)	11 MHz	Vertical	300 Hz	1–4	73
[illegible]rner (1962)	6 kHz	Vertical	300 Hz	6.25‡	134.6
	11 MHz	Vertical	300 Hz	6.25	81
[illegible]llgren and MacDonald (1962)	30 MHz	Vertical	50 kHz	1‡	50
	75 MHz	Vertical	50 kHz	1‡	47.5
	90 MHz	Vertical	50 kHz	1‡	42
	150 MHz	Vertical	50 kHz	1‡	45
	400 MHz	Vertical	50 kHz	1‡	43
Hallgren and MacDonald (1963)	100 MHz	Vertical	50 kHz	1‡	50
	200 MHz	Vertical	50 kHz	1‡	48
	400 MHz	Vertical	50 kHz	1‡	45
	600 MHz	Vertical	50 kHz	1‡	42
[illegible]chafer and Goodall (1939)	150 MHz	Vertical	1.5 MHz	2–20	33.25
[illegible]awsey (1957)	200 MHz	Horizontal	100 kHz	100–175	24.4
[illegible]ewitt (1957)	600 MHz	Unknown (Parabola)	1 MHz	4–12	5.8
Brook and Kitagawa (1964)	120 MHz	Circular	1.5 MHz	6–20	17
	850 MHz	Circular	1.5 MHz	6–20	0.2
Japan URSI (1963)	100 kHz	Vertical	10 kHz	18.7	105.4
	200 MHz	Vertical	10 kHz	18.7	25.4

* Calculated from data of L. F. Florman, NBS Rept. 5525, November 10, 1955.
† Normalized by author; actual bandwidth of receiver not given.
‡ Normalized by author; actual distance not given.

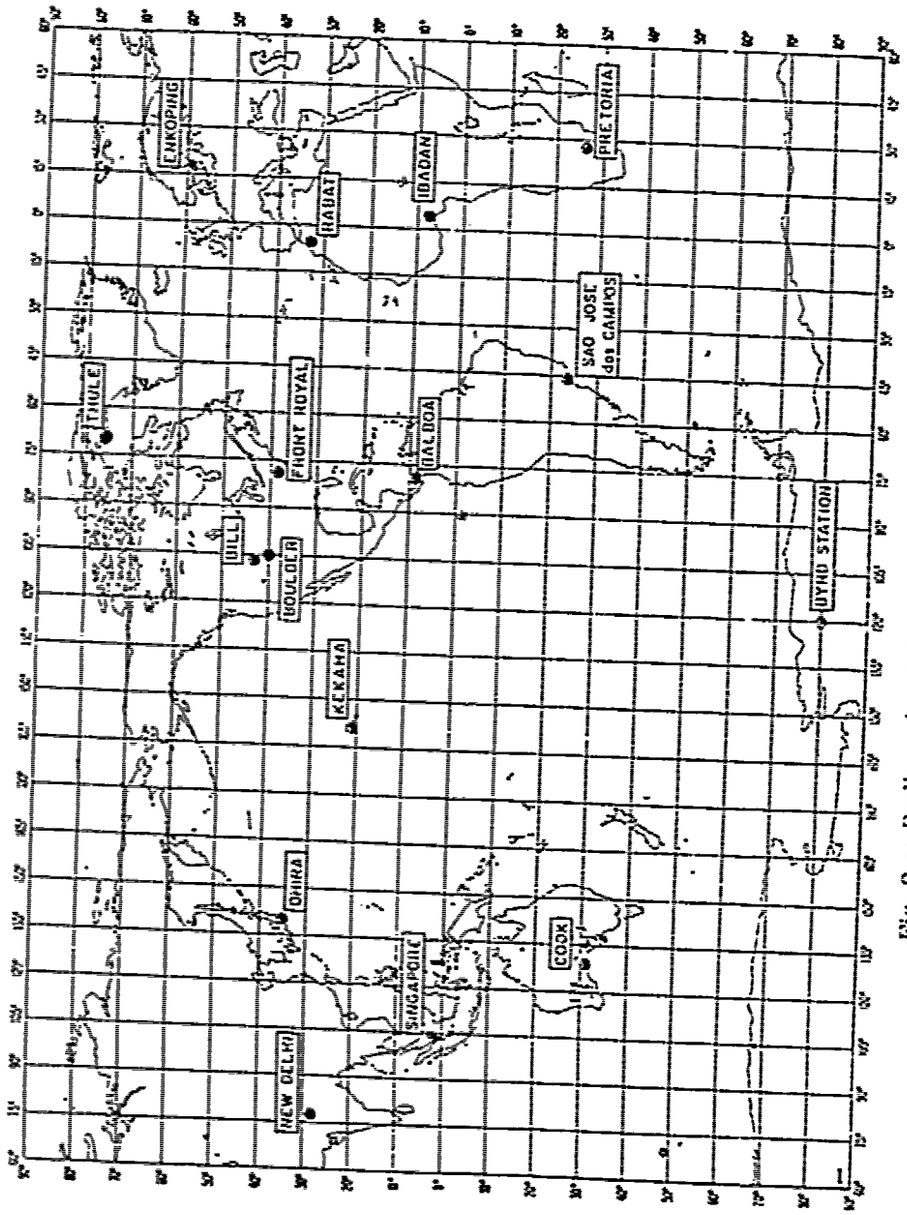

Fig. 2 — Radio noise stations using ARN-2 recorders

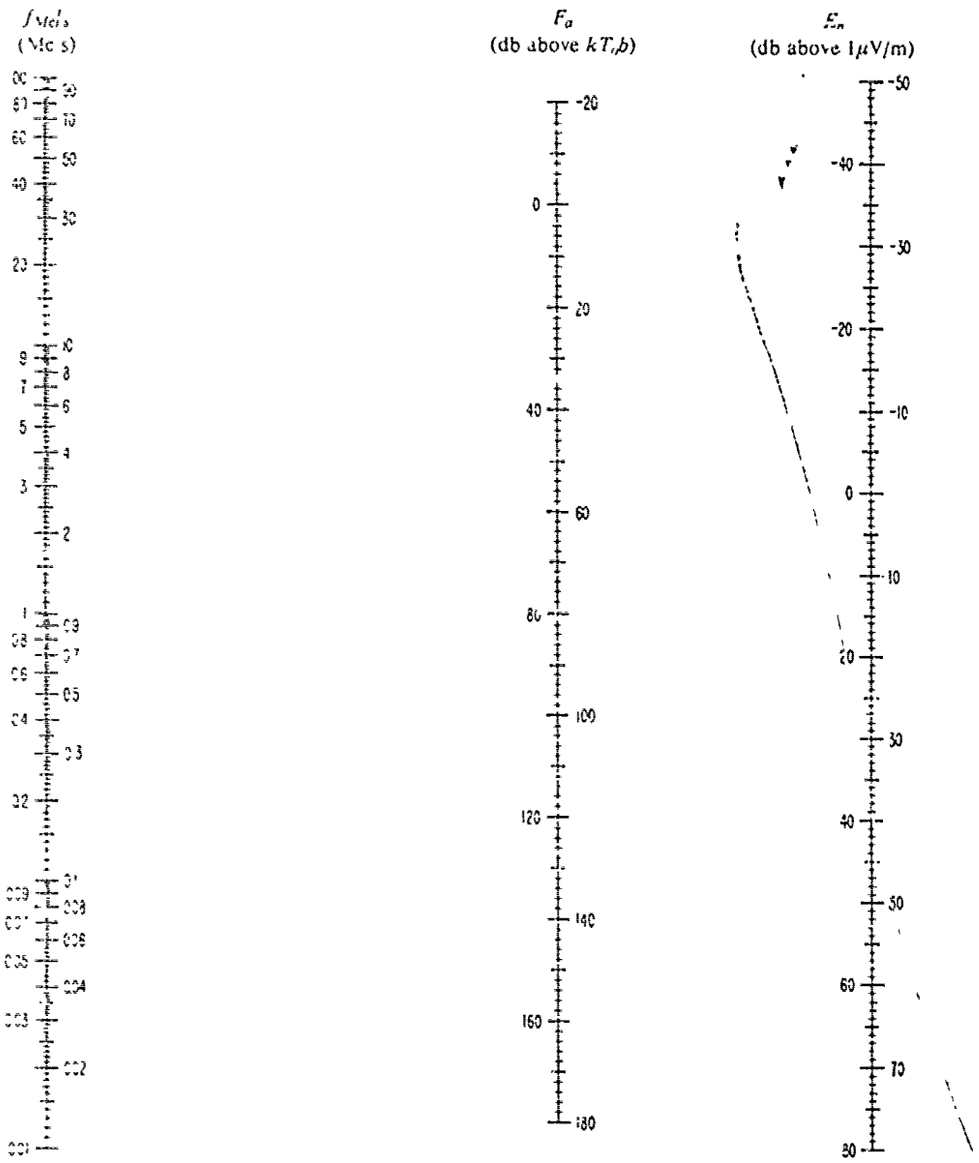

Nomogram for transforming effective antenna noise factor to noise field-strength as a function of frequency

$E_n = F_a + 20 \log_{10} f_{Mc/s} - 65{\cdot}5$

(E_n, F_a and $f_{Mc/s}$ are defined in the list of symbols)

Figure 3

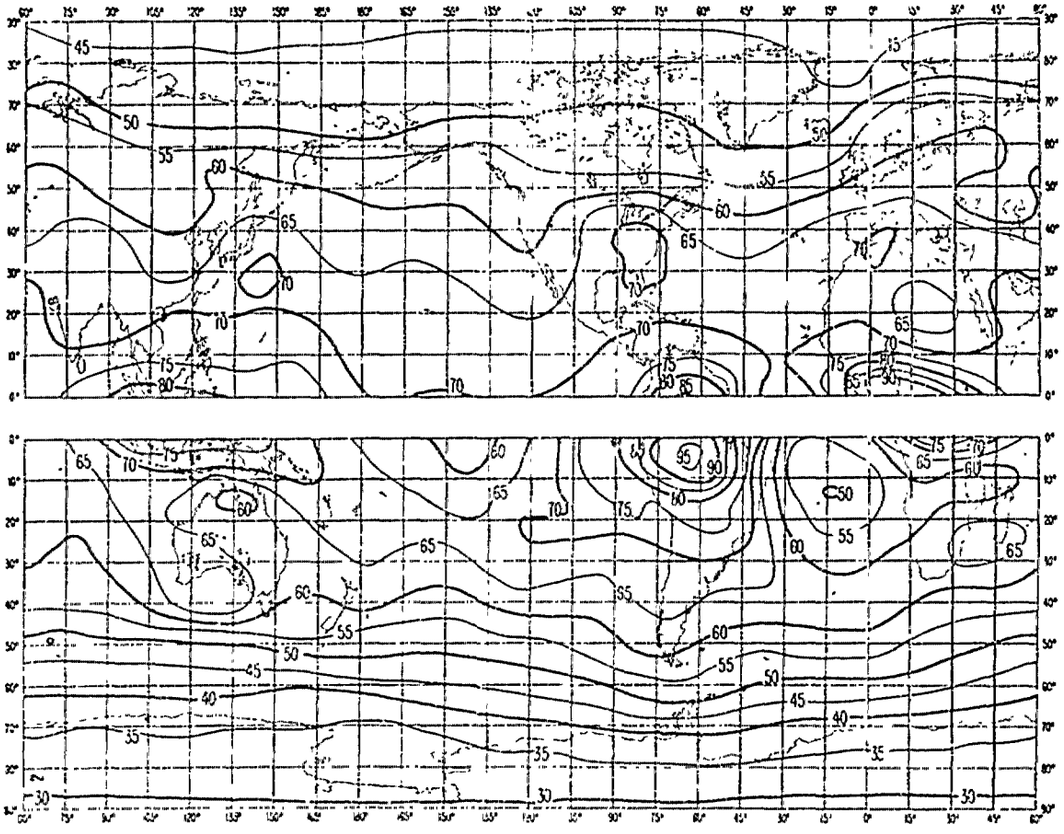

Expected values of atmospheric radio noise, F_{am}
(db above kT_0b at 1 Mc/s)
(Winter, Band 0.489 h)

Figure 4(a)

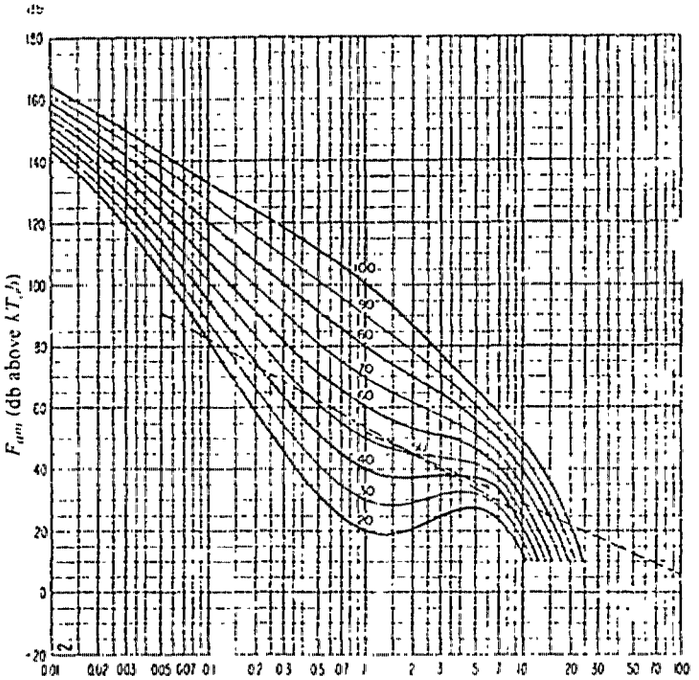

Variation of radio noise with frequency (Winter; 0000-0400 h.)

——— Expected values of atmospheric noise
—·—·— Expected values of man-made noise at a quiet receiving location
– – – – Expected values of galactic noise

Figure 4(b)

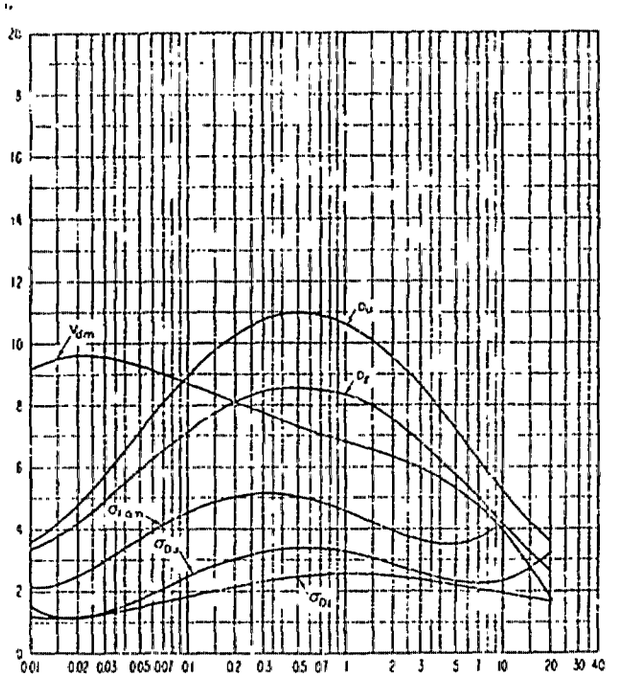

Data on noise variability and character (Winter; 0000-0400 h.)

σ_{Fam} = Standard deviation of values of F_{am}
D_u = Ratio of upper decile to median value, F_{am}
σ_{Du} = Standard deviation of values of D_u
D_l = Ratio of median value, F_{am}, to lower decile
σ_{Dl} = Standard deviation of value of D_l
V_{dm} = Expected value of median deviation of average voltage. The values shown are for a bandwidth of 200 c/s.

Figure 4(c)

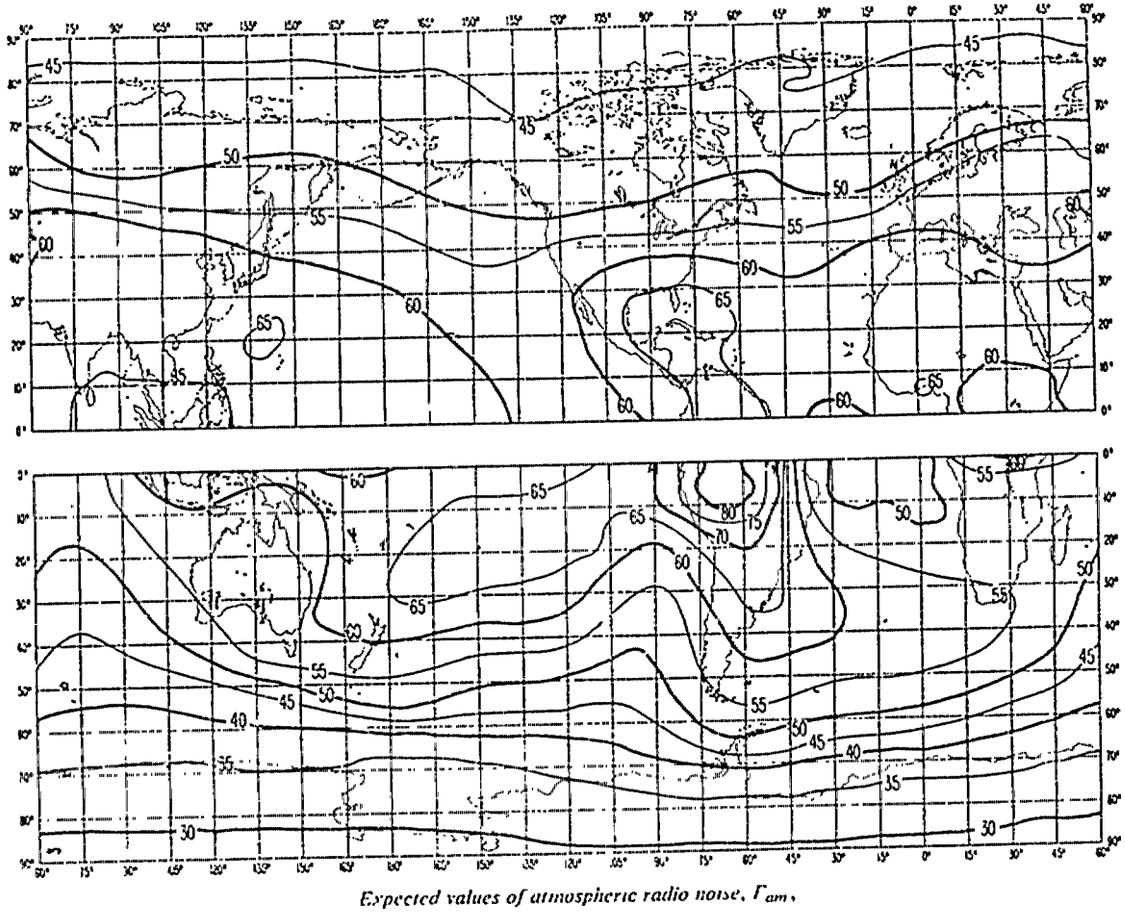

Expected values of atmospheric radio noise, F_{am},
(db above kT_0b at 1 Mc/s)
(Winter: 0400-0800 h.)

Figure 5(a)

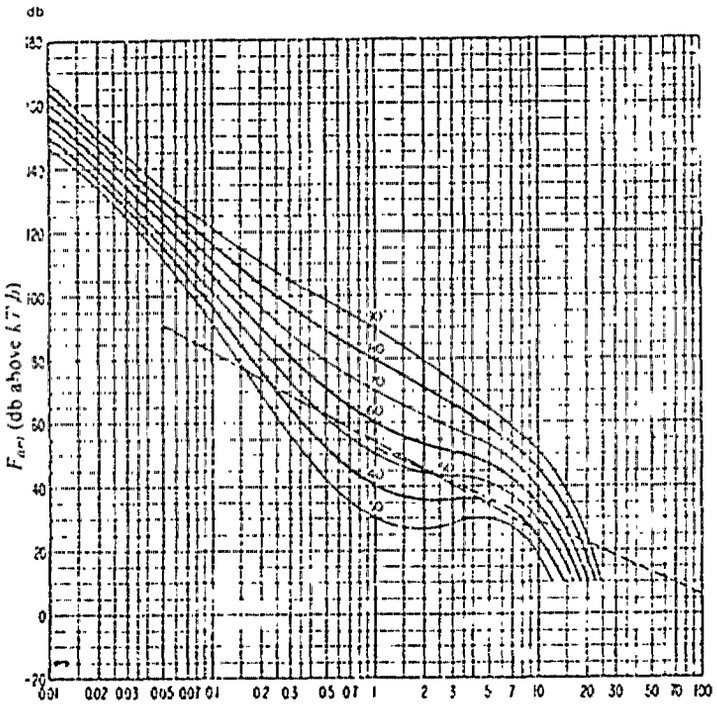

Variation of radio noise with frequency
(Winter; 0400-0800 h.)

——— Expected values of atmospheric noise
– – ..... Expected values of man-made noise at a quiet receiving location
. . . . . Expected values of galactic noise

Figure 5(b)

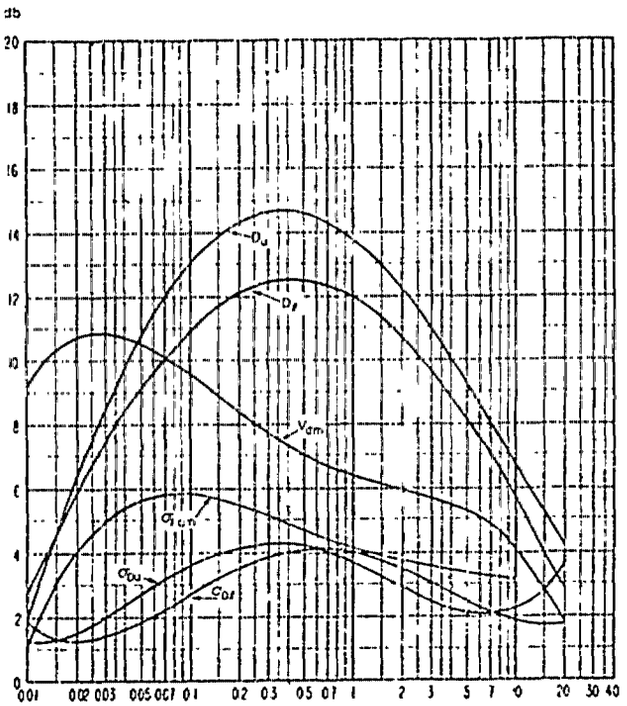

Data on noise variability and character
(Winter; 0400-0800 h.)

σ_{Fam} = Standard deviation of values of F_{am}
D_u = Ratio of upper decile to median value, F_{am}
σ_{Du} = Standard deviation of values of D_u
D_l = Ratio of median value, F_{am}, to lower decile
σ_{Dl} = Stantard deviation of value of D_l
V_{dm} = Expected value of median deviation of average voltage. The values shown are for a bandwidth of 200 c/s.

Figure 5(c)

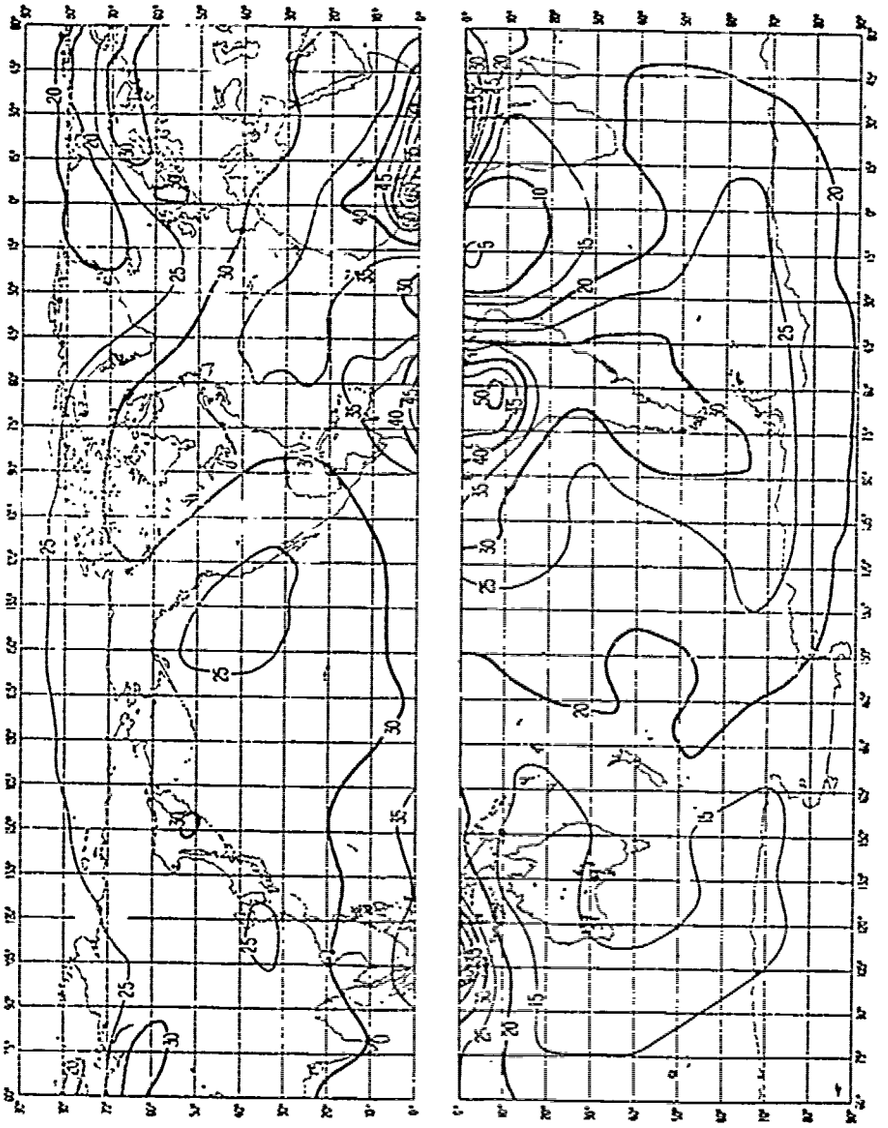

Expected values of atmospheric radio noise, F_{am},
(db above kT_0b at 1 Mc/s)
(Winter: 0800–1200 h.)

Figure 6(a)

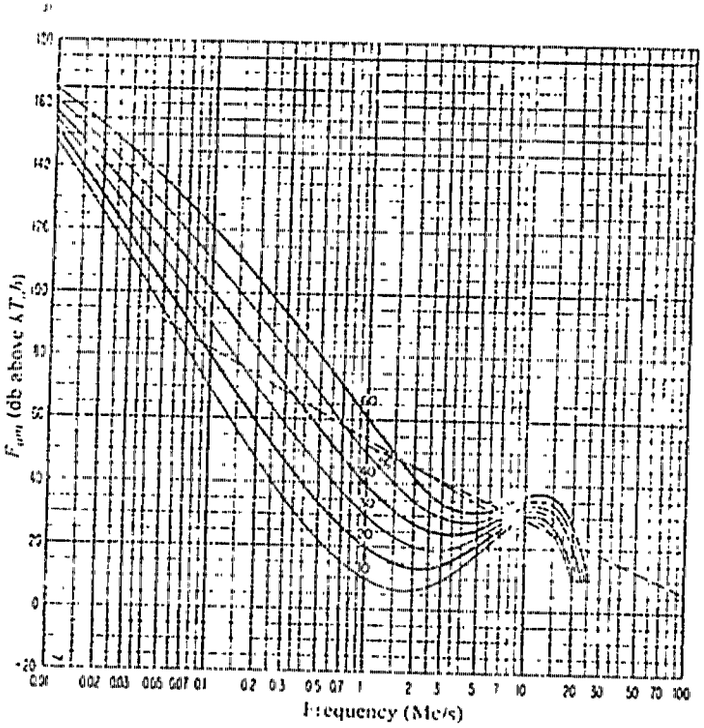

Variation of radio noise with frequency
(Winter; 0800-1200 h.)

——— Expected values of atmospheric noise
— — — Expected values of man-made noise at a quiet receiving location
– – – – – Expected values of galactic noise

Figure 6(b)

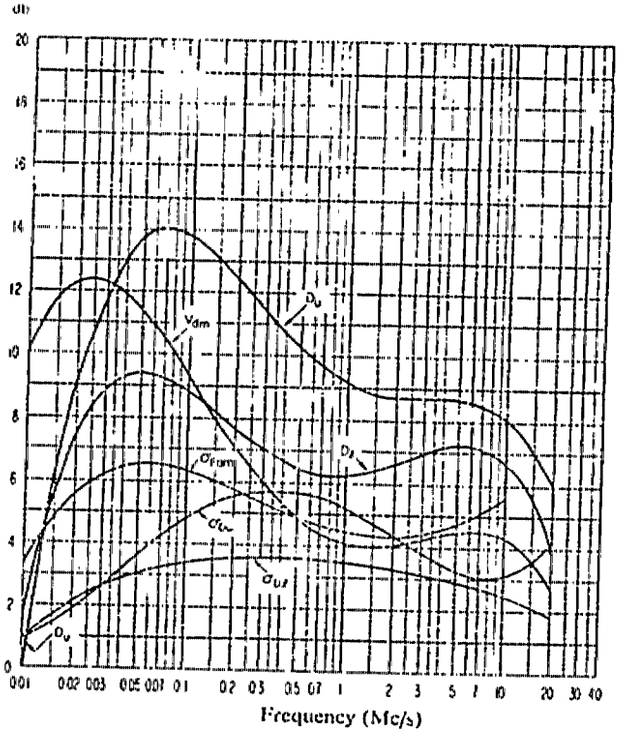

Data on noise variability and character
(Winter: 0800–1200 h.)

σ_{Fam} = Standard deviation of values of F_{am}
D_u = Ratio of upper decile to median value, F_{am}
σ_{Du} = Standard deviation of values of D_u
D_l = Ratio of median value, F_{am}, to lower decile
σ_{Dl} = Standard deviation of value of D_l
V_{dm} = Expected value of median deviation of average voltage. The values shown are for a bandwidth of 200 c/s.

Figure 6(c)

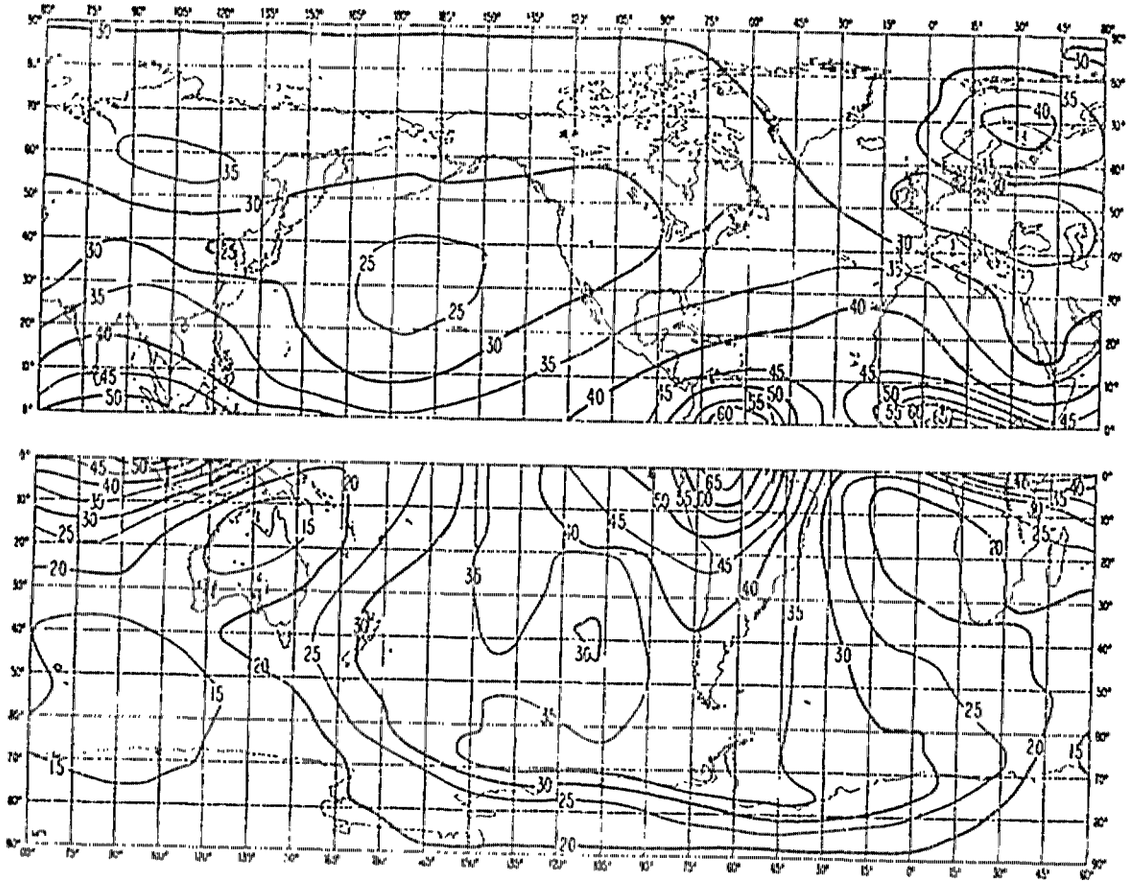

Expected values of atmospheric radio noise, F_{am},
(db above kT_0b at 1 Mc/s)
(Winter 1200–1600 h)

Figure 7(a)

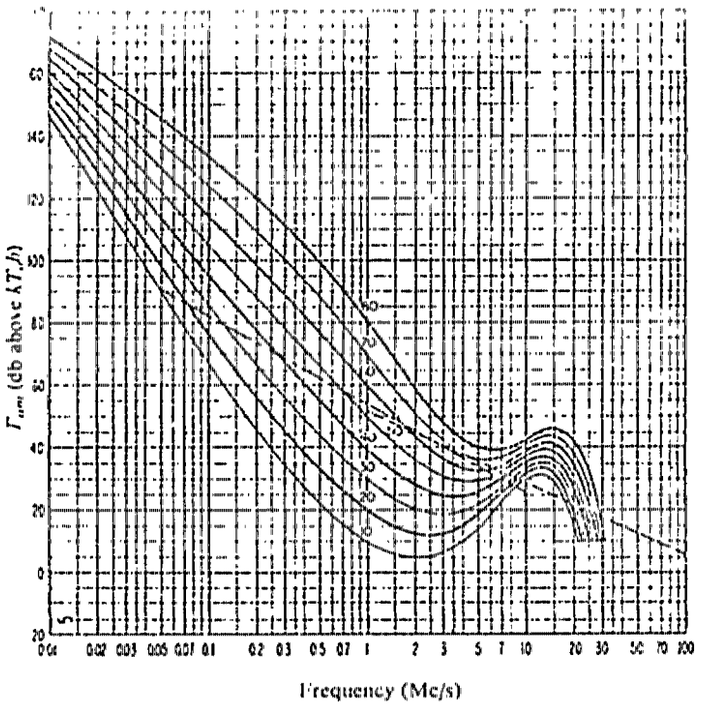

Variation of radio noise with frequency
(Winter: 1200–1600 h.)

——— Expected values of atmospheric noise
—·—·— Expected values of man-made noise at a quiet receiving location
– – – – Expected values of galactic noise

Figure 7(b)

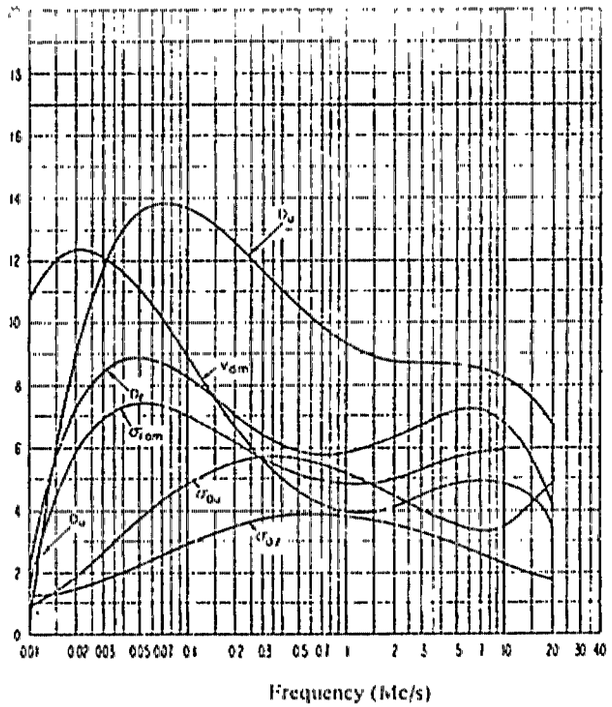

Data on noise variability and character
(Winter, 1200–1600 h.)

σ_{Fam} = Standard deviation of values of F_{am}
D_u = Ratio of upper decile to median value, F_{am}
σ_{Du} = Standard deviation of values of D_u
D_l = Ratio of median value, F_{am}, to lover decile
σ_{Dl} = Stantard deviation of value of D_l
V_{dm} = Expected value of median deviation of average voltage. The values shown are for a bandwidth of 200 c/s.

Figure 7(c)

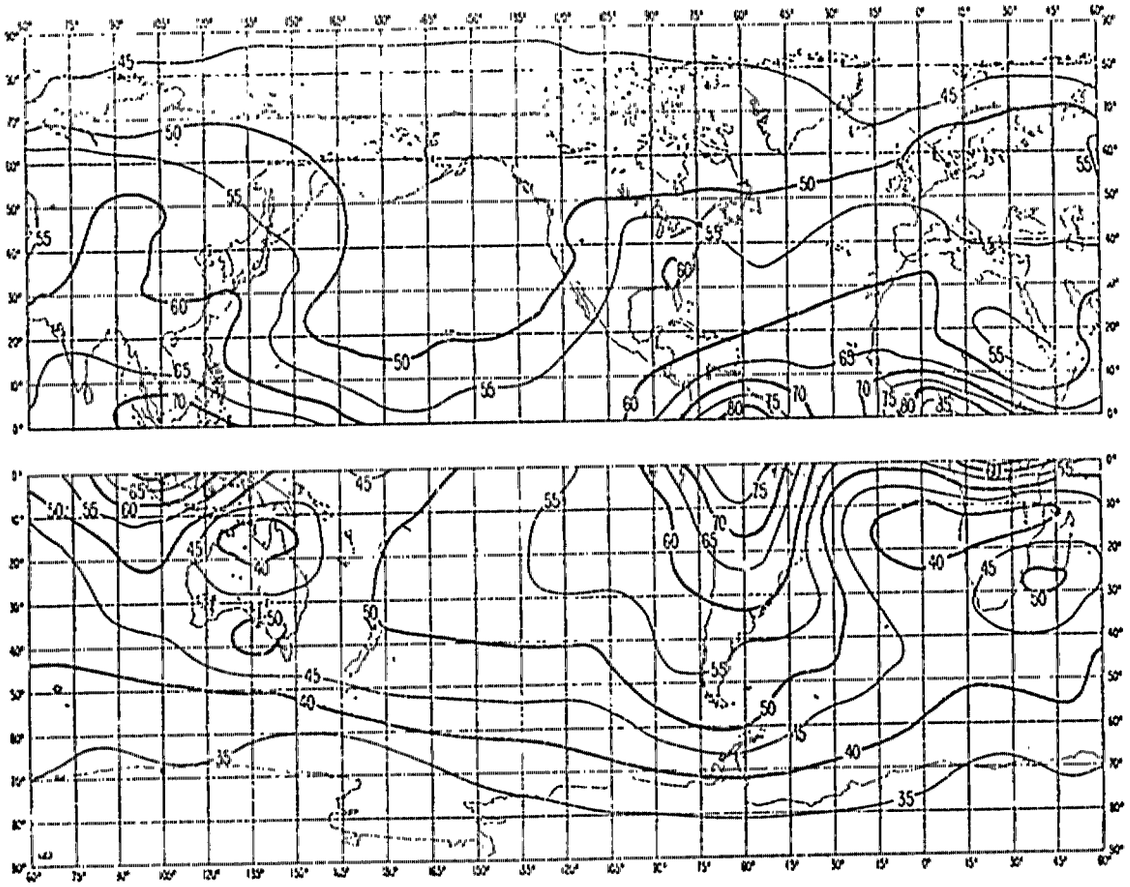

Expected values of atmospheric radio noise, F_{am}.
(db above kT_0b at 1 Mc/s)
(Winter; 1600–2000 h.)

Figure 8(a)

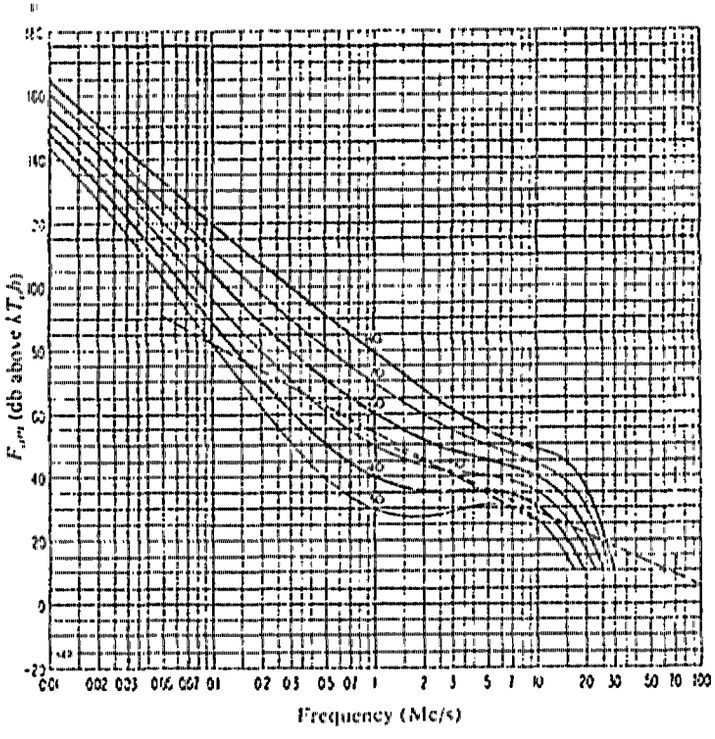

Variation of radio noise with frequency
(Winter; 1600-2000 h.)

——— Expected values of atmospheric noise
—·— · Expected values of man-made noise at a quiet receiving location
– – – – Expected values of galactic noise

Figure 8(b)

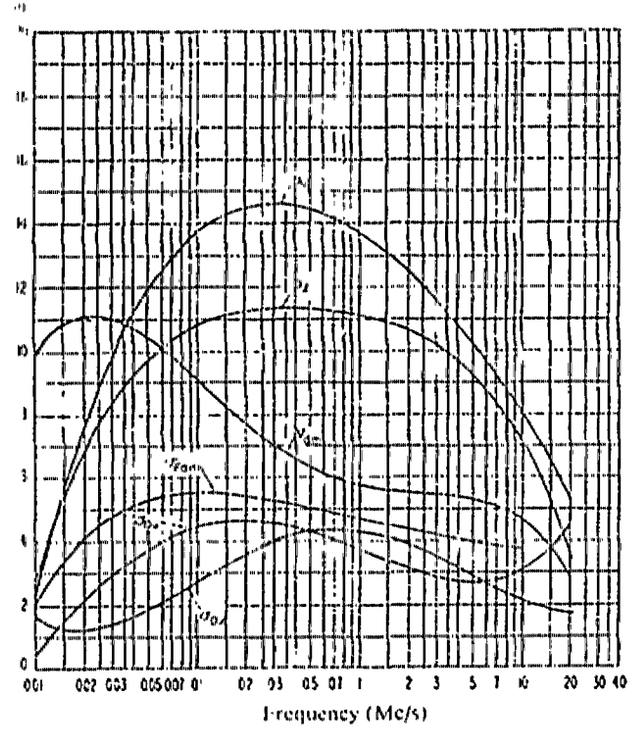

Data on noise variability and character
(Winter; 1600-2000 h.)

σ_{Fam} = Standard deviation of values of F_{am}
D_u = Ratio of upper decile to median value, F_{am}
σ_{Du} = Standard deviation of values of D_u
D_l = Ratio of median value, F_{am} to lower decile
σ_{Dl} = Standard deviation of value of D_l
V_{dm} = Expected value of median deviation of average voltage. The values shown are for a bandwidth of 200 c/s.

Figure 8(c)

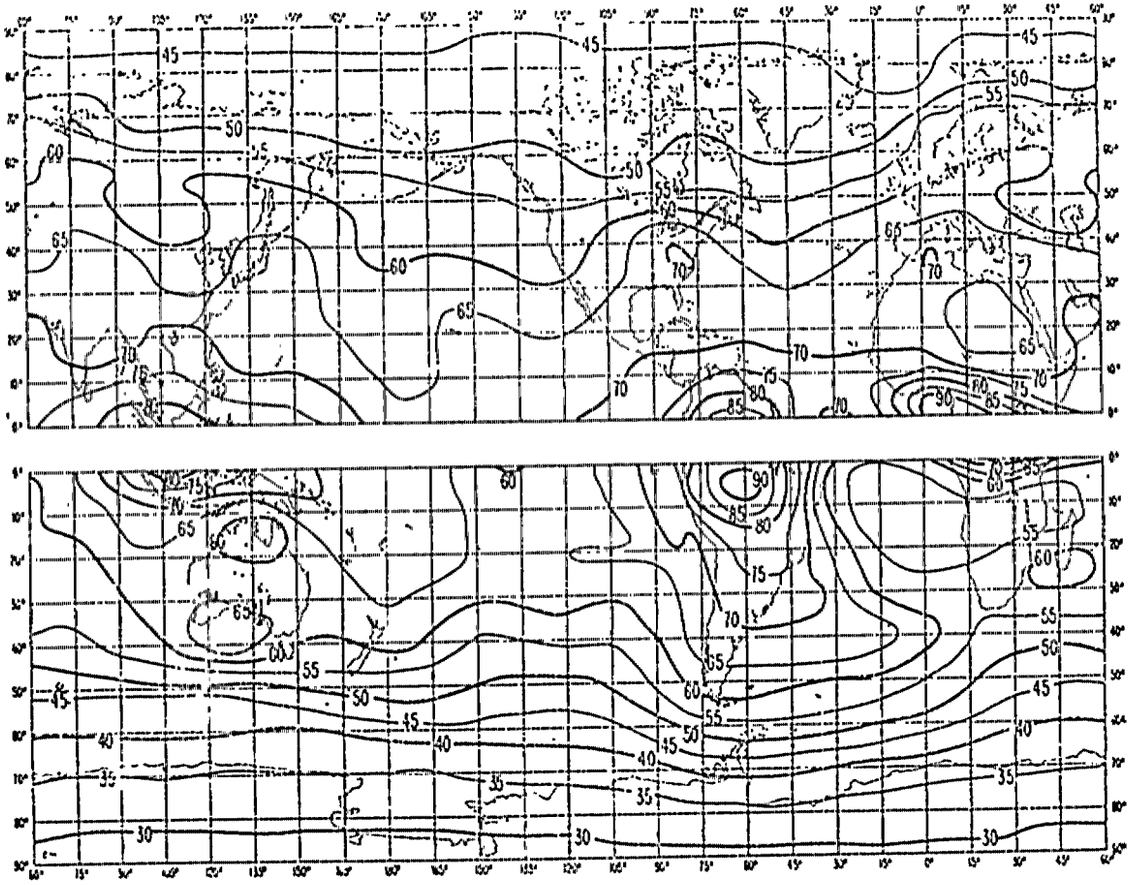

Expected values of atmospheric radio noise, F_{am},
(db above kT_0b at 1 Mc/s)
(Winter; 2000–2400 h.)

Figure 9(a)

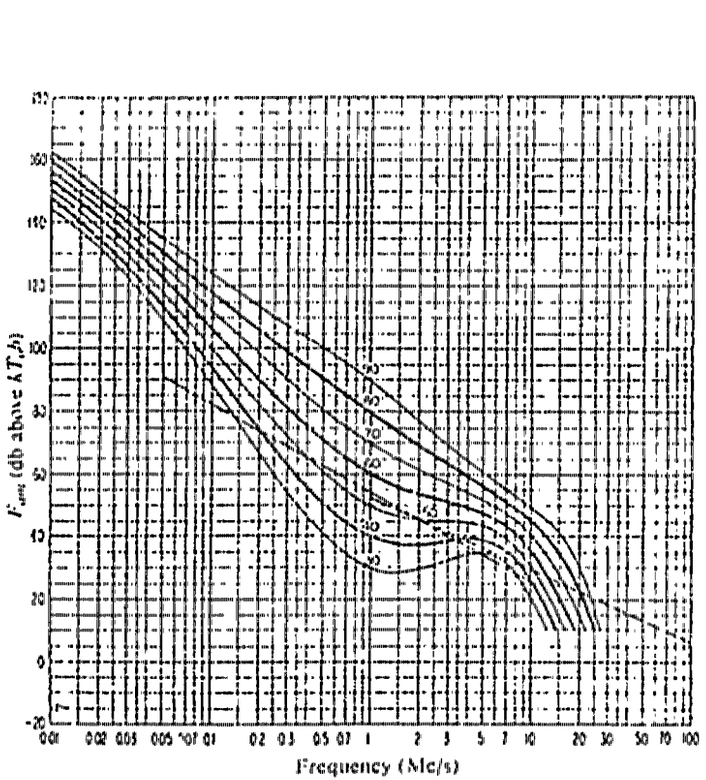

Variation of radio noise with frequency
(Winter; 2000–2400 h.)

——— Expected values of atmospheric noise
—·—·— Expected values of man-made noise at a quiet receiving location
– – – – Expected values of galactic noise

Figure 9(b)

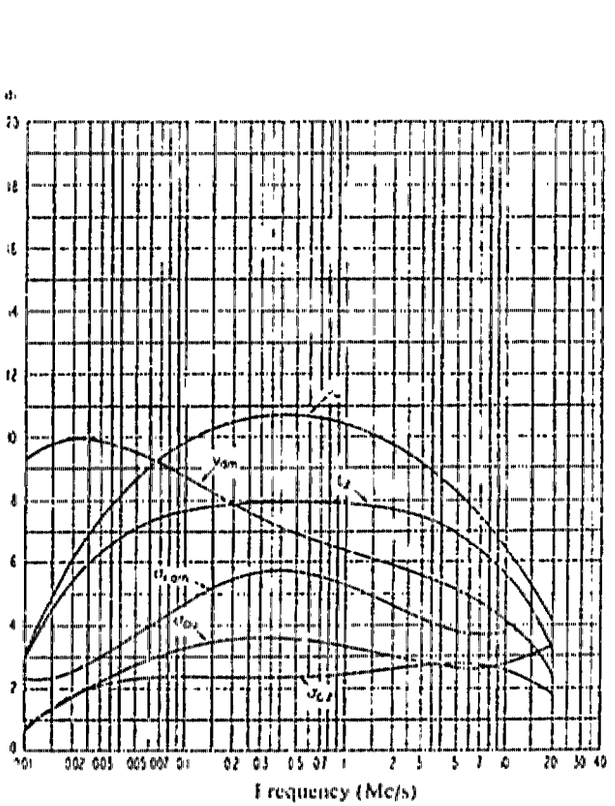

Data on noise variability and character
(Winter; 2000–2400 h)

σ_{Fam} = Standard deviation of values of F_{am}
D_u = Ratio of upper decile to median value, F_{am}
σ_{Du} = Standard deviation of values of D_u
D_l = Ratio of median value, F_{am}, to lower decile
σ_{Dl} = Stantard deviation of value of D_l
V_{dm} = Expected value of median deviation of average voltage. The values shown are for a bandwidth of 200 c/s.

Figure 9(c)

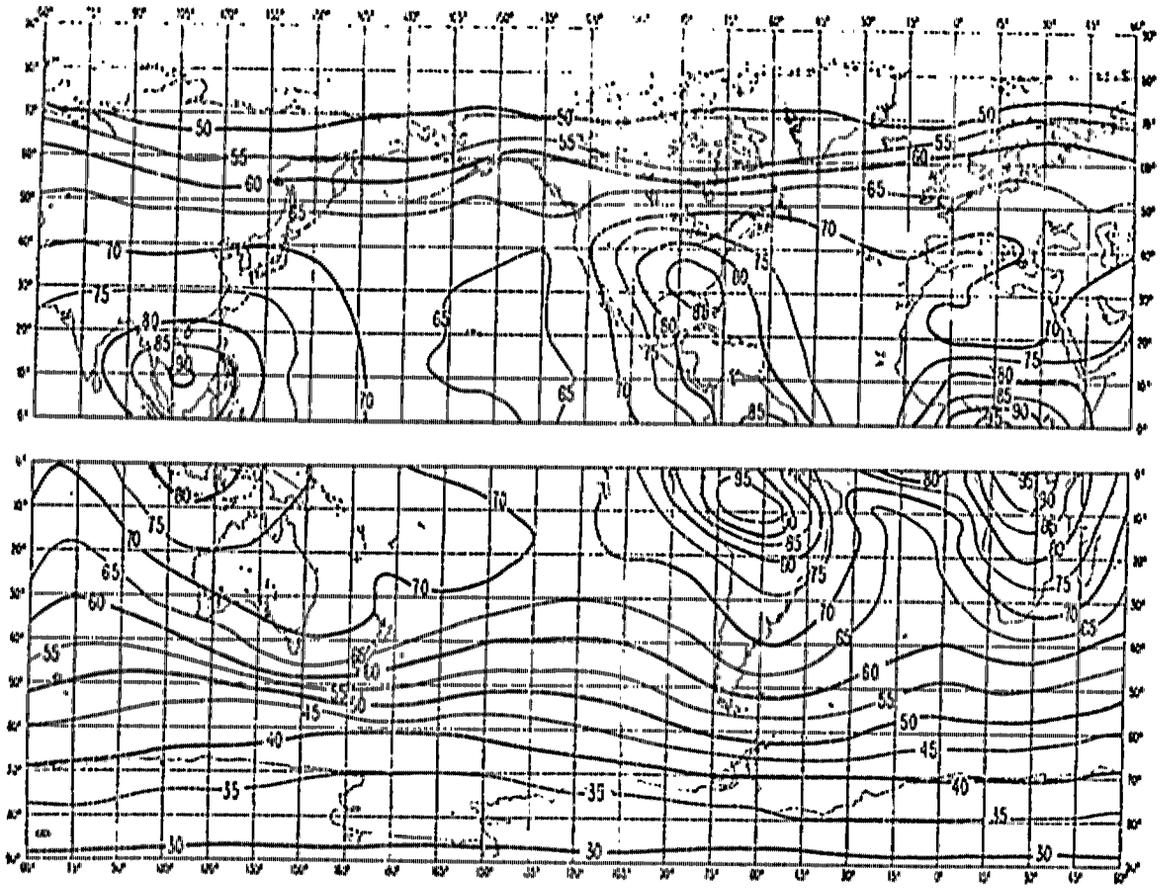

Expected values of atmospheric radio noise, F_{am},
(db above kT_0b at 1 Mc/s)
(Spring: 0900-0400 h.)

Figure 10(a)

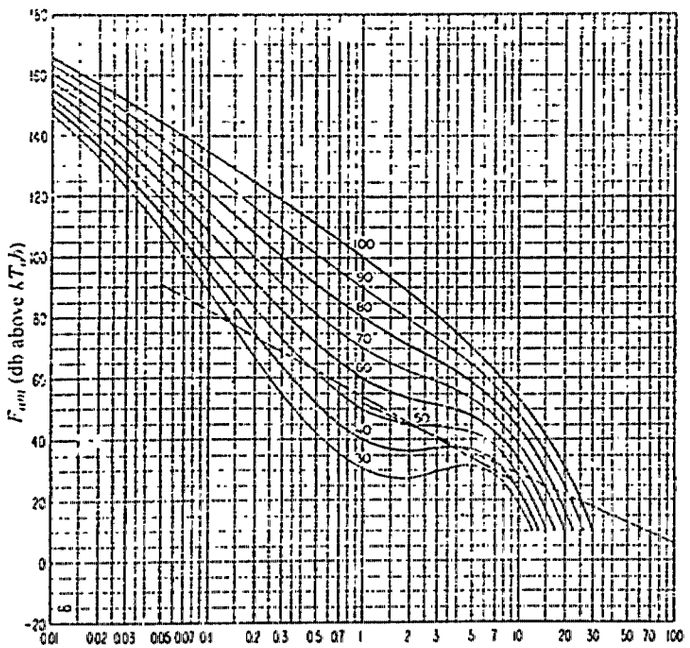

Variation of radio noise with frequency
(Spring; 0000-0400 h.)

——— Expected values of atmospheric noise
—·—·— Expected values of man-made noise at a quiet receiving location
– – – – Expected values of galactic noise

Figure 10(b)

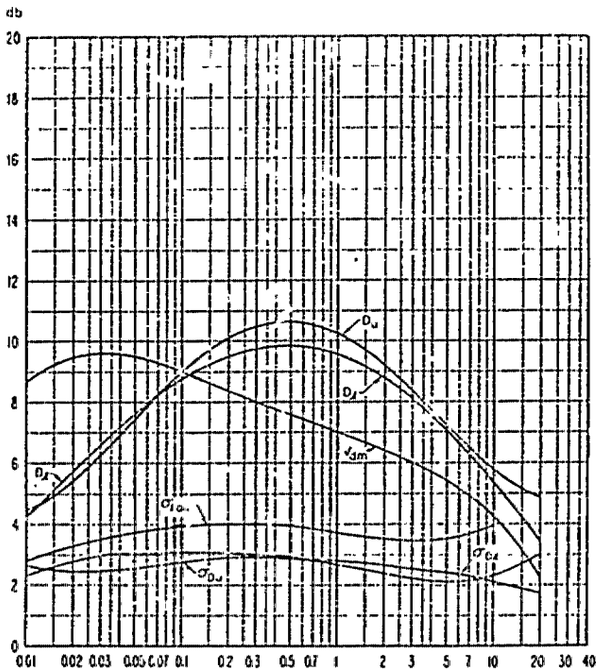

Data on noise variability and character
(Spring; 0000-0400 h.)

σ_{Fam} = Standard deviation of values of F_{am}
D_u = Ratio of upper decile to median value, F_{am}
σ_{Du} = Standard deviation of values of D_u
D_l = Ratio of median value, F_{am}, to lower decile
σ_{Dl} = Standard deviation of value of D_l
V_{dm} = Expected value of median deviation of average voltage. The values shown are for a bandwidth of 200 c/s.

Figure 10(c)

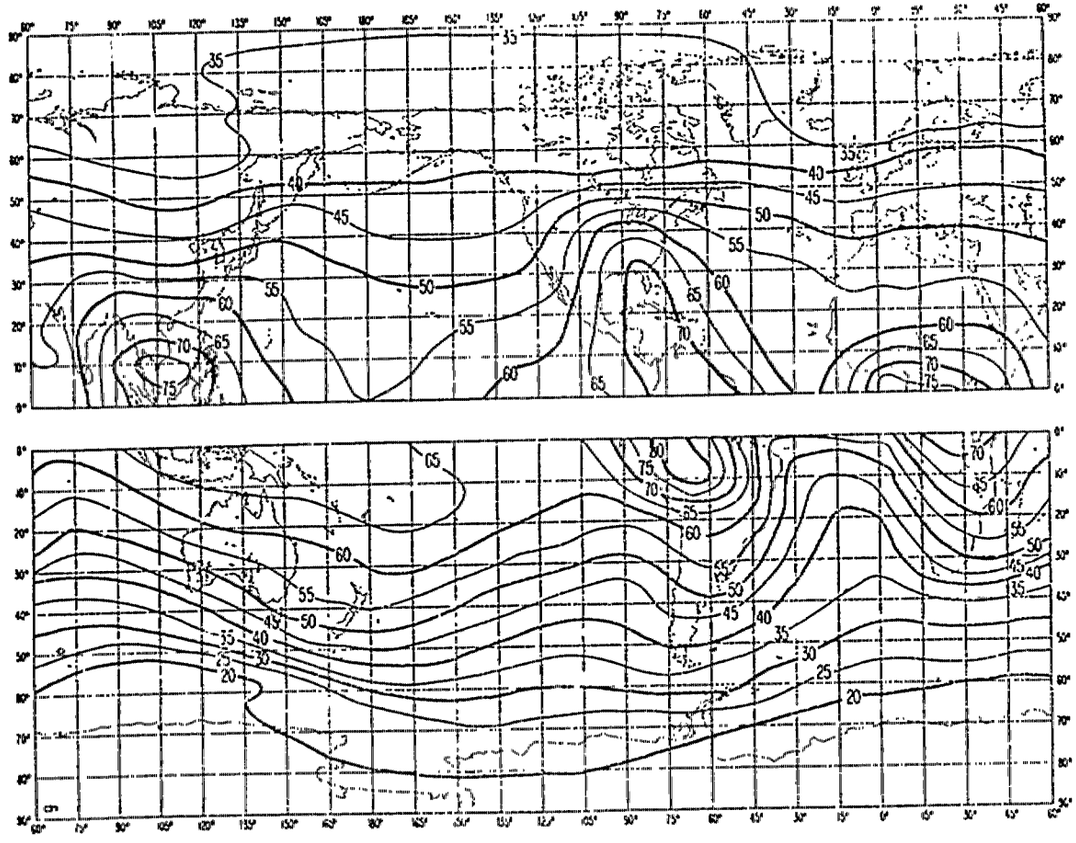

Expected values of atmospheric radio noise, F_{am}
(db above kT_0b at 1 Mc/s)
(Spring: 0400-0800 h.)

Figure 11(a)

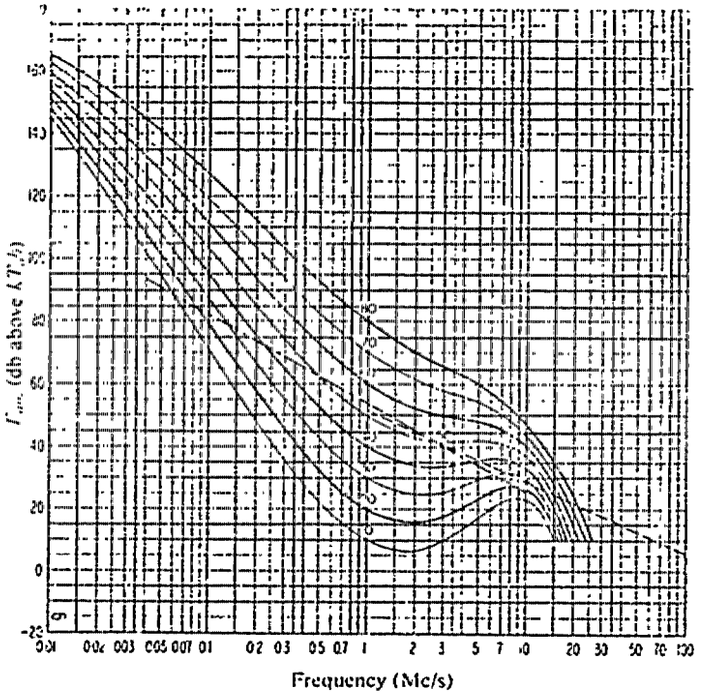

Variation of radio noise with frequency
(Spring; 0400-0800 h.)

——— Expected values of atmospheric noise
—·—·— Expected values of man-made noise at a quiet receiving location
– – – – Expected values of galactic noise

Figure 11(b)

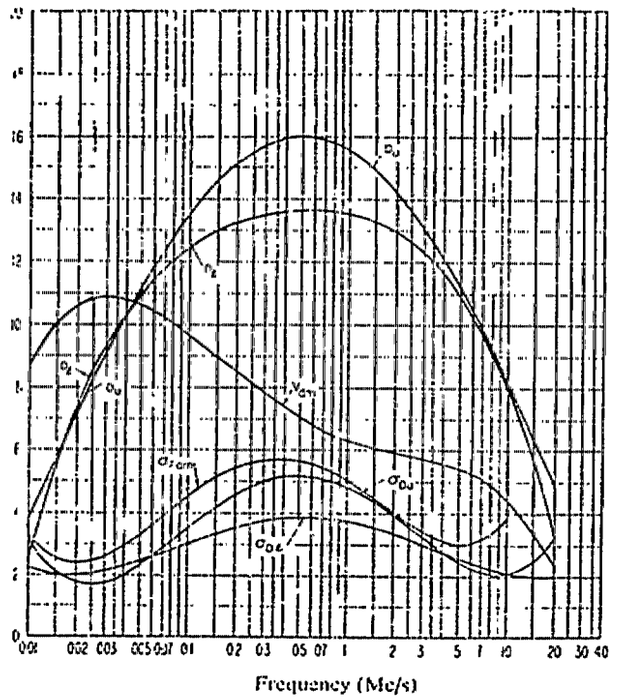

Data on noise variability and character
(Spring; 0400-0800 h)

σ_{Fam} = Standard deviation of values of F_{am}
D_u = Ratio of upper decile to median value, F_{am}
σ_{Du} = Standard deviation of values of D_u
D_l = Ratio of median value, F_{am}, to lover decile
σ_{Dl} = Stantard deviation of value of D_l
V_{am} = Expected value of median deviation of average voltage.. The values shown are for a bandwidth of 200 c/s.

Figure 11(c)

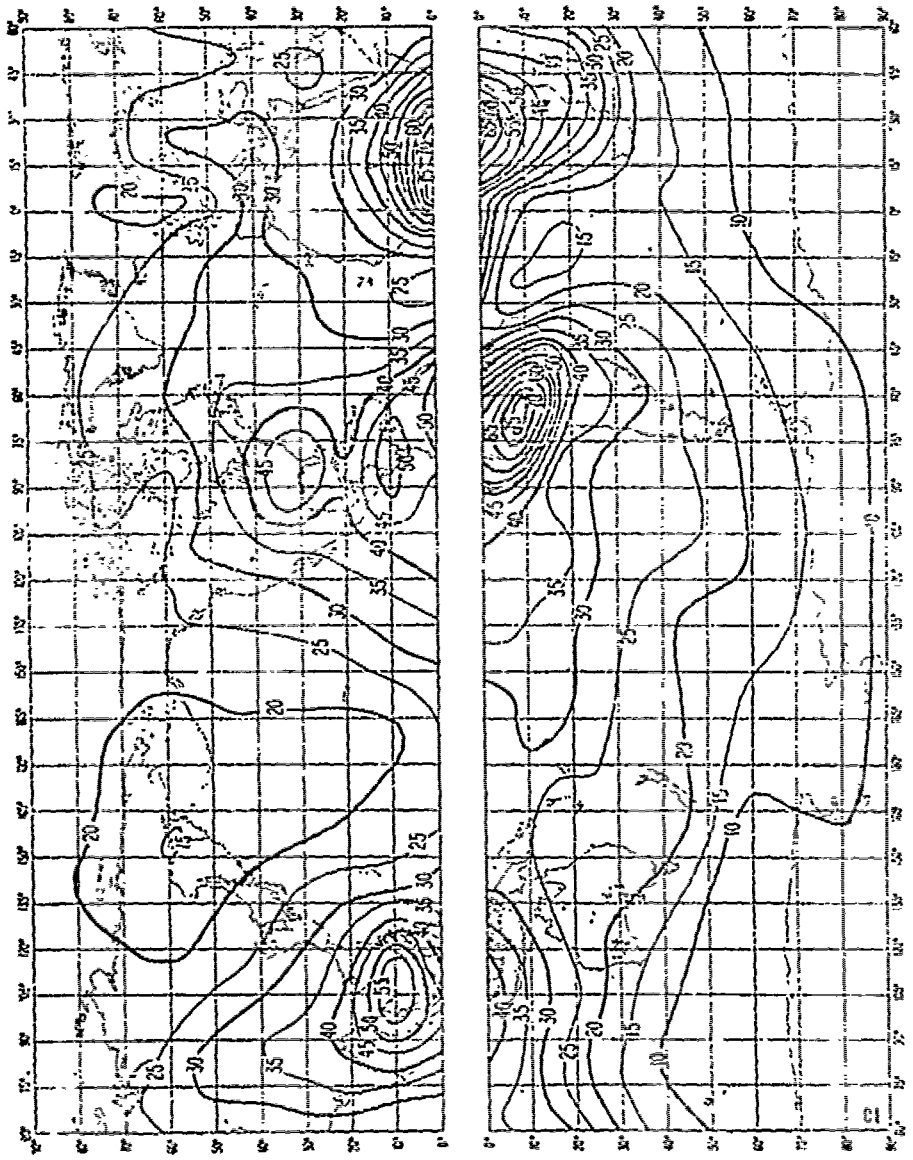

Expected values of atmospheric radio noise, F_{am},
(db above kT$_0$b at 1 Mc/s)
(Spring, 0400-1200 hr.)

Figure 12(a)

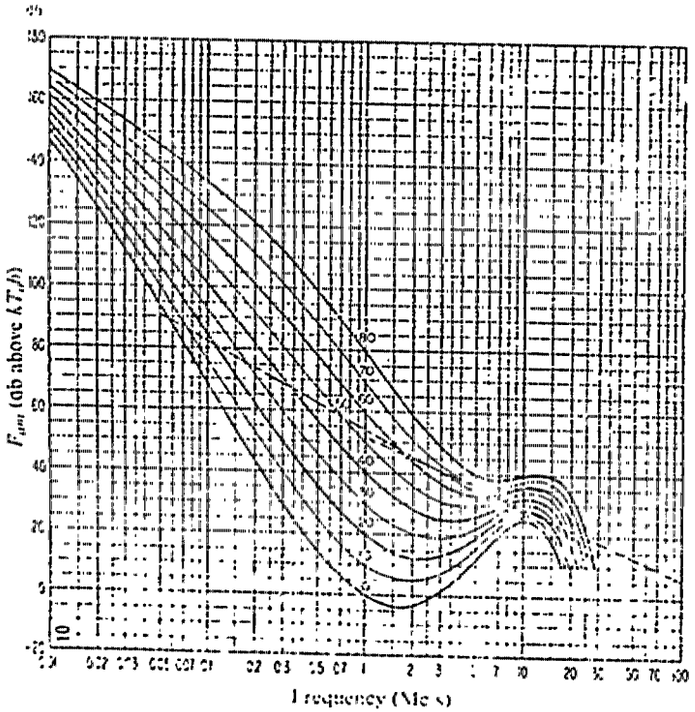

Variation of radio noise with frequency (Spring, 0800–1200 h.)

——— Expected values of atmospheric noise
— — — Expected values of man-made noise at a quiet receiver location
– – – – Expected values of galactic noise

Figure 12(b)

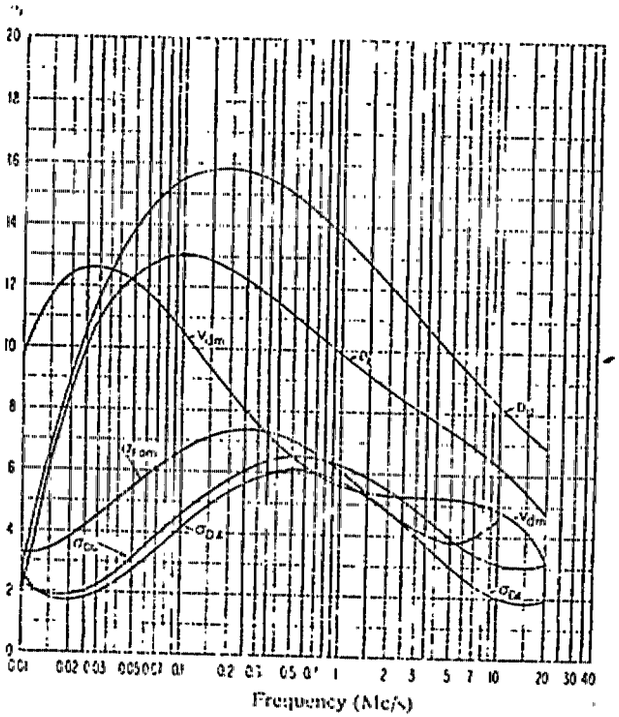

Data on noise variability and character (Spring; 0800–1200 h.)

σ_{Fam} = Standard deviation of values of F_{am}
D_u = Ratio of upper decile to median value, F_{am}
σ_{Du} = Standard deviation of values of D_u
D_l = Ratio of median value, F_{am} to lower decile
σ_{Dl} = Standard deviation of value of D_l
V_{dm} = Expected value of median deviation of average voltage. The values shown are for a bandwidth of 200 c/s.

Figure 12(c)

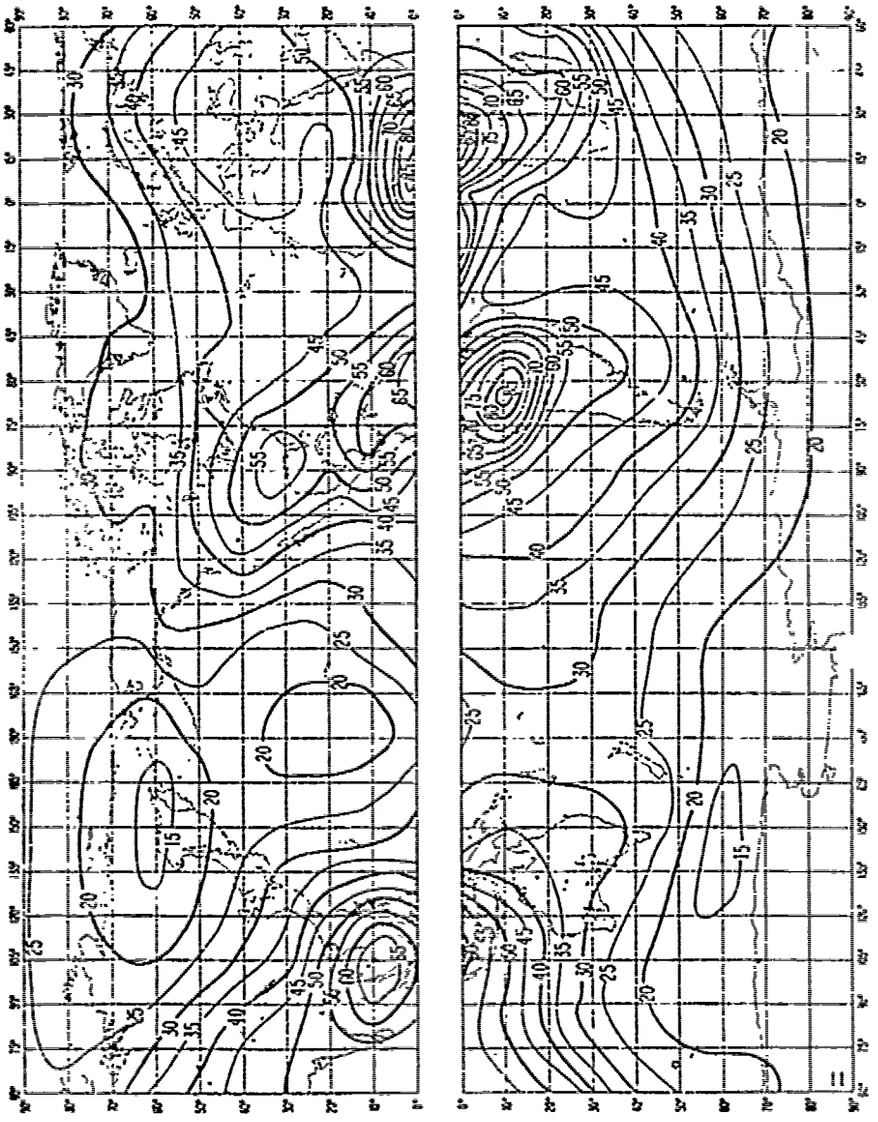

Expected values of atmospheric radio noise, F_{am}.
(db above kT₀b at 1 Mc/s)
(Spring: 1200-1600 h.)

Figure 13(a)

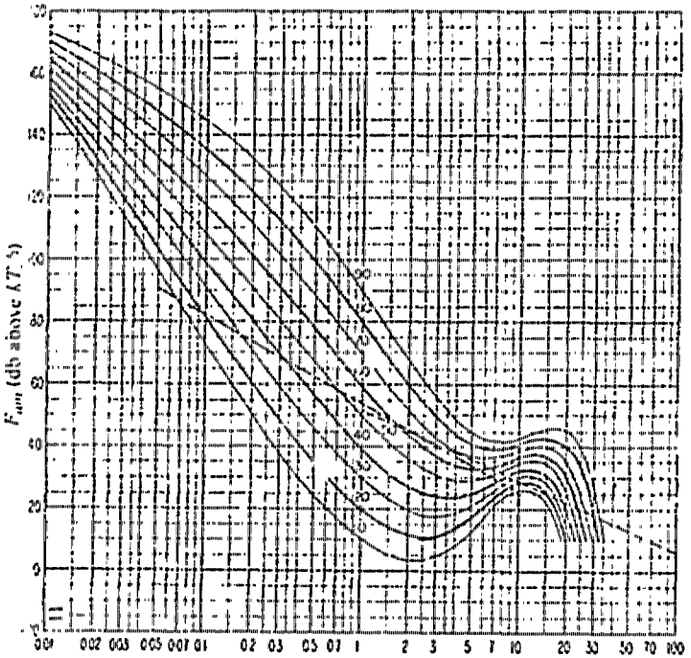

Variation of radio noise with frequency (Spring, 1200–1600 h.)

——— Expected values of atmospheric noise
—·—·— Expected values of man-made noise at a quiet receiving location
– – – – Expected values of galactic noise

Figure 13(b)

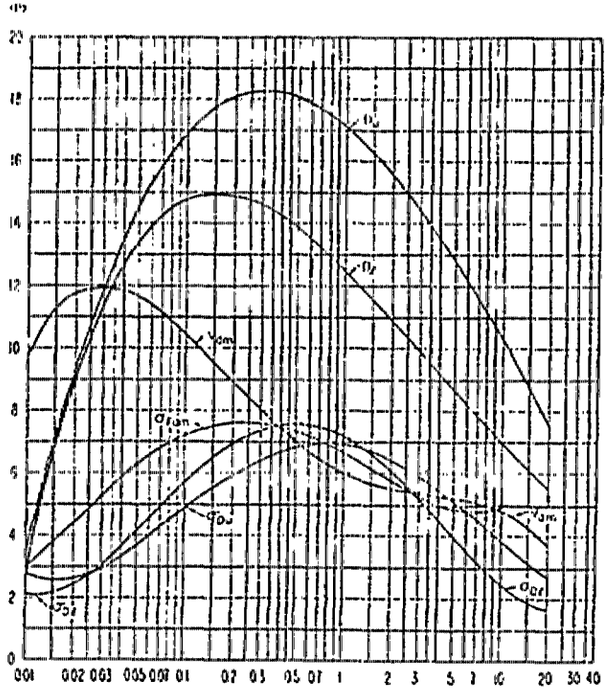

Data on noise variability and character (Spring: 1200–1600 h.)

σ_{Fam} = Standard deviation of values of F_{am}
D_u = Ratio of upper decile to median value, F_{am}
σ_{Du} = Standard deviation of values of D_u
D_l = Ratio of median value, F_{am} to lover decile
σ_{Dl} = Stantard deviation of value of D_l
V_{dm} = Expected value of median deviation of average voltage. The values shown are for a bandwidth of 200 c/s.

Figure 13(c)

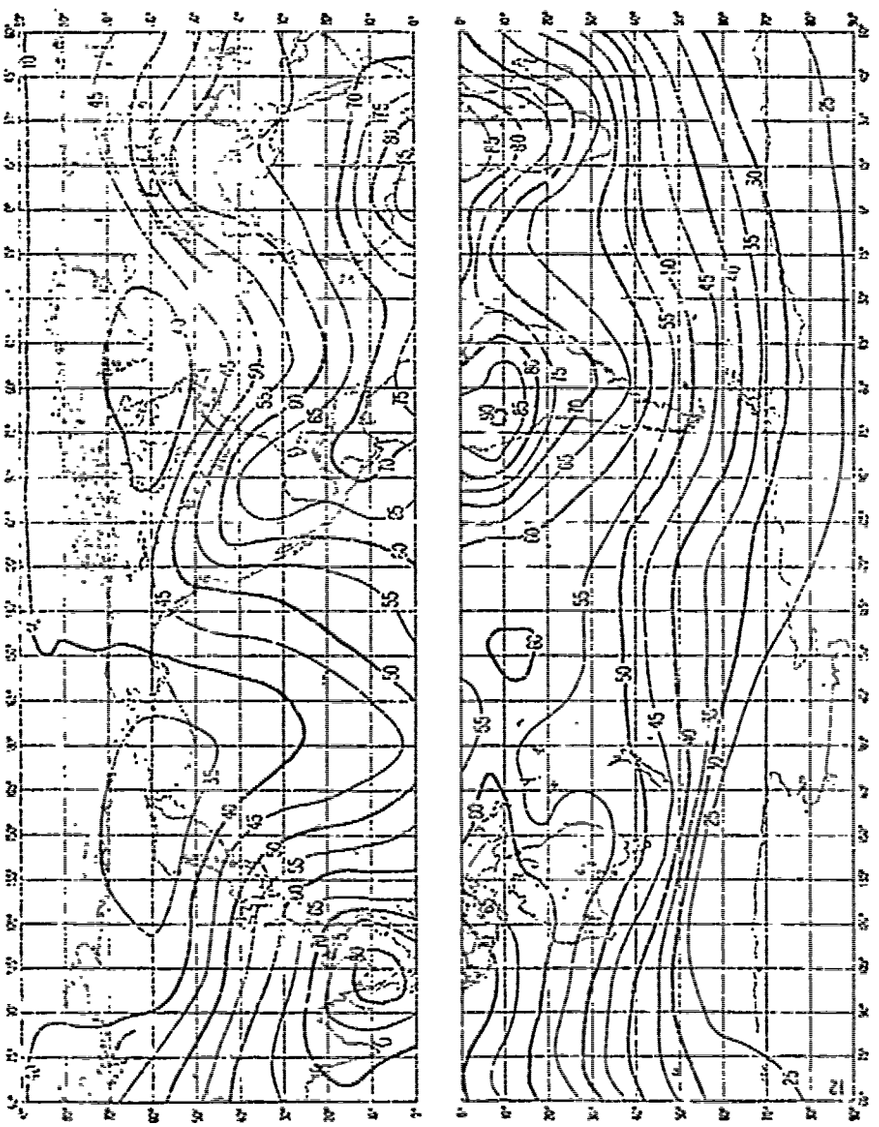

Expected values of atmospheric radio noise, F_{am}.
(db above kT_0b at 1 Mc/s)
(Spring, 1400–2000 h.)

Figure 14(a)

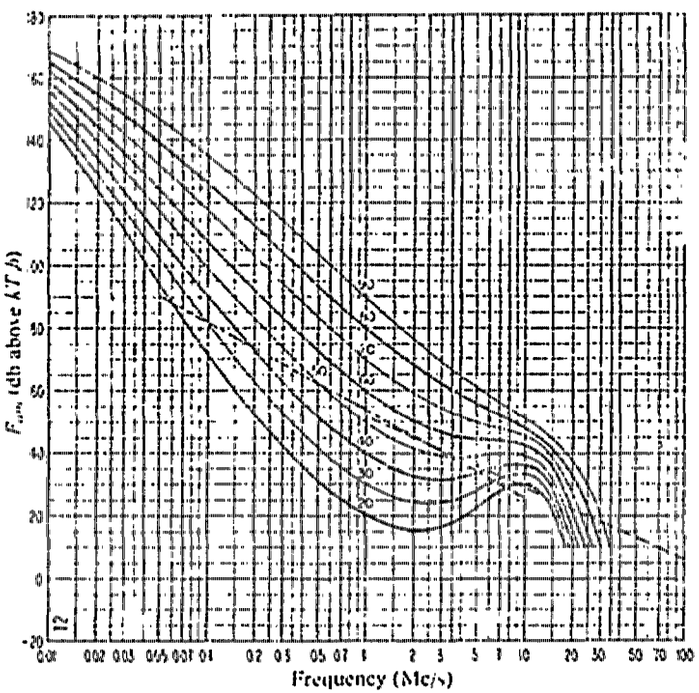

Variation of radio noise with frequency
(Spring: 1600–2000 h.)

——— Expected values of atmospheric noise
—·—·— Expected values of man-made noise at a quiet receiving location
– – – – Expected values of galactic noise

Figure 14(b)

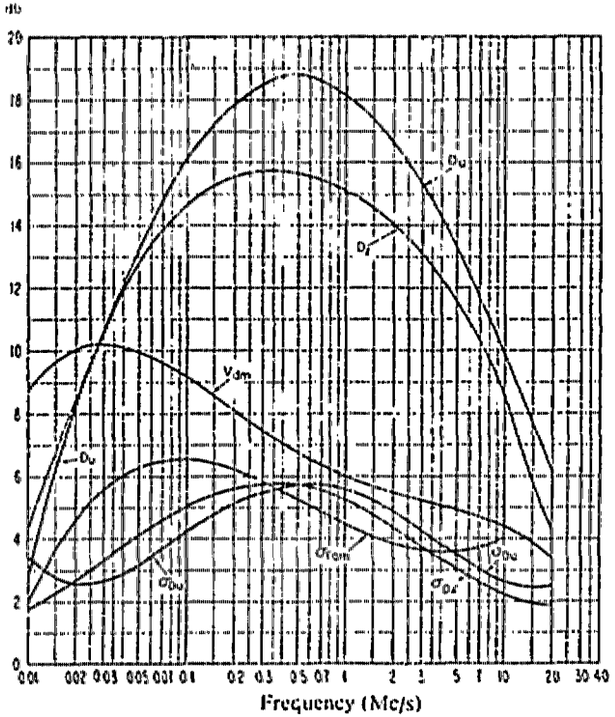

Data on noise variability and character
(Spring: 1600–2000 h.)

σ_{Fam} = Standard deviation of values of F_{am}
D_u = Ratio of upper decile to median value, F_{am}
σ_{Du} = Standard deviation of values of D_u
D_l = Ratio of median value, F_{am}, to lower decile
σ_{Dl} = Standard deviation of value of D_l
V_{dm} = Expected value of median deviation of average voltage. The values shown are for a bandwidth of 200 c/s.

Figure 14(c)

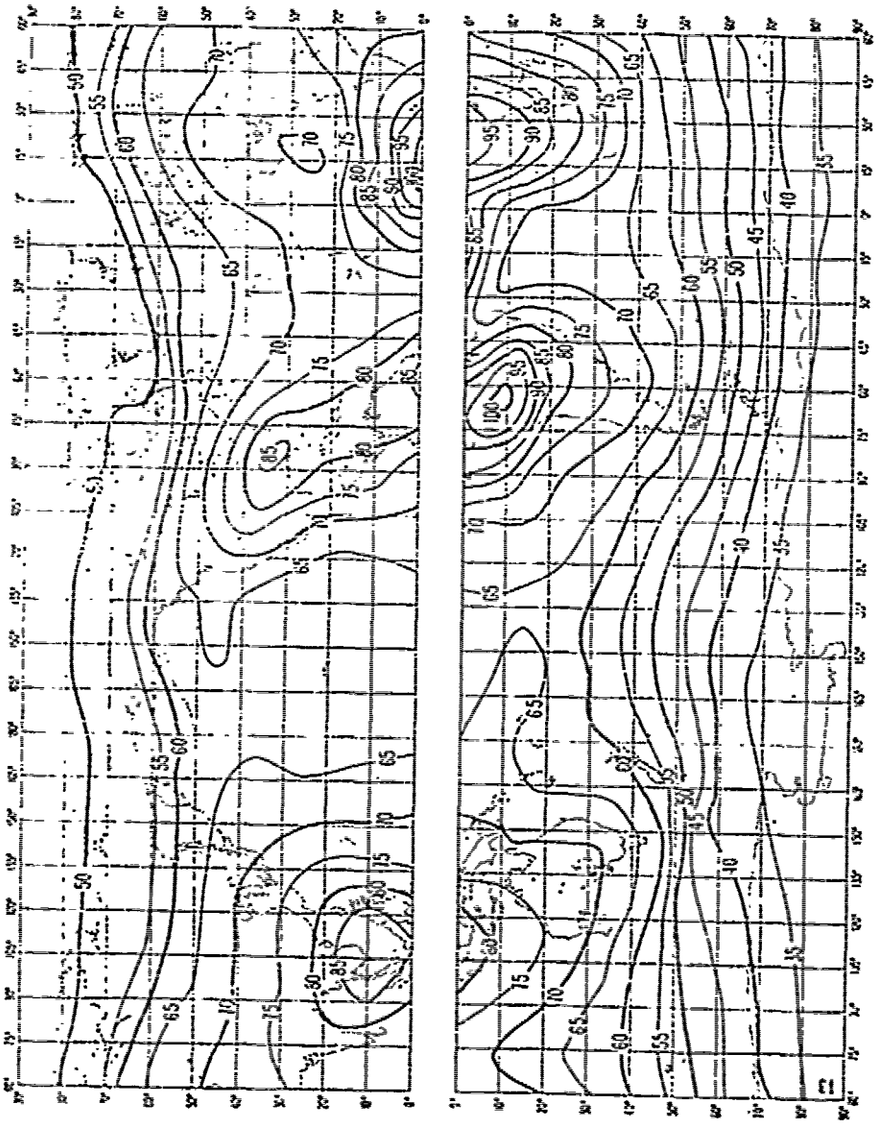

Expected values of atmospheric radio noise, F_{am},
(db above kT_0b at 1 Mc/s)
(Spring: 2000–2400 h)

Figure 15(a)

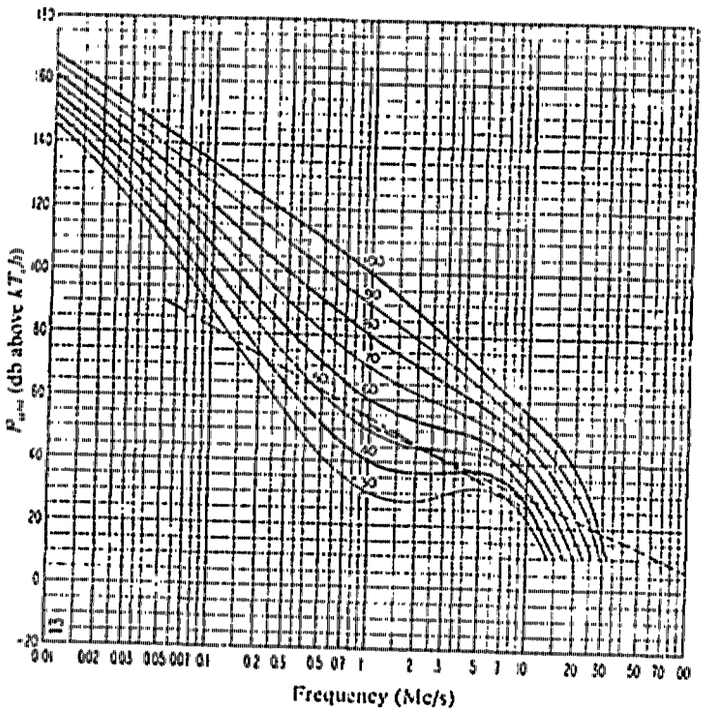

Variation of radio noise with frequency
(Spring: 2000-2400 h.)

——— Expected values of atmospheric noise
——.——.—— Expected values of man-made noise at a quiet receiving location
– – – – Expected values of galactic noise

Figure 15(b)

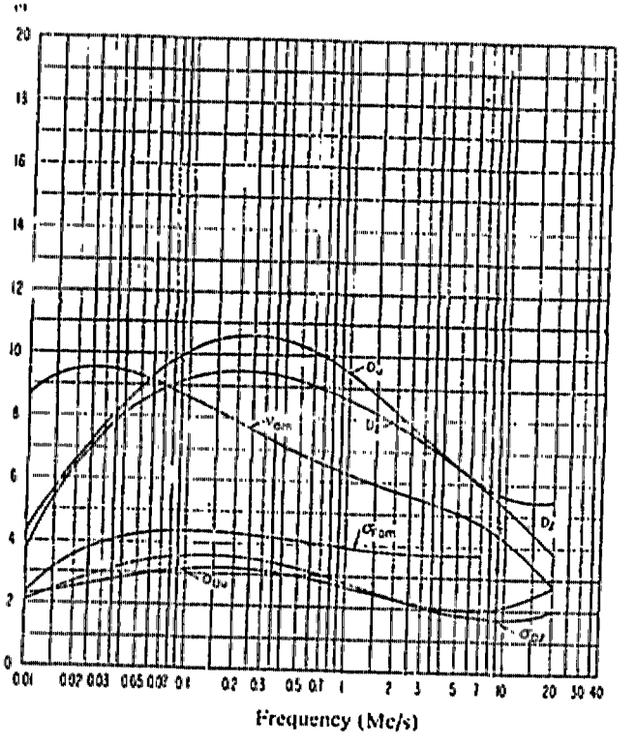

Data on noise variability and character
(Spring: 2000-2400 h.)

σ_{Fam} = Standard deviation of values of F_{am}
D_u = Ratio of upper decile to median value, F_{am}
σ_{Du} = Standard deviation of values of D_u
D_l = Ratio of median value, F_{am} to lover decile
σ_{Dl} = Stantard deviation of value of D_l
V_{dm} = Expected value of median deviation of average voltage. The values shown are for a bandwidth of 200 c/s.

Figure 15(c)

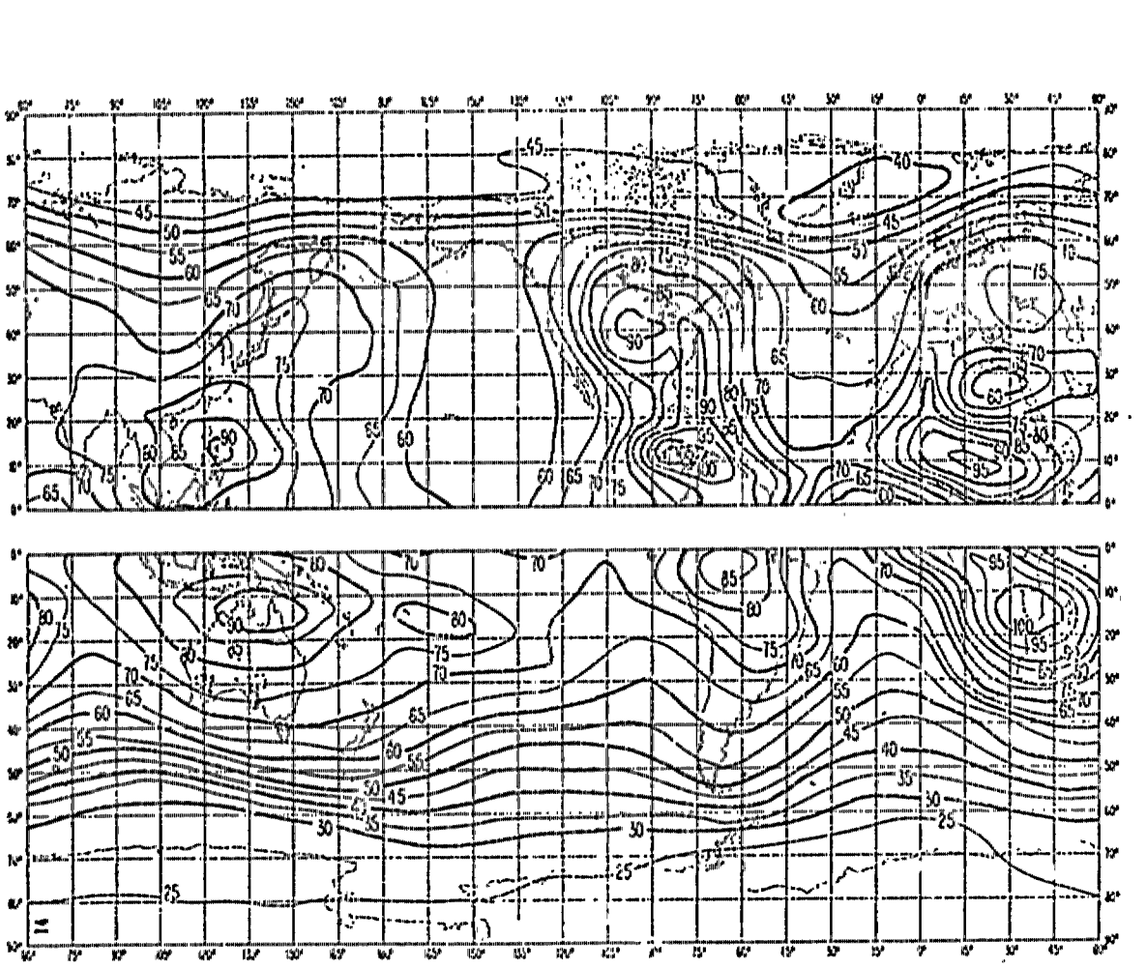

Expected values of atmospheric radio noise, F_{am}.
(db above kT_0b at 1 Mc/s)
(January; 0000–0400 h.)

Figure 16(a)

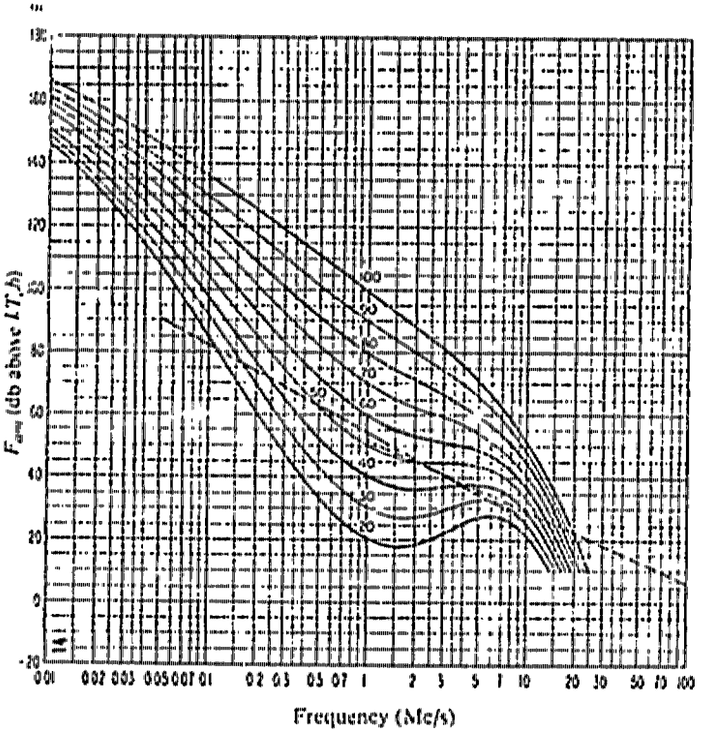

Variation of radio noise with frequency
(Summer; 0000-0400 h.)

——— Expected values of atmospheric noise
—·—·— Expected values of man-made noise at a quiet receiving location
– – – – Expected values of galactic noise

Figure 16(b)

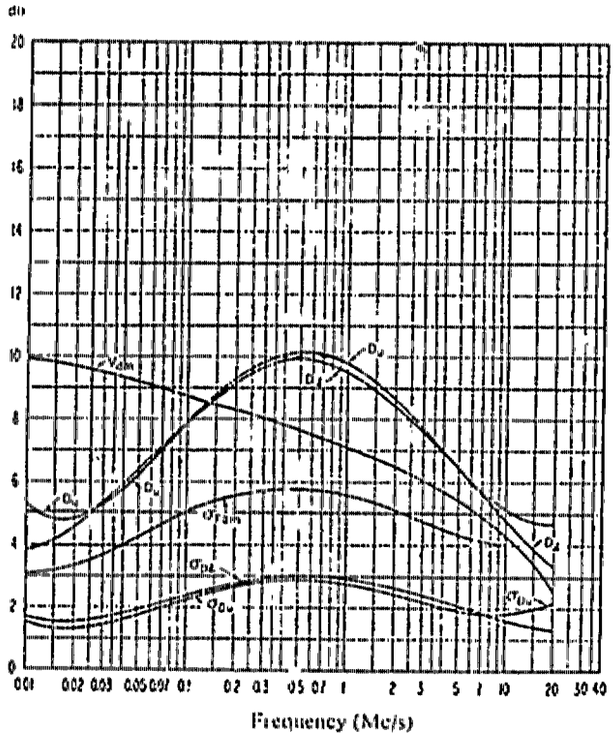

Data on noise variability and character
(Summer; 0000-0400 h.)

σ_{Fam} = Standard deviation of values of F_{am}
D_u = Ratio of upper decile to median value, F_{am}
σ_{Du} = Standard deviation of values of D_u
D_l = Ratio of median value, F_{am}, to lover decile
σ_{Dl} = Standard deviation of value of D_l
V_{dm} = Expected value of median deviation of average voltage. The values shown are for a bandwidth of 200 c/s.

Figure 16(c)

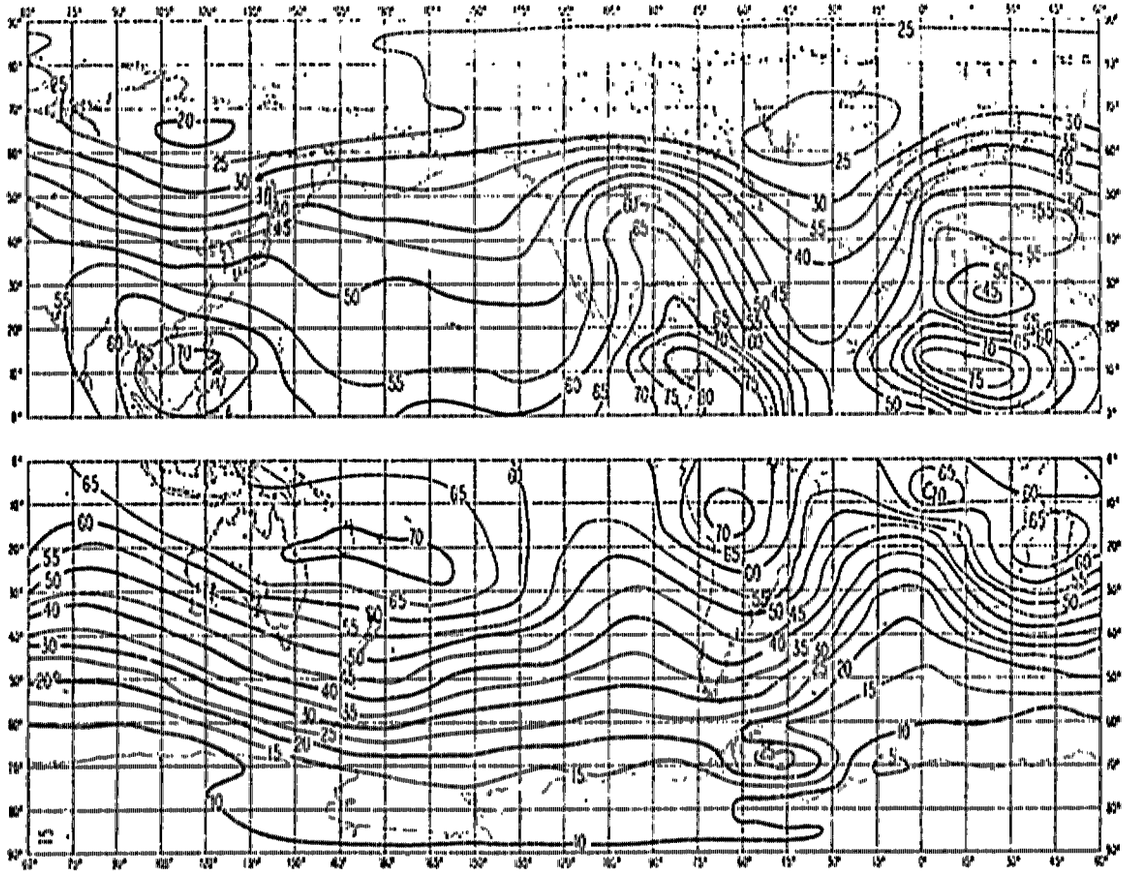

Expected values of atmospheric radio noise, F_{am}
(db above kT_0b at 1 Mc/s)
(Summer, 0400–0800 h.)

Figure 17(a)

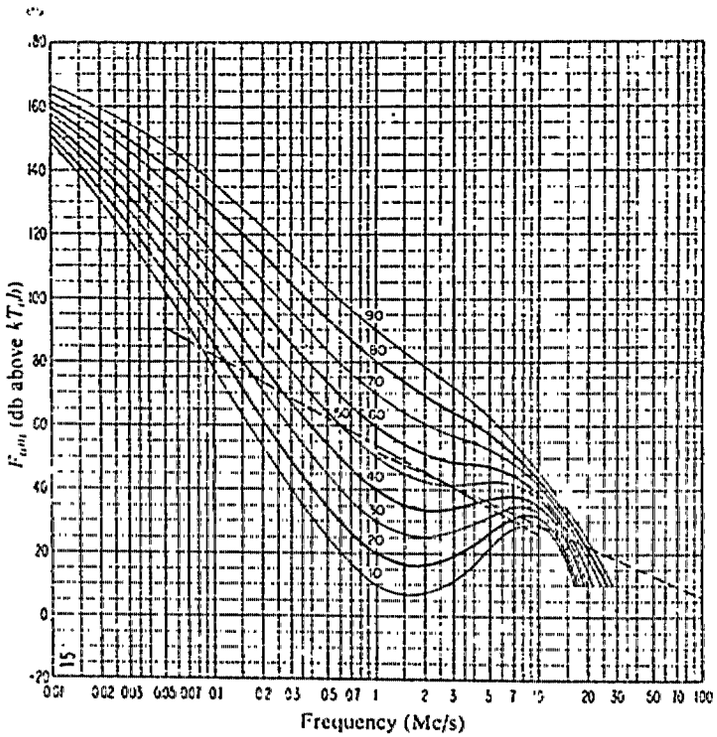

Variation of radio noise with frequency
(Summer; 0400-0800 h.)

——— Expected values of atmospheric noise
—·—·— Expected values of man-made noise at a quiet receiving location
– – – – Expected values of galactic noise

Figure 17(b)

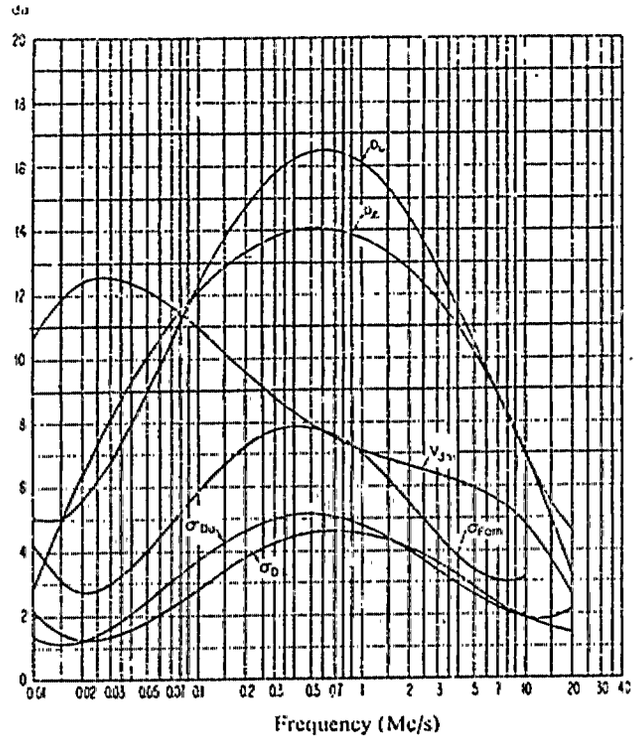

Data on noise variability and character
(Summer; 0400-0800 h.)

σ_{Fam} = Standard deviation of values of F_{am}
D_u = Ratio of upper decile to median value, F_{am}
σ_{Du} = Standard deviation of values of D_u
D_l = Ratio of median value, F_{am}, to lover decile
σ_{Dl} = Stantard deviation of value of D_l
V_{dm} = Expected value of median deviation of average voltage. The values shown are for a bandwidth of 200 c/s.

Figure 17(c)

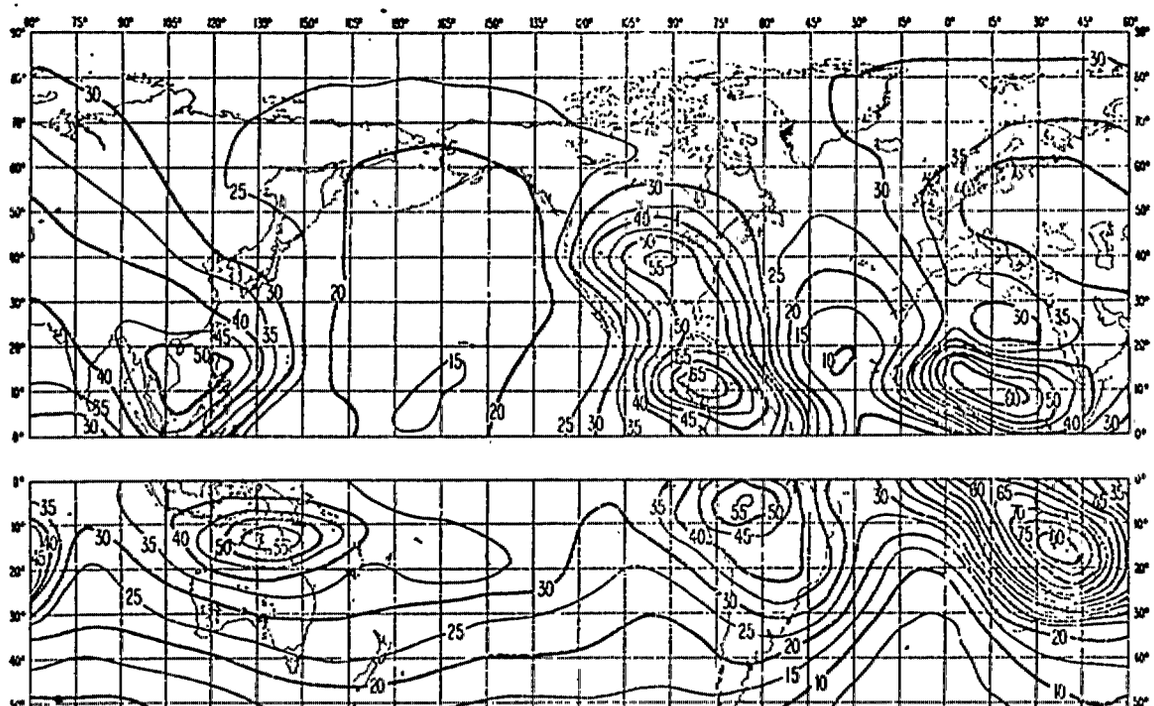

Expected values of atmospheric radio noise, F_{am}.
(db above kT_0b at 1 Mc/s)
(Summer; 0800–1200 h.)

Figure 18(a)

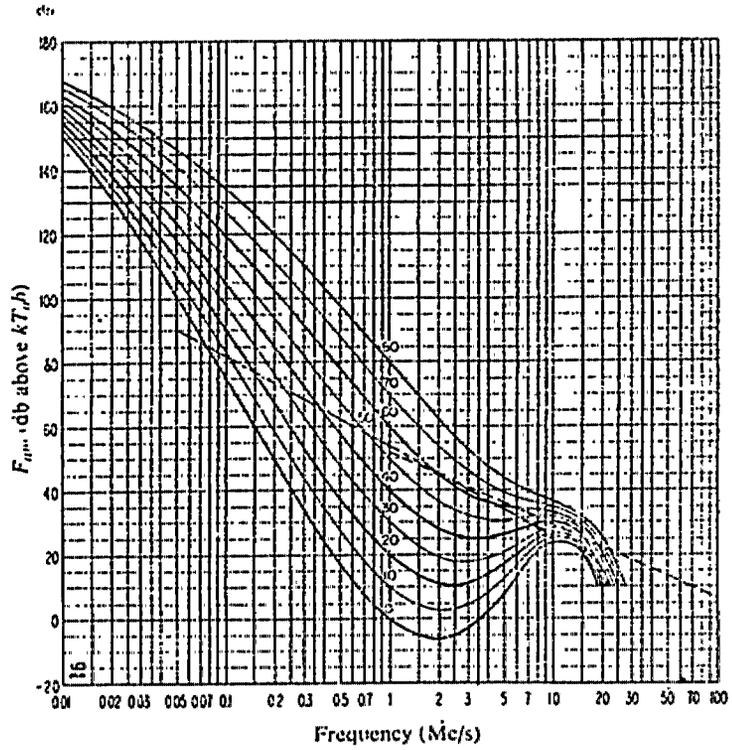

Variation of radio noise with frequency
(Summer; 0800–1200 h.)

——— Expected values of atmospheric noise
—·—·— Expected values of man-made noise at a quiet receiving location
– – – – Expected values of galactic noise

Figure 18(b)

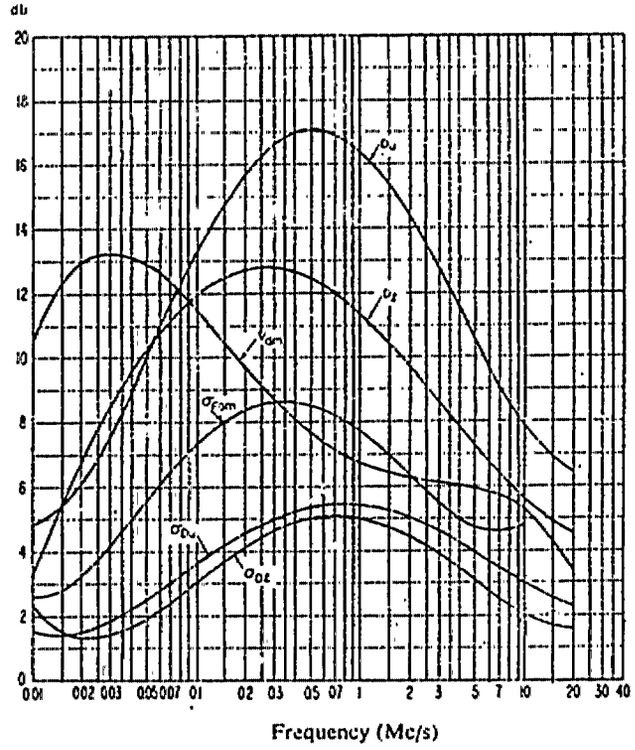

Data on noise variability and character
(Summer; 0800–1200 h.)

σ_{Fam} = Standard deviation of values of F_{am}
D_u = Ratio of upper decile to median value, F_{am}
σ_{Du} = Standard deviation of values of D_u
D_l = Ratio of median value, F_{am}, to lower decile
σ_{Dl} = Stantard deviation of value of D_l
V_{dm} = Expected value of median deviation of average voltage. The values shown are for a bandwidth of 200 c/s.

Figure 18(c)

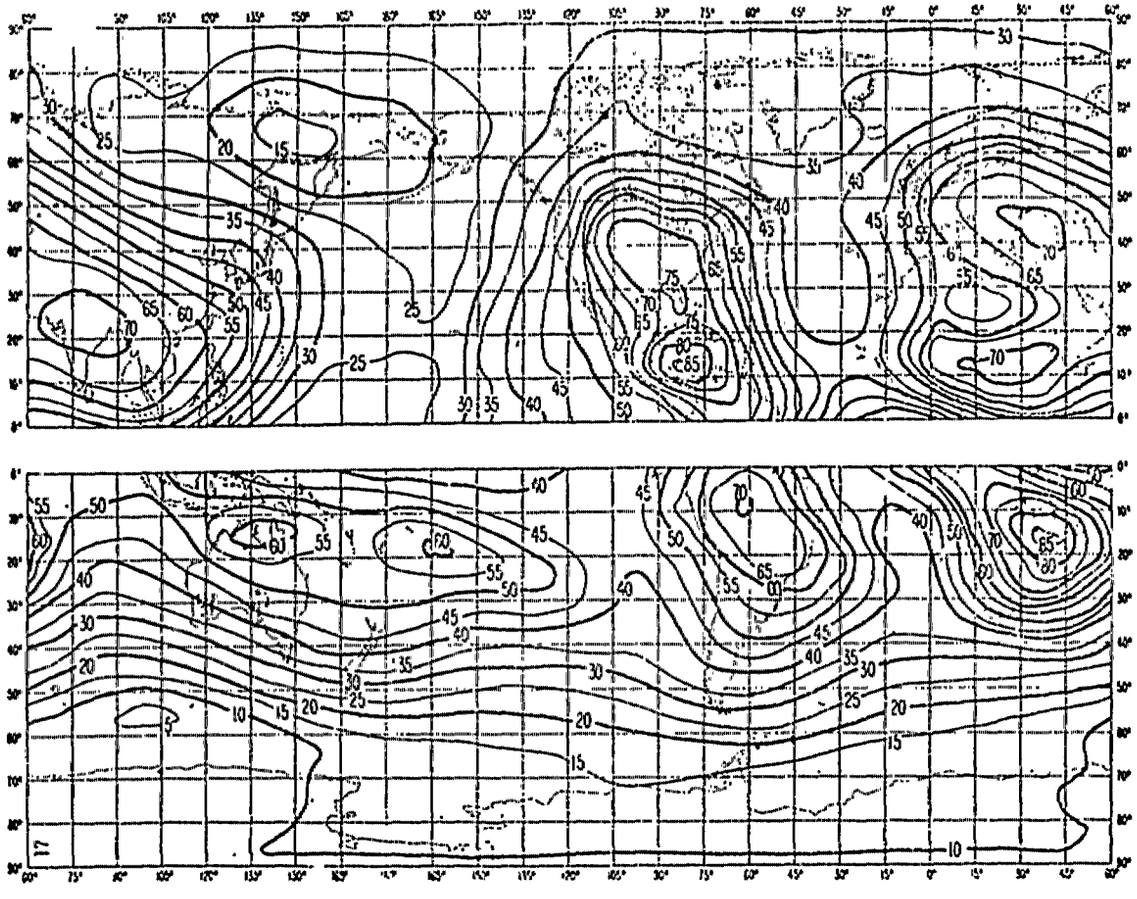

Expected values of atmospheric radio noise, F_{am},
(db above kT_0b at 1 Mc/s)
(Summer; 1200-1600 h.)

Figure 19(a)

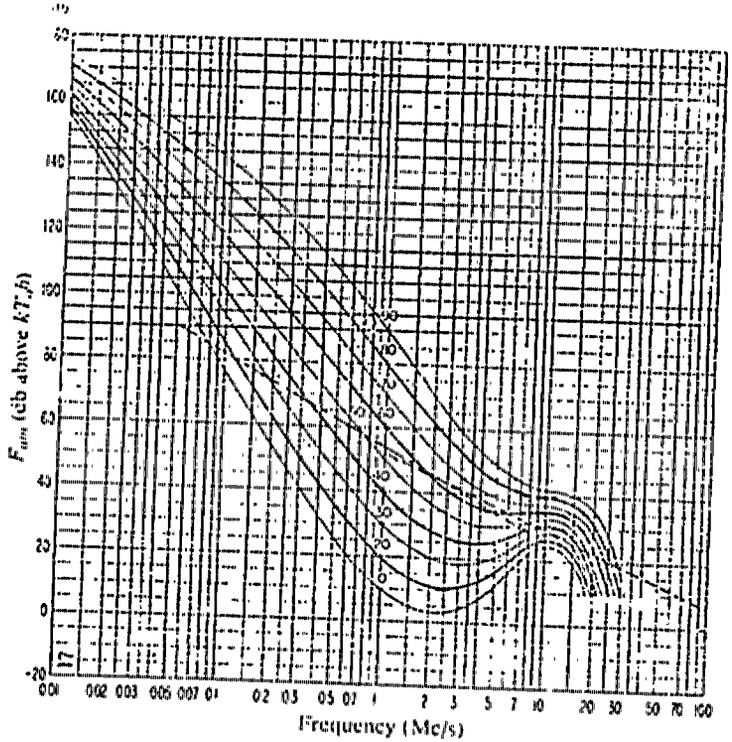

Variation of radio noise with frequency
(Summer; 1200-1600 h.)

——— Expected values of atmospheric noise
—·—·— Expected values of man-made noise at a quiet receiving location
– – – – Expected values of galactic noise

Figure 19(b)

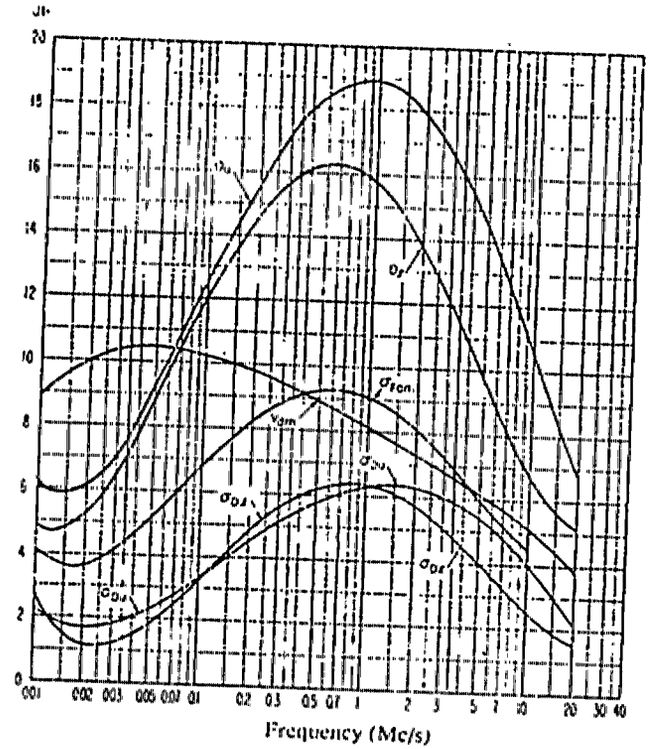

Data on noise variability and character
(Summer, 1200 1600 h.)

σ_{Fam} = Standard deviation of values of F_{am}
D_u = Ratio of upper decile to median value, F_{am}
σ_{Du} = Standard deviation of values of D_u
D_l = Ratio of median value, F_{am}, to lower decile
σ_{Dl} = Standard deviation of value of D_l
V_{dm} = Expected value of median deviation of average voltage. The values shown are for a bandwidth of 200 c/s.

Figure 19(c)

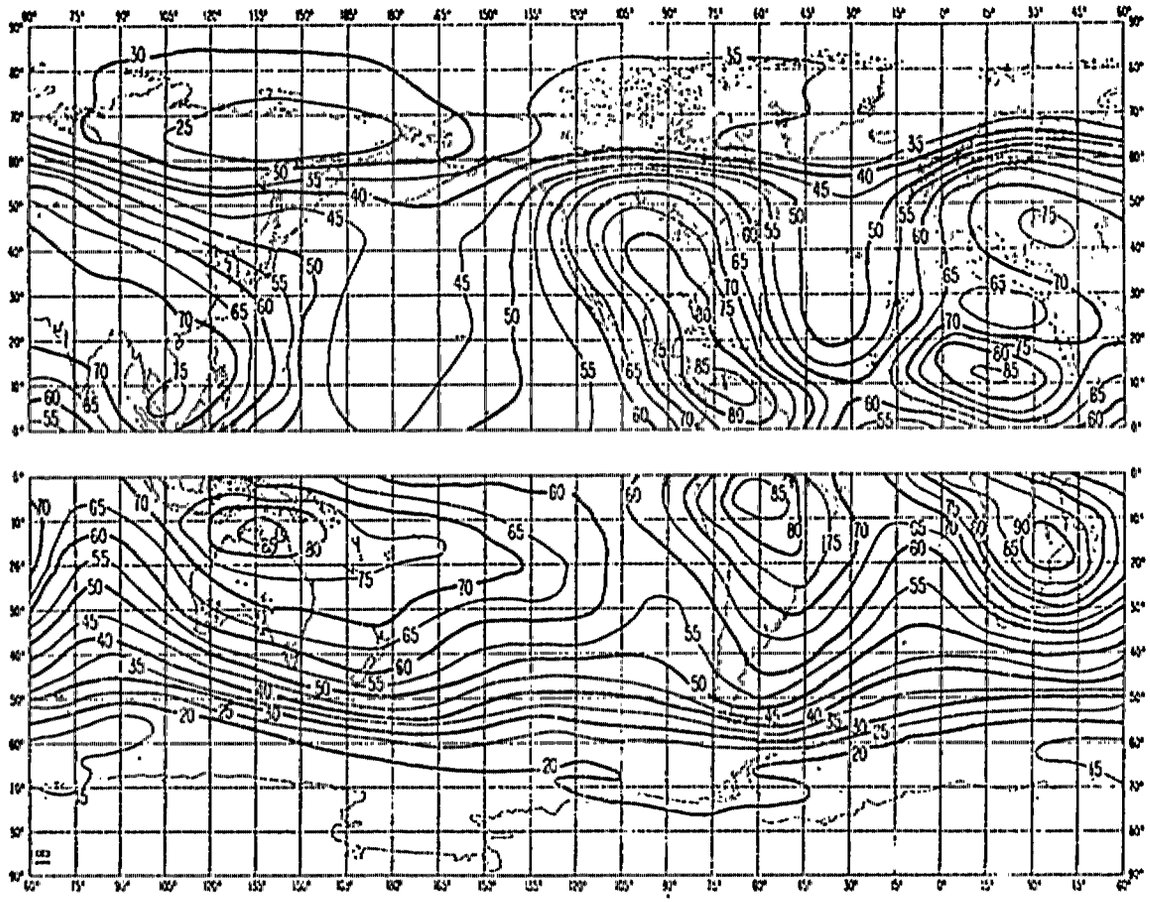

Expected values of atmospheric radio noise, F_{am},
(db above kT_0b at 1 Mc/s)
(Summer; 1600–2000 h)

Figure 20(a)

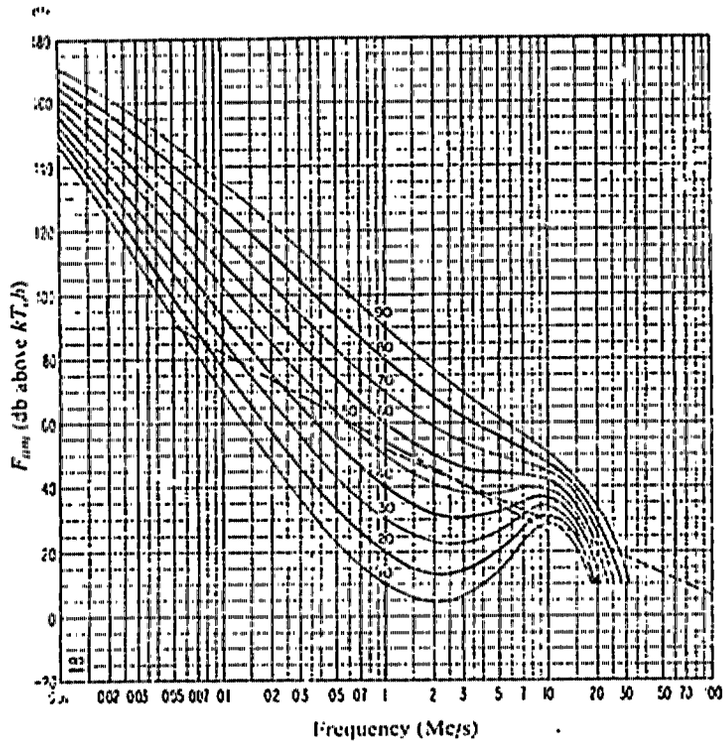

Variation of radio noise with frequency (Summer; 1600–2000 h.)

——— Expected values of atmospheric noise
—·—·— Expected values of man-made noise at a quiet receiving location
– – – – Expected values of galactic noise

Figure 20(b)

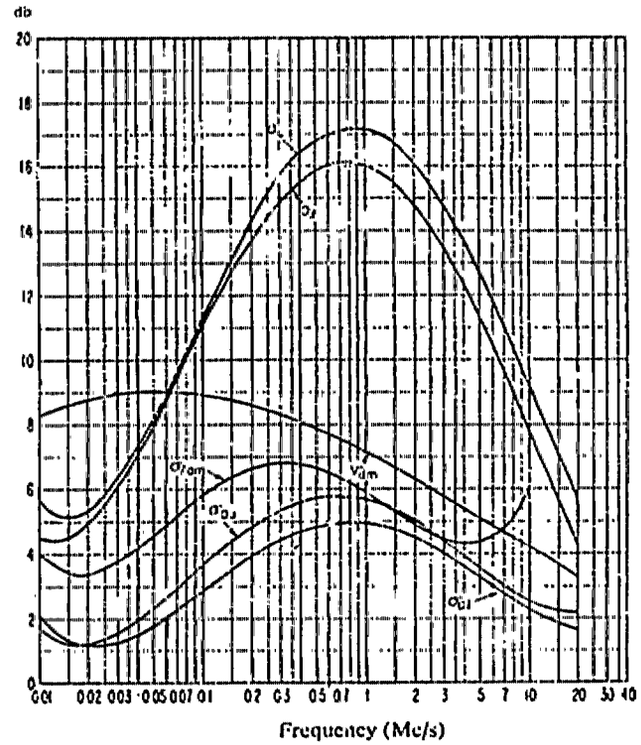

Data on noise variability and character (Summer; 1600–2000 h.)

σ_{Fam} = Standard deviation of values of F_{am}
D_u = Ratio of upper decile to median value, F_{am}
σ_{Du} = Standard deviation of values of D_u
D_l = Ratio of median value, F_{am}, to lower decile
σ_{Dl} = Standard deviation of value of D_l
V_{dm} = Expected value of median deviation of average voltage. The values shown are for a bandwidth of 200 c/s.

Figure 20(c)

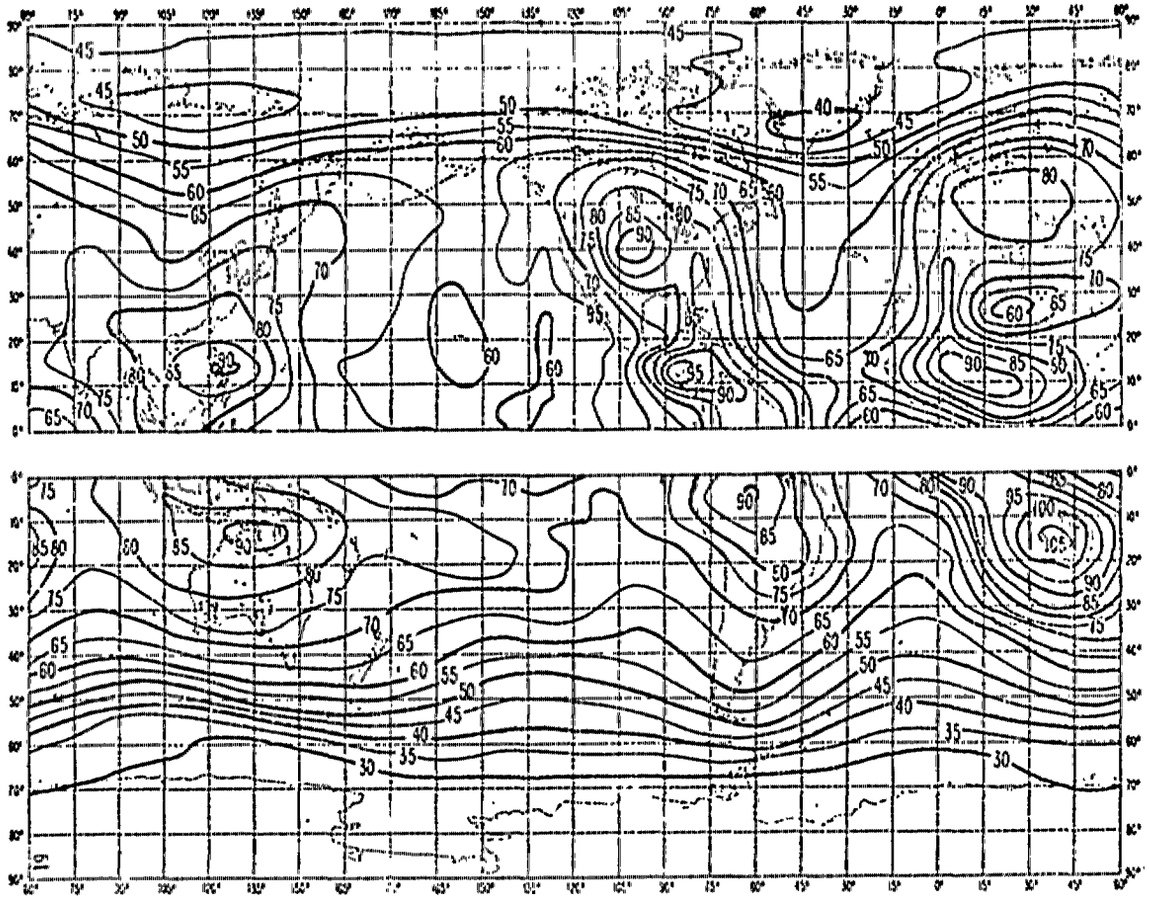

Expected values of atmospheric radio noise, F_{am},
(db above kT_0b at 1 Mc/s)
(Summer; 2000–2400 h.)

Figure 21(a)

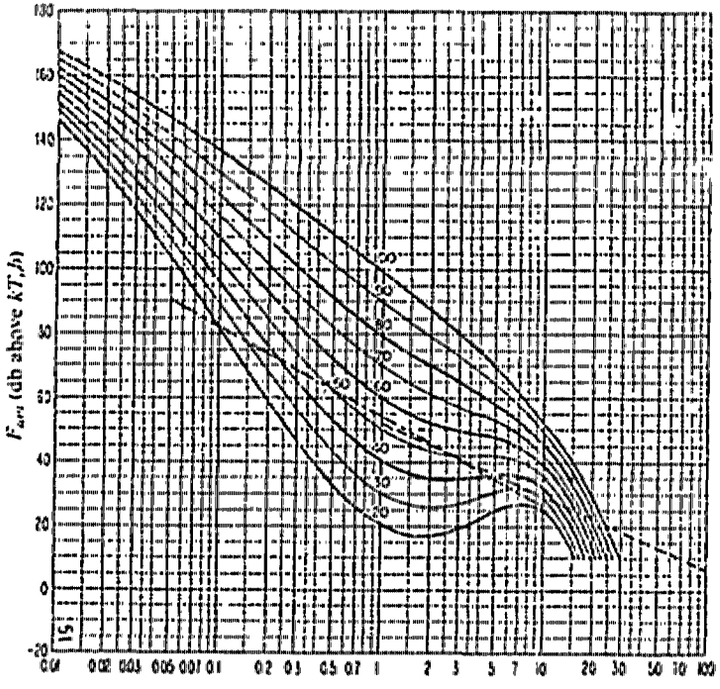

Variation of radio noise with frequency
(Summer; 2000-2400 h.)

——— Expected values of atmospheric noise
—·—·— Expected values of man-made noise at a quiet receiving location
– – – – Expected values of galactic noise

Figure 21(b)

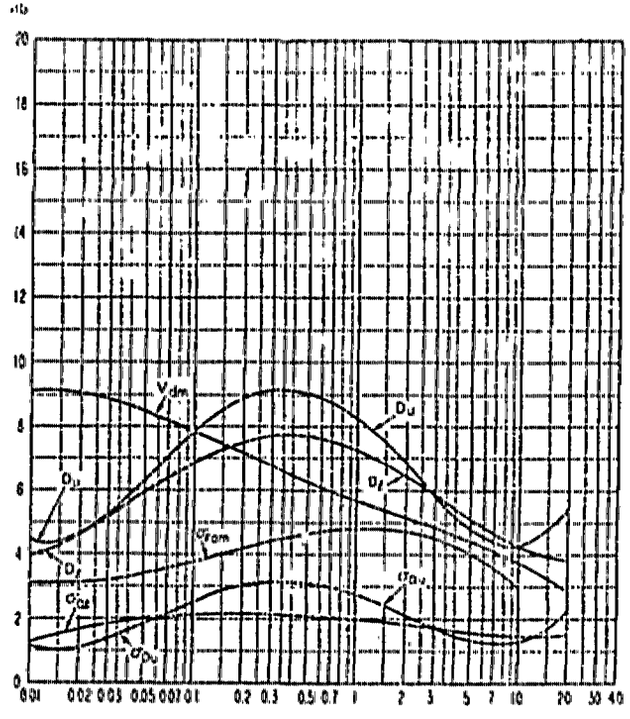

Data on noise variability and character
(Summer; 2000-2400 h.)

σ_{Fam} = Standard deviation of values of F_{am}
D_u = Ratio of upper decile to median value, F_{am}
σ_{Du} = Standard deviation of values of D_u
D_l = Ratio of median value, F_{am}, to lower decile
σ_{Dl} = Standard deviation of value of D_l
V_{dm} = Expected value of median deviation of average voltage.
The values shown are for a bandwidth of 200 c/s.

Figure 21(c)

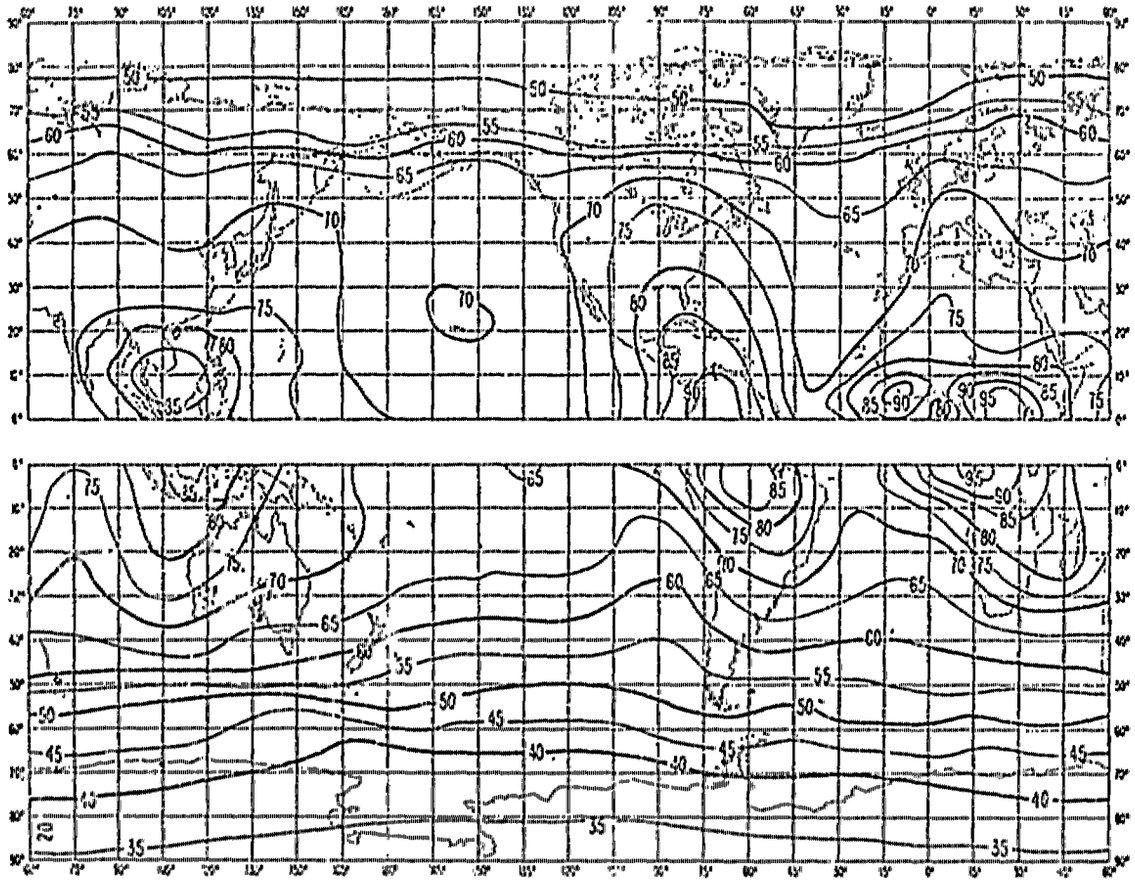

Expected values of atmospheric radio noise, F_{am},
(db above kT_0b at 1 Mc/s)
(Autumn; 0000-0400 h.)

Figure 22(a)

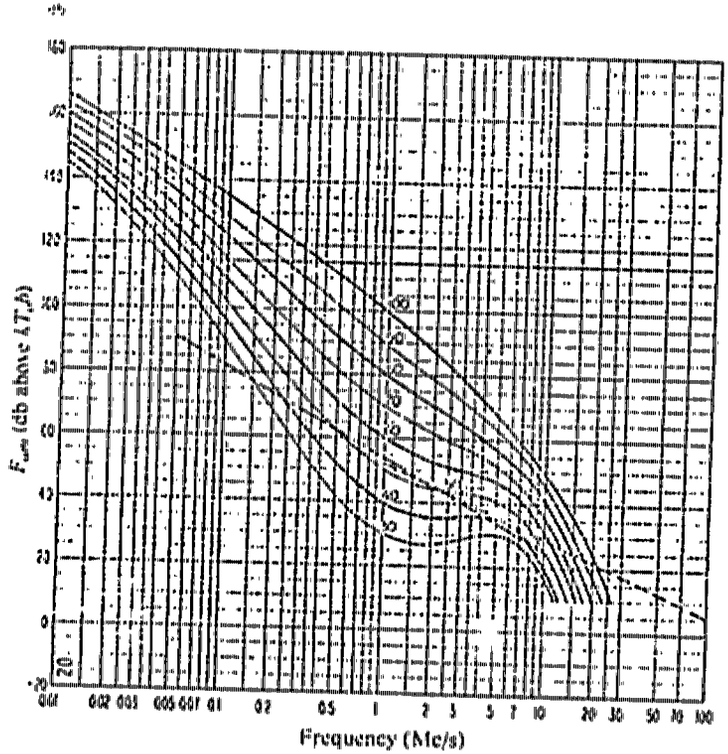

Variation of radio noise with frequency
(Autumn; 0000–0400 h.)

——— Expected values of atmospheric noise
—·—·— Expected values of man-made noise at a quiet receiving location
– – – – Expected values of galactic noise

Figure 22(b)

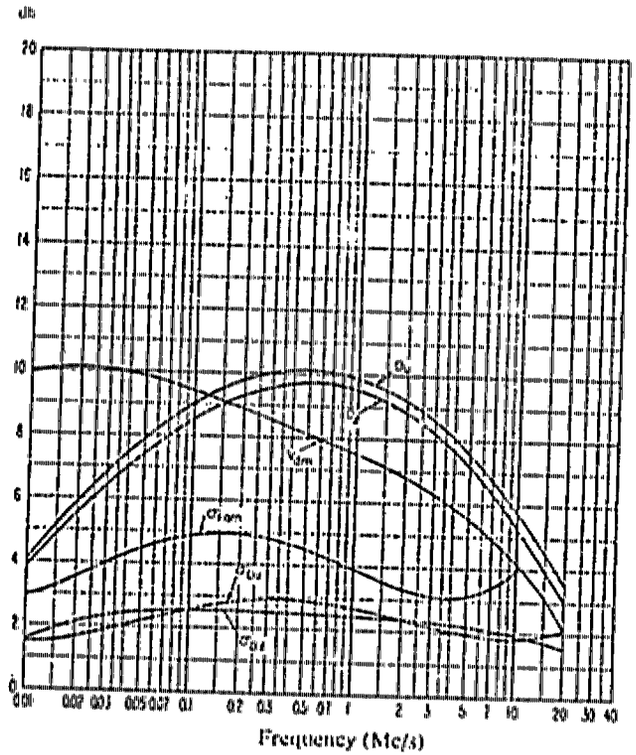

Data on noise variability and character
(Autumn · 0000–0400 h.)

σ_{Fam} = Standard deviation of values of F_{am}
D_u = Ratio of upper decile to median value, F_{am}
σ_{Du} = Standard deviation of values of D_u
D_l = Ratio of median value, F_{am}, to lower decile
σ_{Dl} = Standard deviation of value of D_l
V_{dm} = Expected value of median deviation of average voltage. The values shown are for a bandwidth of 200 c/s.

Figure 22(c)

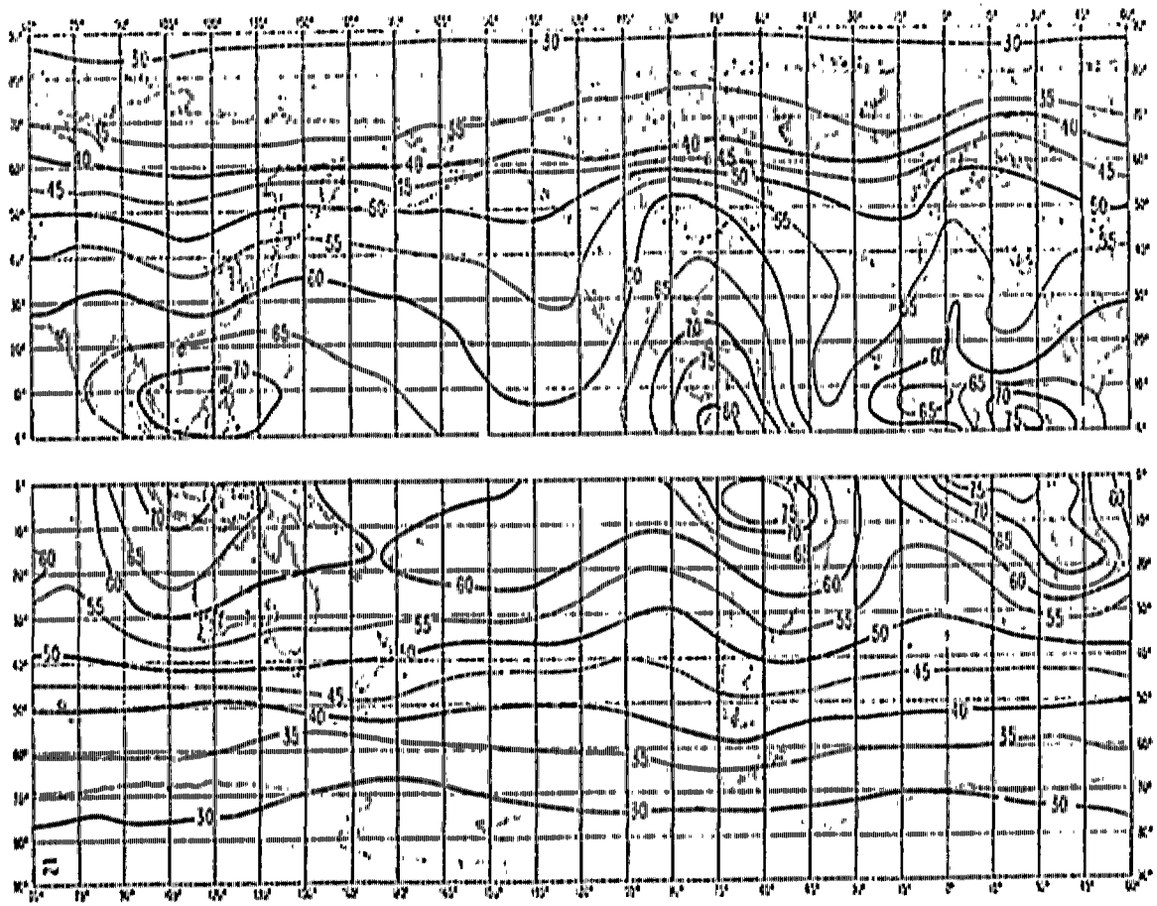

Expected values of atmospheric radio noise, P_{am},
(db above kT_0b at 1 Mc/s)
(Autumn: 0400–0800 h.)

Figure 23(a)

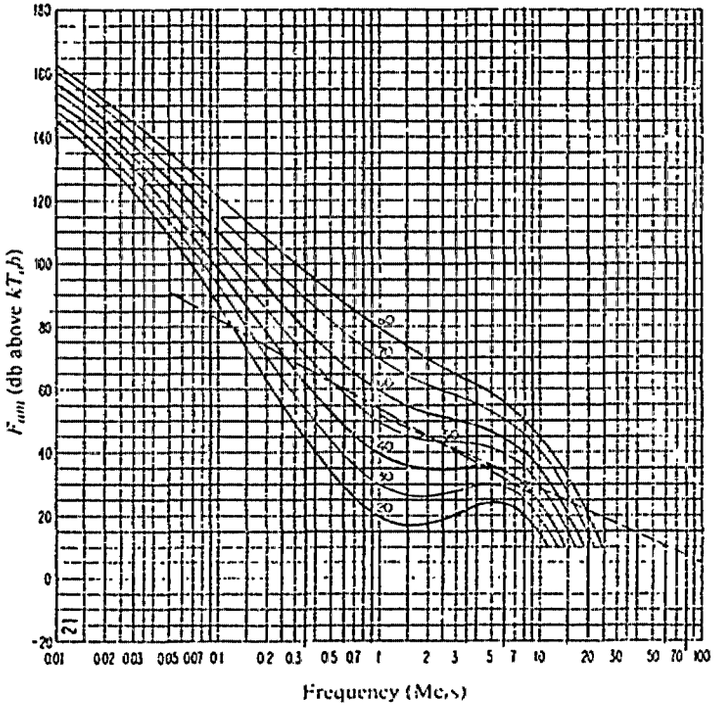

Variation of radio noise with frequency
(Autumn; 0400–0800 h.)

——— Expected values of atmospheric noise
—·—·— Expected values of man-made noise at a quiet receiving location
– – – – Expected values of galactic noise

Figure 23(b)

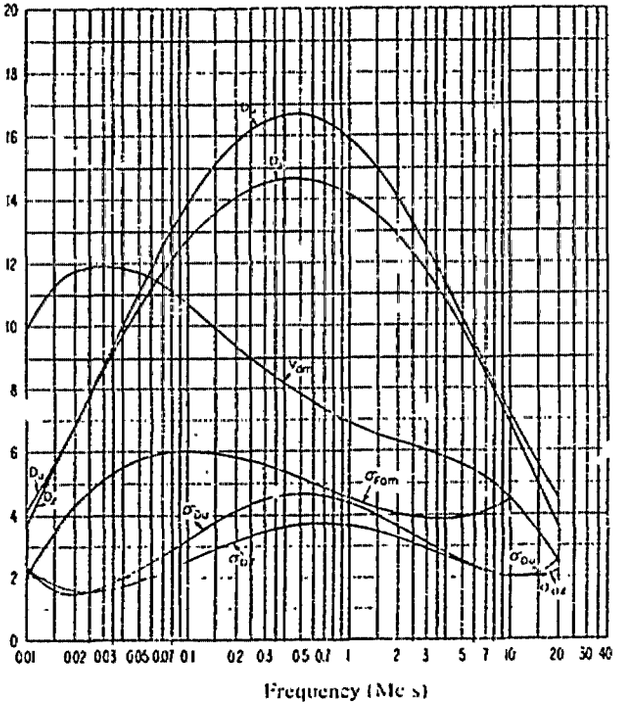

Data on noise variability and character
(Autumn; 0400–0800 h.)

σ_{Fam} = Standard deviation of values of F_{am}
D_u = Ratio of upper decile to median value, F_{am}
σ_{Du} = Standard deviation of values of D_u
D_l = Ratio of median value, F_{am}, to lower decile
σ_{Dl} = Stantard deviation of value of D_l
V_{dm} = Expected value of median deviation of average voltage. The values shown are for a bandwidth of 200 c/s.

Figure 23(c)

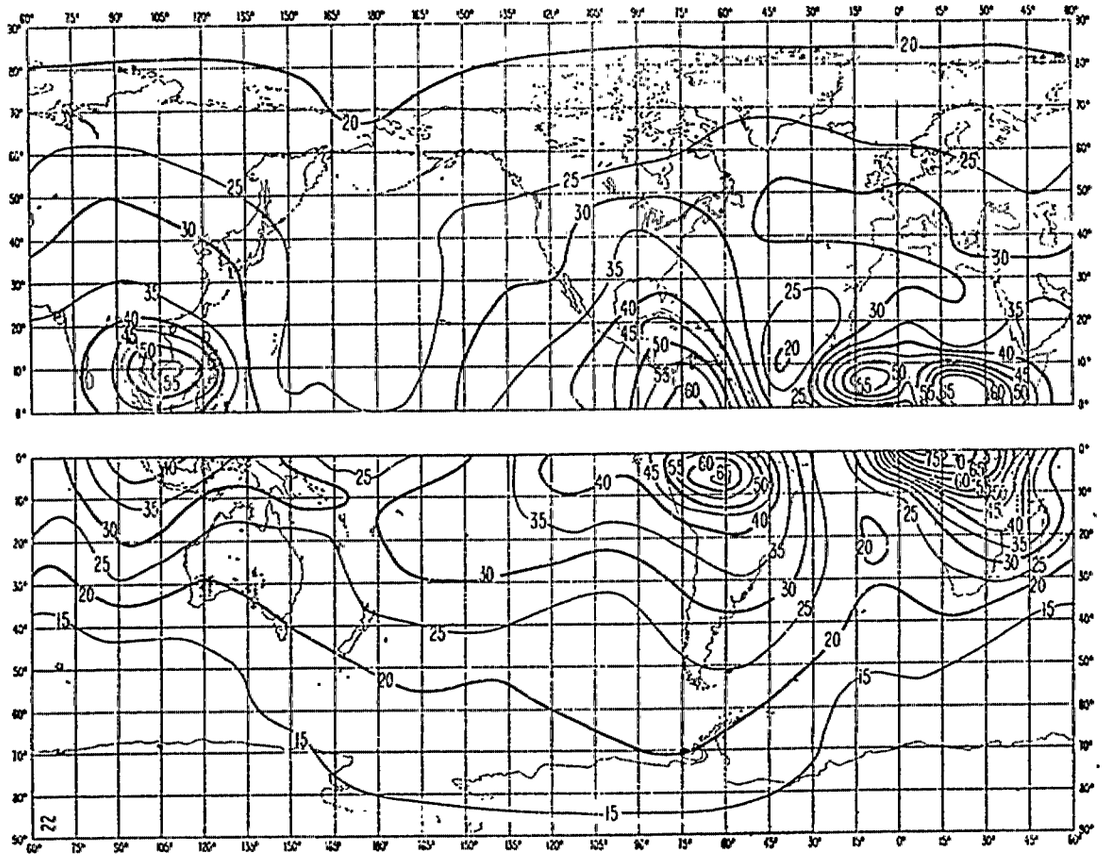

Expected values of atmospheric radio noise, F_{am},
(db above kT_0b at 1 Mc/s)
(Autumn; 0800–1200 h.)

Figure 24(a)

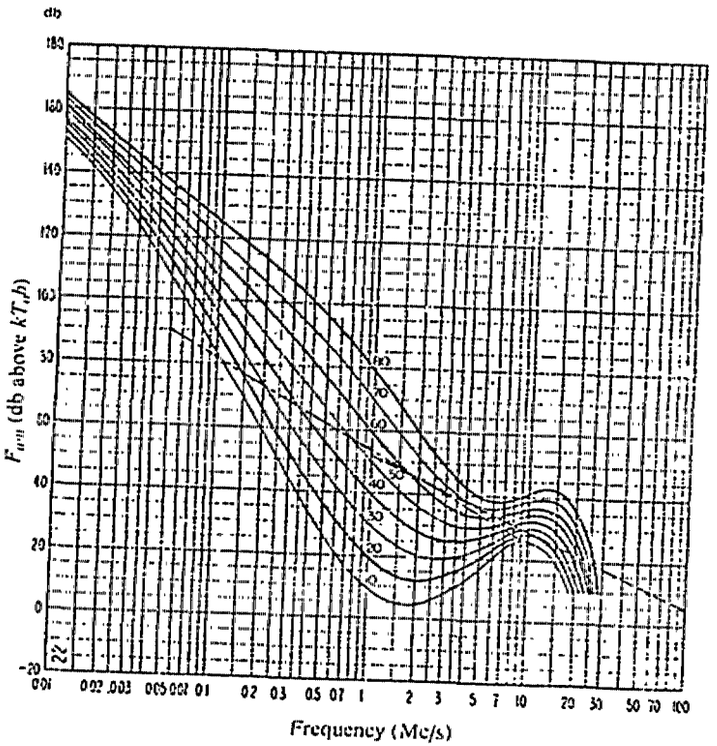

Variation of radio noise with frequency
(Autumn; 0800–1200 h.)

——— Expected values of atmospheric noise
—·—·— Expected values of man-made noise at a quiet receiving location
– – – – Expected values of galactic noise

Figure 24(b)

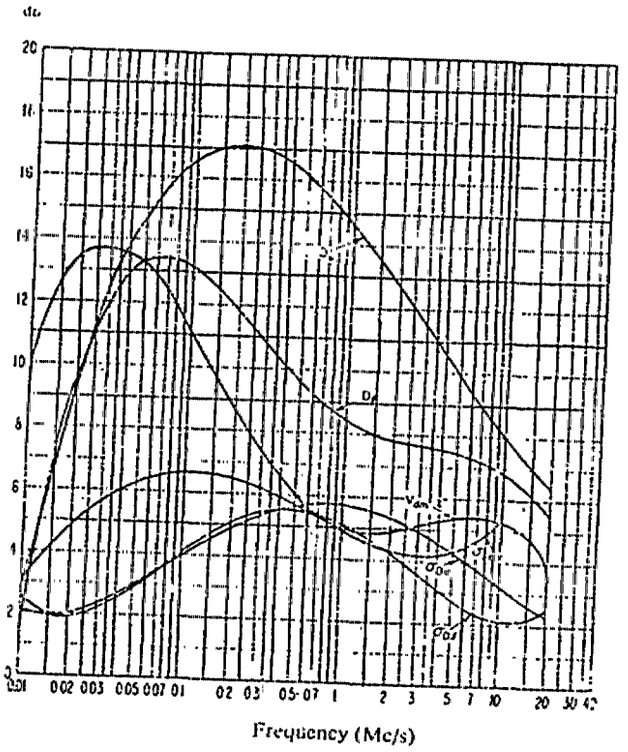

Data on noise variability and character
(Autumn; 0800–1200 h.)

σ_{Fam} = Standard deviation of values of F_{am}
D_u = Ratio of upper decile to median value, F_{am}
σ_{Du} = Standard deviation of values of D_u
D_l = Ratio of median value, F_{am}, to lover decile
σ_{Dl} = Stantard deviation of value of D_l
V_{dm} = Expected value of median deviation of average voltage. The values shown are for a bandwidth of 200 c/s.

Figure 24(c)

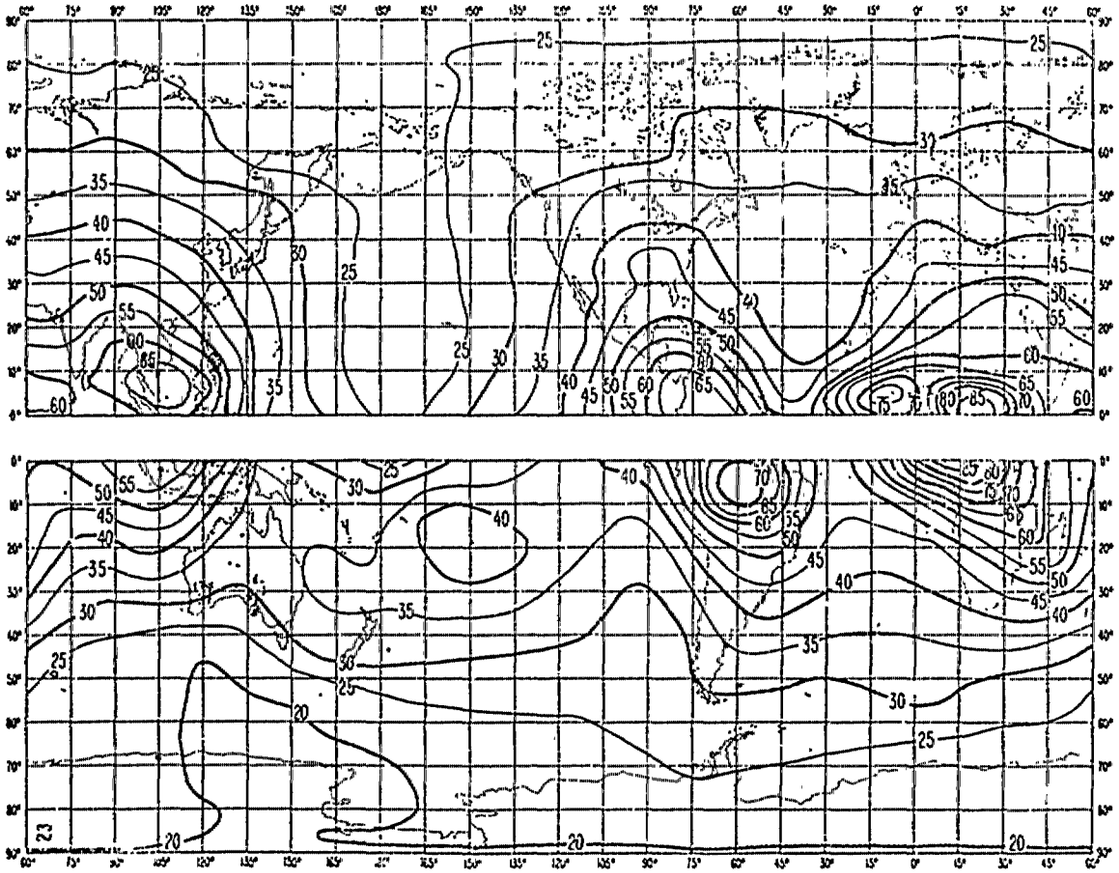

Expected values of atmospheric radio noise, F_{am},
(db above kT_0b at 1 Mc/s)
(Autumn; 1200–1600 h.)

Figure 25(a)

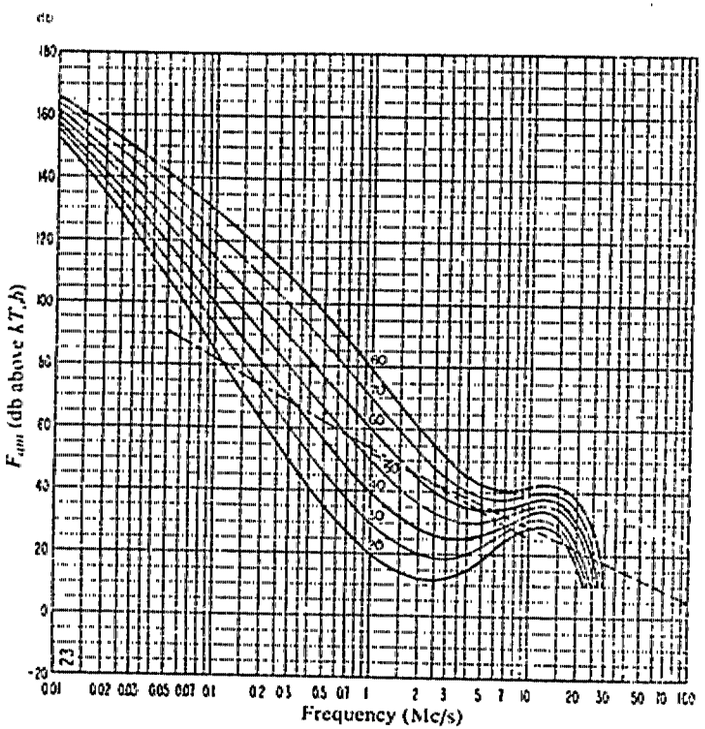

Variation of radio noise with frequency
(Autumn; 1200–1600 h.)

——— Expected values of atmospheric noise
—·—·— Expected values of man-made noise at a quiet receiving location
– – – – Expected values of galactic noise

Figure 25(b)

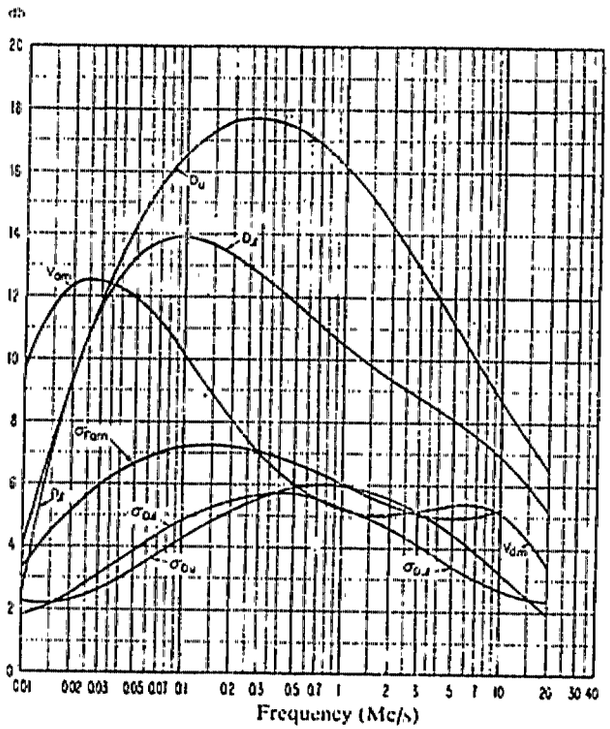

Data on noise variability and character
(Autumn; 1200–1600 h.)

σ_{Fam} = Standard deviation of values of F_{am}
D_u = Ratio of upper decile to median value, F_{am}
σ_{Du} = Standard deviation of values of D_u
D_l = Ratio of median value, F_{am}, to lower decile
σ_{Dl} = Standard deviation of value of D_l
V_{dm} = Expected value of median deviation, average voltage.
The values shown are for a bandwidth of 200 c/s.

Figure 25(c)

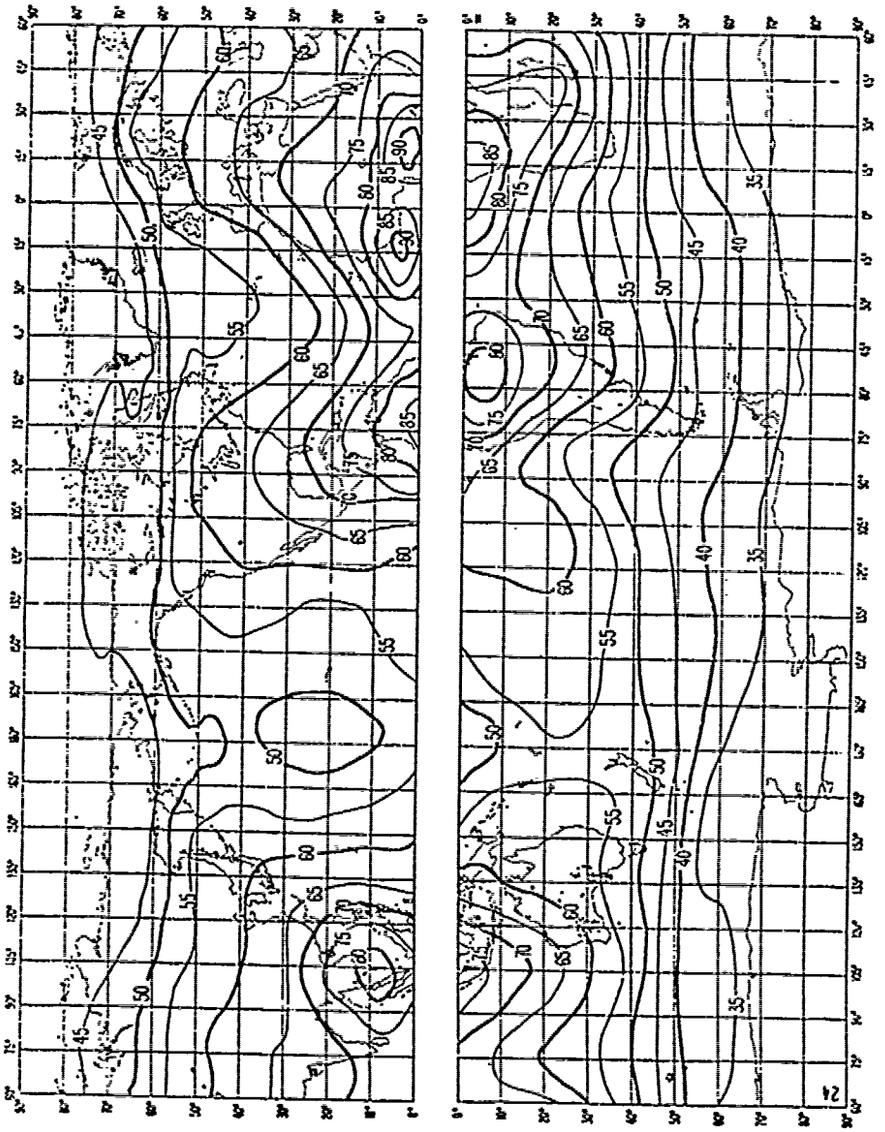

Expected values of atmospheric radio noise, F_{am},
(db above kT_0b at 1 Mc/s)
(Autumn: 1600–2000 h.)

Figure 26(a)

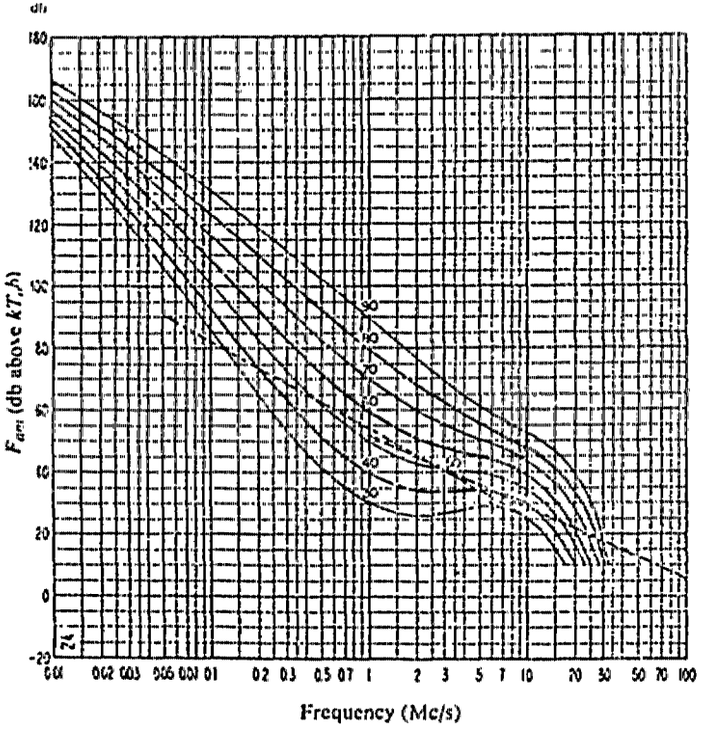

Variation of radio noise with frequency
(Autumn; 1600–2000 h.)

——— Expected values of atmospheric noise
—·—·— Expected values of man-made noise at a quiet receiving location
– – – – Expected values of galactic noise

Figure 26(b)

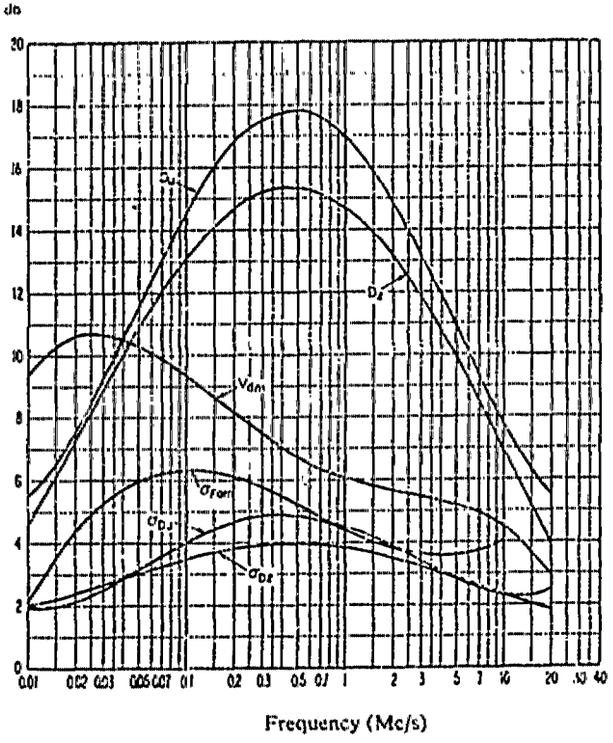

Data on noise variability and character
(Autumn; 1600–2000 h.)

σ_{Fam} = Standard deviation of values of F_{am}
D_u = Ratio of upper decile to median value, F_{am}
σ_{Du} = Standard deviation of values of D_u
D_l = Ratio of median value, F_{am} to lower decile
σ_{Dl} = Stantard deviation of value of D_l
V_{dm} = Expected value of median deviation of average voltage. The values shown are for a bandwidth of 200 c/s.

Figure 26(c)

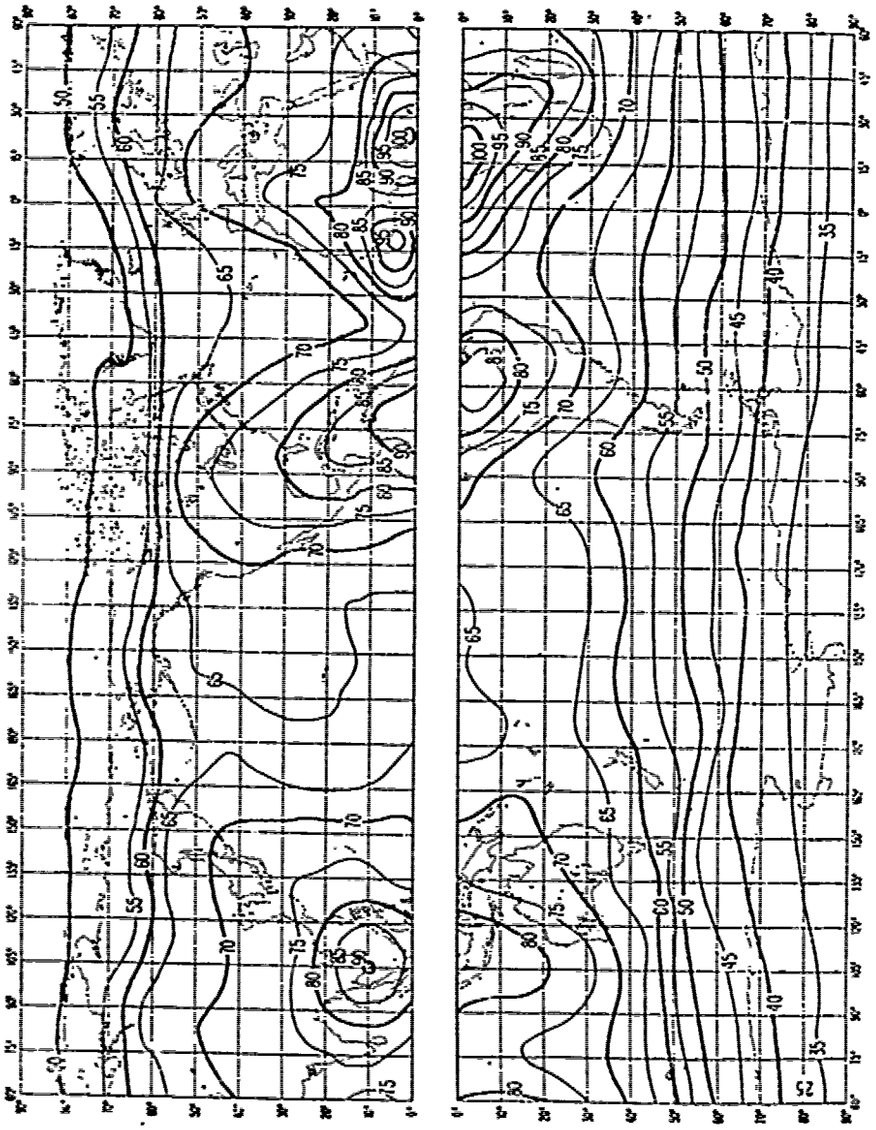

Expected values of atmospheric radio noise, F_{am},
(db above kTb at 1 Mc/s)
(Autumn, 2000 h.)

Figure 27(a)

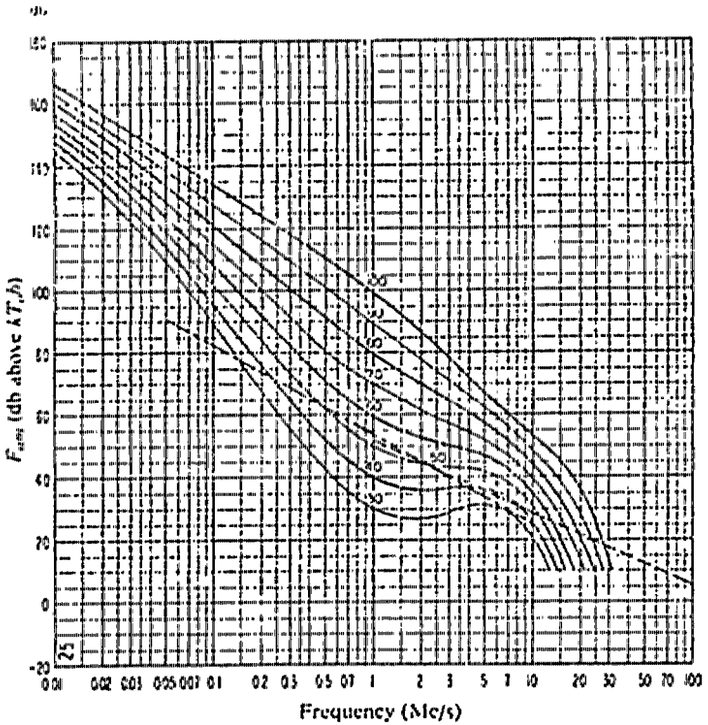

Variation of radio noise with frequency
(Autumn; 2000–2400 h.)

——— Expected values of atmospheric noise
—·—·— Expected values of man-made noise at a quiet receiving location
– – – – Expected values of galactic noise

Figure 27(b)

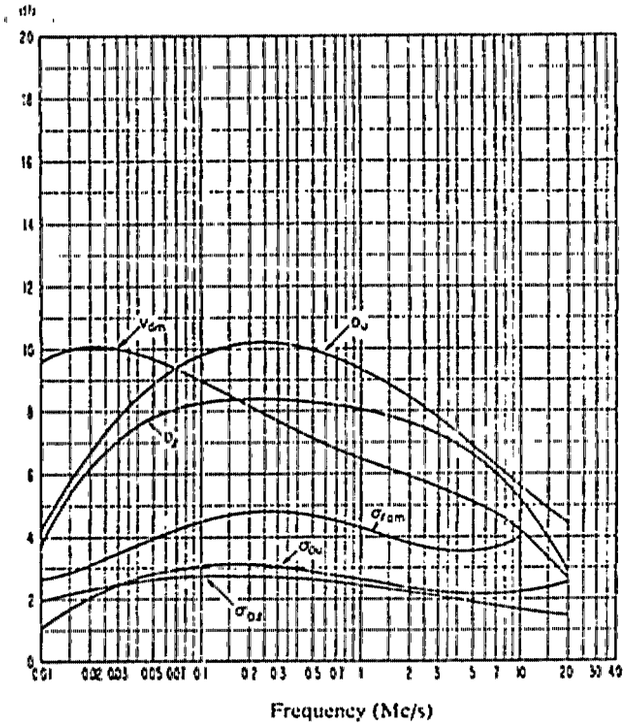

Data on noise variability and character
(Autumn; 2000–2400 h.)

σ_{Fam} = Standard deviation of values of F_{am}
D_u = Ratio of upper decile to median value, F_{am}
σ_{Du} = Standard deviation of values of D_u
D_l = Ratio of median value, F_{am}, to lover decile
σ_{Dl} = Stantard deviation of value of D_l
V_{dm} = Expected value of median deviation of average voltage. The values shown are for a bandwidth of 200 c/s.

Figure 27(c)

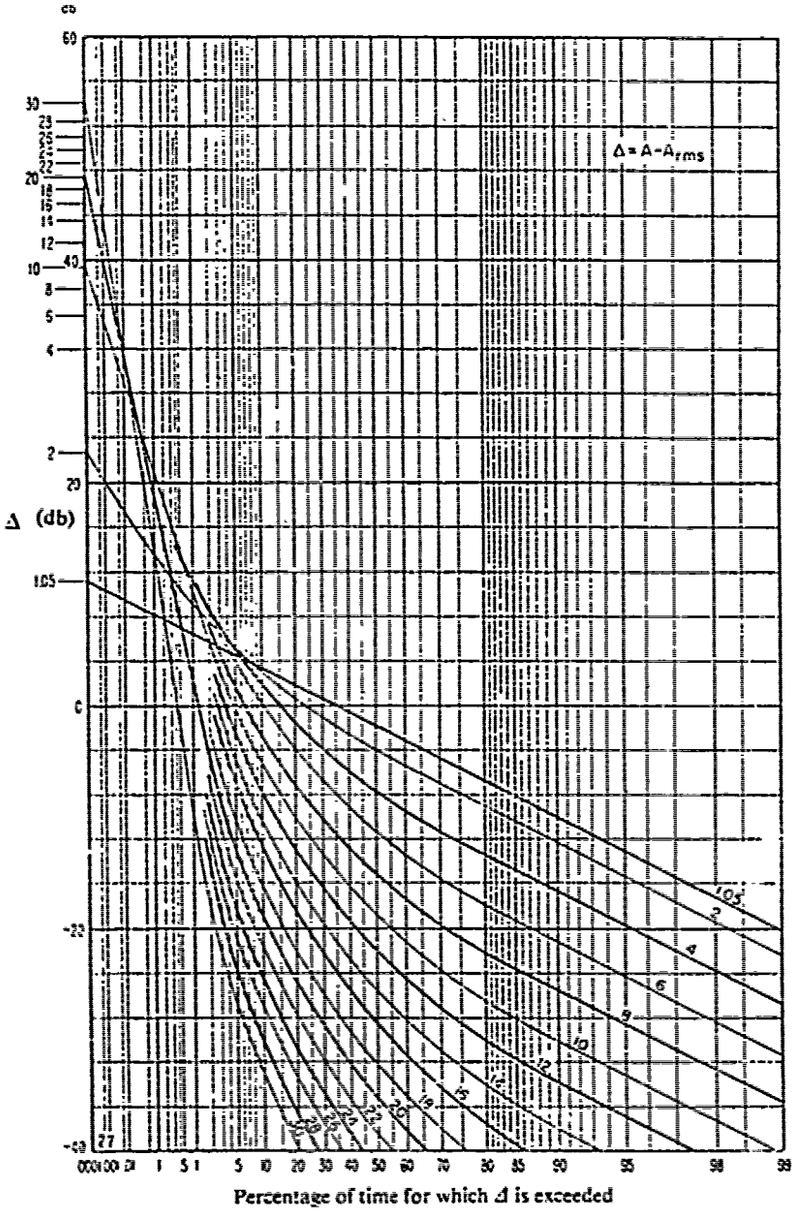

Fig. 28 — Amplitude probability distribution of the noise envelope

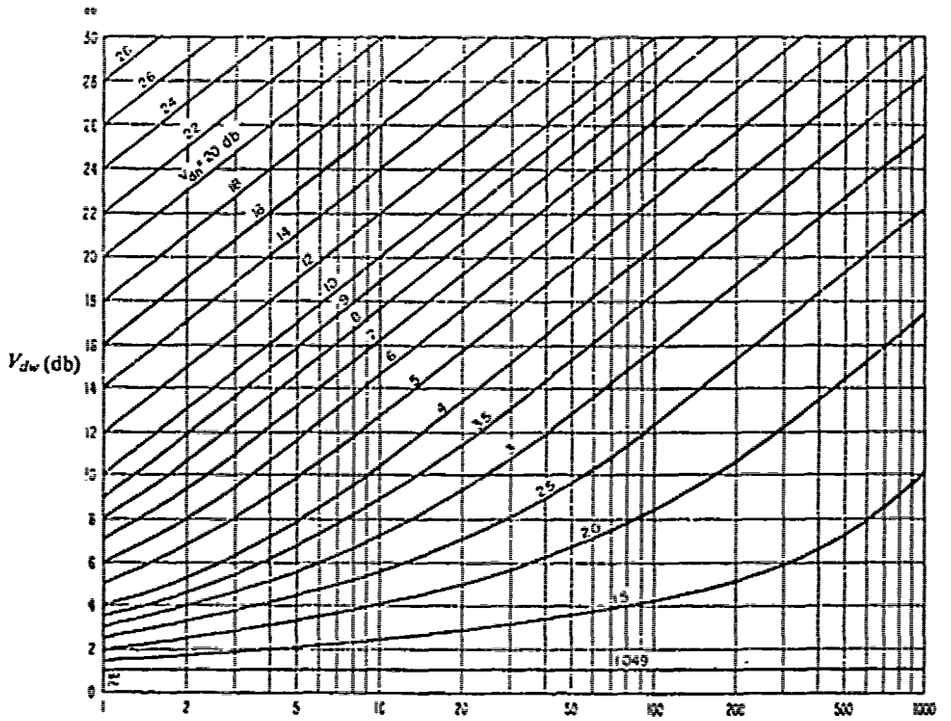

Conversion of V_d in one bandwidth to V_d in another bandwidth

b_w is the wider bandwidth
b_n is the narrower bandwidth

Corresponding values of V_{dw} and V_{dn} are read along the appropriate line for the bandwidth ratio

Figure 29

CHAPTER 5

VERY HIGH FREQUENCY (VHF), ULTRA-HIGH FREQUENCY (UHF), SUPERHIGH FREQUENCY (SHF)

(30-300 mhz, 300-3000 mhz, 3-30 ghz)

INTRODUCTION

At broadcast and short wave frequencies the ambient noise level is high relative to the receiver self-noise such that the receiver sensitivity is limited by the external noise that enters the antenna along with the signal. At microwave frequencies (VHF, UHF, and SHF bands) the external noise level is relatively low and the sensitivity of receivers is defined primarily by internal noise, except for low noise receivers employing masers and parametric amplifiers. The contribution of various types of noise in a receiver can be represented by the effective temperatures of the component noise. The total noise temperature is the sum of the component noise temperatures.

Receiver noise can be separated into two basic components - external and internal. External noise is defined as those energy sources originated external to the antenna Internal noise is due to the receiver noise, loss in the cables and antenna etc. This section concerns mainly with the external noise.

In the microwave frequencies noise originates from many sources. Among the important contribution sources are:

Atmospheric - Mainly due to lightening
Galactric - radiation from extraterrestrial sources
Atmospheric absorption - atmospheric radiations

Man-made - transmission lines, electrical machinery auto ignition systems, co-channel interferences.

Atmospheric

Lightening discharges radiates a large quantity of radio-frequency power. It is estimated that on the average there are 100 lightening strokes per second occur world wide. The combined effects of the lightening strokes give rise to RF noise, which can degrade radio RF communication at frequency below approximately 30 mhz. Noise due to lightening is generally termed "atmospheric noise" and its spectrum decreases with frequency so that it can usually be discounted for frequencies above about 30 mhz. Therefore, atmospheric noise is usually not of concern at microwave frequencies, except perhaps at the lower VHF region.

Man made Noise

Man-made noise originate from automobile ignition, electric tools, machinery, fluorescent lights, and transmission lines. At microwave frequencies, the noise levels due to man-made noise are very low relative to other noise levels so can be neglected.

Cosmic Noise

Cosmic noise are due to electromagnetic radiations from outer space. This extra-terrestrial noise comes from our own galaxy (milky-way), from extra-galactic sources, discrete radio stars, the planets, moon, and the sun.

In general, cosmic noise decreases with increased frequency and is important for frequencies in the VHF and lower UHF region, but may be neglected for frequencies great than 1 gigahertz.

The magnitutude of cosmic noise as seen by an antenna depends upon the antenna pointing direction in space. Cos-

mic noise level is a maximum when the antenna is pointed toward the center of our own galaxy, while minimum levels are observed along the poles about which the galaxy revolves.

A measure of cosmic noise level can be expressed in terms of the parameter called brightness temperature. The brightness temperature of an extended source of radiation measured in a particular direction is the temperature of a black body which yields a brightness equal to that of the source under consideration. Brightness is defined as the power received per unit area per hz bandwidth per unit solid angle. (Watts/m^2-Hz-steradian). Brightness B and the brightness temperature T_B at microwave frequencies are related by the Rayleigh-Jeans formula.

$$B = \frac{2kT_B}{\lambda^2} \qquad (1)$$

k: Boltzmann's constant
λ: wavelength

The brightness temperature specifies the intensity in a specific direction at a given frequency. The measureable temperature is the mean temperature in the field of an antenna and is called antenna temperature. Figure 1 shows the range of expected brightness temperatures in space as seen by an antenna with single polarization [1]. Therefore, the brightness level shown in Fig. 1 is one-half the value that would be observed with an antenna responsive to two orthogonal polarizations.

Figure 1 also shows the effects of atmospheric absorption losses discussed in the next section.

Atmospheric Absorption Noise

From the theory of blackbody radiation it is known that any body which absorbs radiated electromagnetic energy also radiates the same amount of energy it abosrbs. Since

the atmosphere body is an absorber of radiated energy frc space, the energy radiated from the atmosphere is continu and noise like.

Let us consider the atmosphere as an absorbing body surrounded by an imaginary black body at temperature T_a.

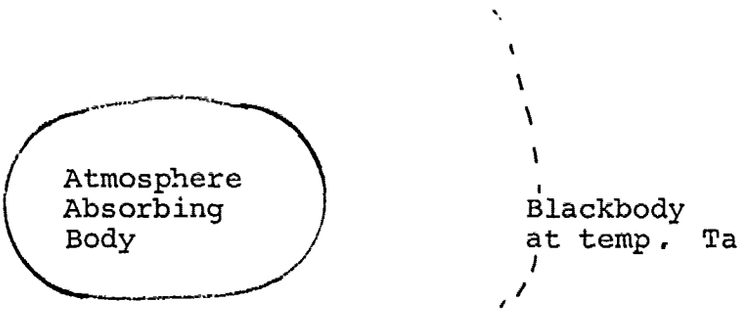

Energy available from black body at temperature T_a within bandwidth B_n is $E_B = kT_a B_n$

Suppose the atmosphere absorbs a certain amount of energy, as when the quantity E_B is passed through, such the remaining energy is $\frac{E_B}{L}$ where L is a loss factor. Then the amount of energy absorbed by the atmosphere is E_{ab}

$$E_{ab} = E_B - \frac{E_B}{L}$$
$$= kT_a B_n \left(1 - \frac{1}{L}\right)$$
$$= kT_e B_n / L \quad , \qquad T_e = T_a(L-1) \tag{2}$$

T_e is called the effective temperature. But from our earlier discussion on black body theory, a body radiates an amount of energy precisely corresponding to its abosrbe energy. Let ΔN be the radiated noise energy. so

$$\Delta N = E_{ab} = \frac{kT_e B_n}{L} \tag{3}$$

Example: $T_a = 260^\circ K$, $L = 1\ dB$

What is T_e?

$$T_e = T_a (L - 1)$$

$$10 \log \frac{E_b}{E_b/L} = 1$$

$$L = 1.26$$

$$\therefore\ T_e = 260^\circ K (1.26 - 1) = 67.6^\circ K$$

Atmospheric absorption noise is plotted in Fig. 1 as a solid curves, assuming an ambient temerature of 260°K. The cosmic noise is shown as dotted curves with higher levels for antennas pointed toward the galactic center. For atmospheric abosrption noise, the higher level corresponds to antenna pointing towards the horizon, and the minimum level occurs when antenna is verticle. From Fig. 1 we note that at lower frequencies cosmic noise dominate while at higher frequencies the atmospheric absorption noise dominates. A region of frequency from about 1000 mhz to 10,000 mhz appear to be favorable for radio systems operation because of a relatively quiet noise region.

Atmospheric absorption noise is greatest near the horizon because the antenna sees a thicker layer of atmosphere.

Sun, Moon, Radio stars

The sun is a strong emitter of electromagnetic radiation which has an intensity that depends upon solar activities. The minimum level of solar noise corresponds to a black body radiation at a temperature of about 6000°K. The flux density received on earth from a thermal source at the distance of a sun is [2]

$$S = \frac{1.88 \times 10^{-27} T_b}{\lambda^2} \qquad (4)$$

Where,

S = flux density in watts/m^2-hz

T_d = apparent disc. temperature, °K

λ = wavelength, m

A plot of the flux density as a function of frequency for the basic thermal noise component from the quiet sun is shown in Fig. 2. It does not exactly follow the relationship of Fig. 1 because Fig. 2 takes into account the effects of solar atmospheric absorption [3].

When the sun is disturbed by solar storms (sunspots and flares) the solar noise level can be several orders of magnitude above that of the "quiet" sun. The disturbed solar radiation levels can exceed that of an undisturbed level by 40 dB. This can be seen on Fig. 2. Also plotted on Fig. 2 are some expected flux density levels from the radio star cassioplid and the moon.

Flux Density and Brightness Temperature

The flux density S is related to the brightness T_B by integrating the brightness B over the entire solid angle

$$S = \int B \, d\Omega = \int \frac{2k T_B}{\lambda^2} \, d\Omega \qquad (5)$$

The sun and the moon may be considered point sources only if the angle subtended by the sources (on the order of $\frac{1}{2}^o$ in both cases) is less than the antenna beamwidth.

LIST OF REFERENCES

1. Green, J. C. and M. T. Lebenbaum, Letter in Micro J. Vol. 2, pp. 13-14, October, 1959.

2. Pawsey, J. L., and R. N. Bracewell, Radio Astronomy, Oxford University Press, London, 1955.

3. Wild, J. P., Observational Radio Astronomy, Advances in Electronics and Electron Physics, Vol. 7, 1955.

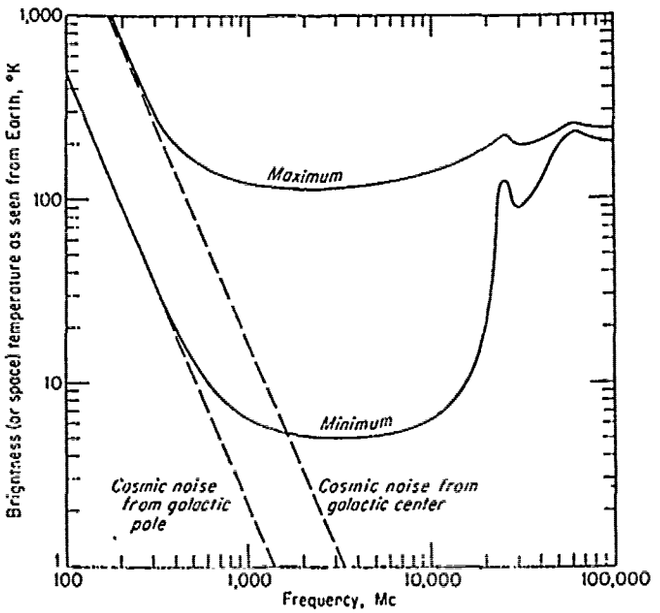

Maximum and minimum brightness (or space) temperatures of the sky as seen by an ideal single-polarization antenna on earth. Dashed curves apply to cosmic noise. Cosmic noise predominates at lower frequencies; atmospheric absorption noise, at higher frequencies. Maximum and minimum cosmic noise correspond to the directions of the galactic center and the galactic pole, respectively. Maximum atmospheric absorption corresponds to the antenna beam pointing along the horizon, while minimum absorption corresponds to antenna pointed at the zenith.

Figure 1

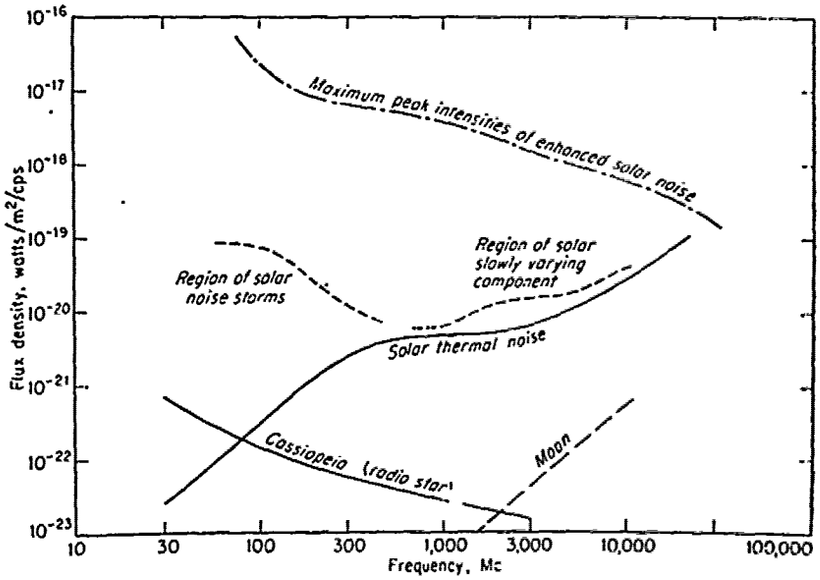

Fig. 2 — Noise flux density as a function of frequency from the sun, Cassiopeia, and the moon

CHAPTER 6

OPTICAL
(300-3000 Gigahertz)

INTRODUCTION

At optical frequencies two basic types of noise are encountered: (1) thermal noise, generated internally within the optical receiver, and (2) quantum noise, which has both an internal component (dark current noise) and an external component from radiations incident upon the receiver optics. Thermal noise spectrum can be described by [1]

$$\frac{hv}{e^{hv/kT} - 1} \qquad (1)$$

where h is the Planck's constant (6.624×10^{-34} joules-sec.), V is the optical frequency in hertz, k is the Boltzmann's constant (1.38×10^{-23} joules/°K), and T is the temperature in degress absolute. At very low temperatures and at optical frequencies, thermal noise decreases exponentially with increasing frequency.

Quantum noise in an optical receiver is dependent upon the type of optical detection scheme used. In general, optical detection makes use of one of two techniques: (1) coherent or heterdyne detection, and (2) incoherent or direct detection. Coherent detection operates in a phase-locked mode and provides a measure of gain against background noise. An incoherent detector, on the otherhand, is a "square law" device and is more susceptible to background noise.

Since the incoherent detector is more susceptible to background noise at optical frequencies, in the following we will consider the background noise as the output of an incoherent detector. For this case, the average detector output current due to incident power P can be modeled as a Poisson process [1]

$$I = \frac{\eta q}{h\nu} P \qquad (2)$$

where I is the average current in amperes; n(v) is the detector quantum efficiency, the ratio of the average number of current carriers generated by the detector to the average number of incident photons; q is charge on an electron, $(1.6 \times 10^{-19} C)$; h is the Planck's constant; v is the frequency in hertz; and P is the average incident power in watts. The noise current for this case is given by

$$\sqrt{2qIB} \qquad (3)$$

with B being the detector bandwidth in hertz.

The current I in Eq. 3 is actually made up of three component: (1) I_s, a current due to incident signal power, P_s, (2) I_b, a current due to incident power, P_b, from the background, and (3) I_d, a dark current, generated internally. Equation 2 now becomes

$$I = I_s + I_b + I_d = \frac{\eta q}{h\nu}(P_s + P_b) + I_d \qquad (4)$$

Our main interest will be to present some available information on the component of noise due to the background. For a discussion on the dark current, I_d, we refer to Ross [3] and Pratt [4] .

BACKGROUND NOISE

Background noise incident upon receiver optics either by direct radiation, by reflection from a surface, or by scattering from a medium. All bodies at a temperature above absolute zero is known to radiate thermal (electromagnetic) energy. For a body with a radiant absorptance equal to unity, $\alpha=1$, the spectral radiant emittance, W_λ, has the value

$$W_\lambda = \frac{2\pi hc^2}{\lambda^5}\left[\exp(hc/\lambda kT)-1\right]^{-1} \quad (w\cdot m^{-2}\cdot\mu m^{-1}) \qquad (5)$$

Where k is the Boltzmann's constant, T is the absolute temperature, h is Planck's constant, C is the velocity of light in free space (m/s), and λ is the wavelength in meters. Equation 5 is Planck's radiation law for a blackbody. Most radiating bodies encountered in practice are not precisely blackbodies. However the radiation characteristics of non-blackbodies (greybodies) can often be approximated by a blackbody. The relation between the spectral radiant emittances is

$$W_{\lambda\,(greybody)} = \alpha\, W_{\lambda\,(blackbody)}$$

Figure 1 is a plot of Eq. 5 at several temperatures.

At a particular temperature, the spectral radiant emittance has a maximum value which occurs at a wavelength, λ_m. This value is obtained by differentiating Eq. 5 with respect to the wavelength and solve for

$$\lambda_m = \frac{2897}{T} \qquad (6)$$

This is known as Wien's Displacement law.

DIRECT RADIATION

If the radiations from a background source arrive normal to the surface of the receiver optics, the detector output power can be written as [2]

$$P_b = N_\lambda \Omega_s A_r \tau_o \tau_a B_{opt} \quad (watts) \qquad (7)$$

where P_b is the detector output power due the background radiation, Ω_s is the solid angle subtended by the radiating source at the receiver (steradians), N_λ is the spectral radiance of the source in watts/$m^2 \cdot sr \cdot \mu m$, τ_o is the transmittance of the receiver optics, τ_a is the transmittance of Earth's atmosphere, and Bopt is the optical bandwidth in hertz. At optical wavelengths most backgrounds have diffuse surfaces [3] so

$$N_\lambda = \frac{W_\lambda}{\pi} \qquad (8)$$

The detector noise power due to blackbody radiation in Eq. 7 can now be written in terms of Eqs. 5 and 8 as

$$P_{bb} = \frac{2hc^2 \Omega_s A_r \tau_o \tau_a B_{opt}}{\lambda^5 [\exp(hc/\lambda kT) - 1]} \qquad (9)$$

In space communication systems, $\tau_a = 1$; while, in Earth's atmosphere τ_a has two components

$$\tau_a = e^{-aR} = e^{-(\sigma_a + \sigma_s)R} \qquad (10)$$

where a, σ_a, σ_s are the atmospheric extinction, absorption and scattering coefficients, respectively, and R is the distance between source and receiver. The absorption characteristic of Earth's atmosphere at optical wavelengths has been studied by Battelle [5] and this is shown in Fig. 2. In the region of optical windows the

absorption coefficient is very small, so $a \simeq \sigma_s$, and scattering attenuation dominates. Figure 3 is a plot of scattering data by Battelle [5] for various atmospheric conditions.

Direct background radiations may result from many sources. Among these sources are the sun, stars, planets, the Earth, Earth's moon, and the atmosphere at high elevations. Figure 4 shows the spectral irradiance of the sun at zenith obtained by Gast [6] , which is seen to follow closely blackbody radiation characteristics at $5900^{o}K$. Since radiation data is often given in spectral irradiance H_λ, its relation to the background power P_b can be written as

$$P_b = H_\lambda A_r \tau_o \tau_a \beta_{opt} \qquad (11)$$

Calculated values of spectral, irradiance for the moon and planets outside the terrestrial atmosphere [7] are shown in Fig. 5. Figure 6 shows the spectral irradiance values for some of the brightest stars, also calculated by Remsey [7] . Earth and its atmosphere has a radiation characteristic similar to blackbody radiation and which general lies between blackbody radiation curves of $218^{o}K$ and $288^{o}K$, the differences resulting from the atmospheric absorption bands shown in Fig. 2. This thermal background noise is referred to as "earthshine" [8] and is shown in Fig. 7.

REFLECTED BACKGROUND NOISE

Thermal radiation can arrive at the receiver optics, even when the radiating source is not in view, by reflection from a surface or scattering from a medium. The reflection of solar energy from the moon and the planets are examples. In general, the spectral distribution of

reflected solar radiations by the moon and the planets is similar to that of the sun, but diminished in magnitude. Some calculated values of reflected irradiance from the moon and some planets are shown in Fig. 5.

The atmosphere, as a medium, introduces volume scattering to incident solar radiations. The spectral radiance of scattered solar radiation is dependent upon the solar zenith angle, the angle through which light is scattered, the atmospheric condition, and other factors. Figures 7 and 8 show scattered spectral radiance levels for the cases of day and night sky backgrounds, respectively, due to Stewart and Hopfield [9] . In both Figures 8 and 9, curve E is the spectral radiance for a blackbody radiation at $283^{o}K$, which approximates that for the Earth. Curve F in both figures shows the expected level of atmospheric radiations caused largely by water vapor and CO_2.

LIST OF REFERENCES

1. Oliver, B. M., Thermal and Quantum Noise, Proceedings of the IEEE, Vol. 53, May 1965, pp. 436-454.

2. Melchior, H., M. B. Fisher, and F. R. Arams, Photodetectors for Optical Communication Systems, Proceedings of the IEEE, Vol. 58, No. 10, October 1970, pp. 1466-1486.

3. Ross, M., Laser Receivers, John, Wiley and Sons, Inc., New York, 1965. pp. 54-57.

4. Pratt, W. K., John Wiley and Sons, Inc., New York, 1969, chapter 8.

5. Battelle, R. B., P. R. Gillette, and R. C. Honey, An Analysis of the Feasibility of Laser Systems for Naval Applications (U), Defense Documentation Center Rep. ASTIA Doc. AD-350353, November 1963.

6. Gast, P. R., Solar Irradiance, Handbook of Geophysics and Space Environments, S. L. Valley, Editor, Cambridge, Mass., Air Force Cambridge Res. Lab., 1965.

7. Ramsey, R. C., Spectral Irradiance from Stars and Planets Above the Atmosphere from 0.1 to 100 microns, Applied Optics, Vol. 1, No. 4, July 1962, pp.465-471.

8. Wolfe, W. L., Handbook of Military Infrared Technology, Washington, D. C., Government Printing Office, 1965, Chapter 2.

9. Stewart, H. S., and R. F. Hopfield, Atmospheric Effects, Applied Optics and Optical Engineering, R. Kingslake, Editor, Vol. 1, New York, Academic Press, 1965, pp. 131-140.

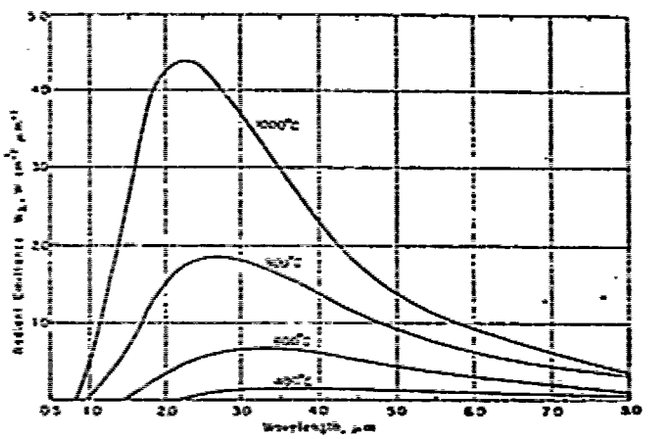

Fig. 1 — Planck's law represented as a plot of object radiant emittance W_1 versus wavelength λ for several values of temperature

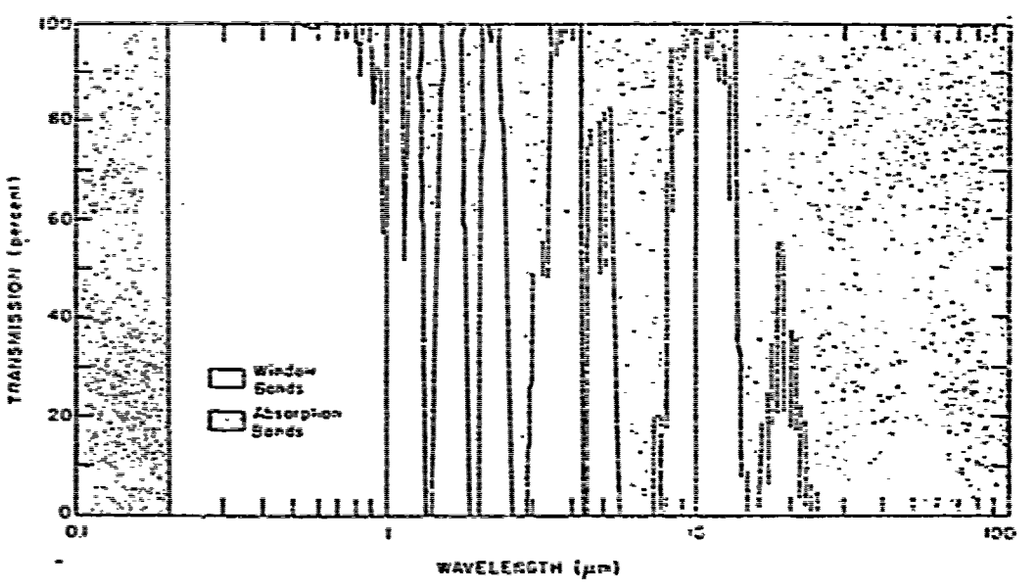

Fig. 2 — Spectral characteristics of optical wave atmospheric absorption per millimeter of percipitable water vapor per kilometer path length along Earth's surface

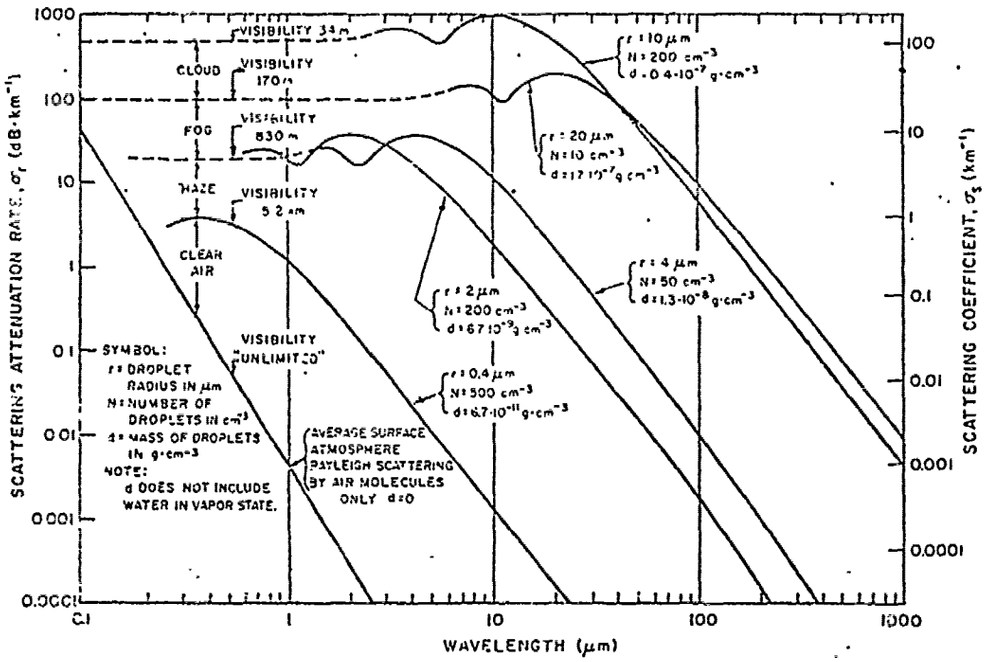

Fig. 3 — Optical wave atmospheric scattering data

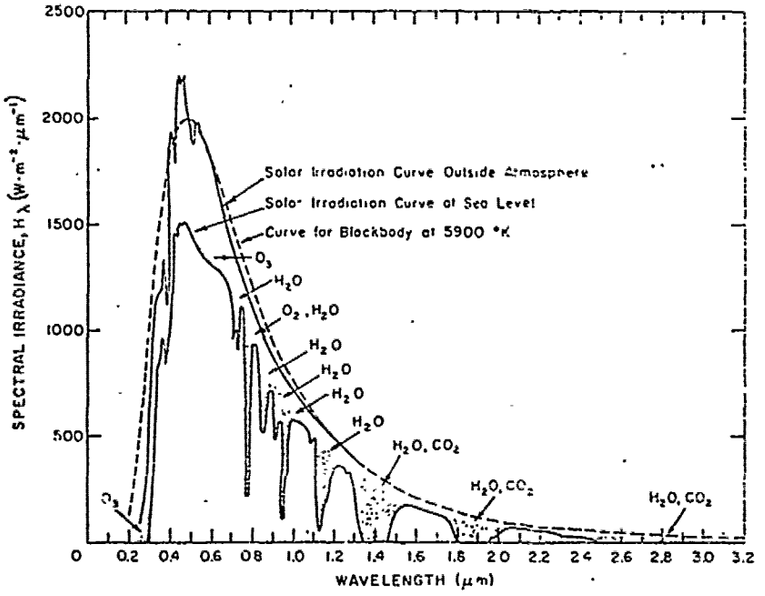

Fig. 4 — Solar spectral irradiance with Sun at zenith. Absorption bands are shown shaded (after Gast [18]).

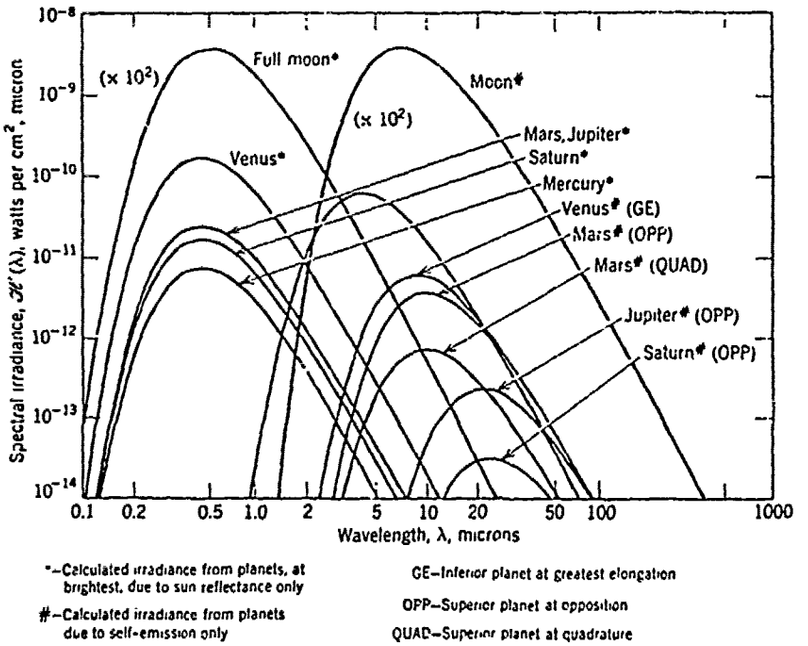

Fig. 5 — Calculated planetary and lunar spectral irradiance outside the terrestrial atmosphere

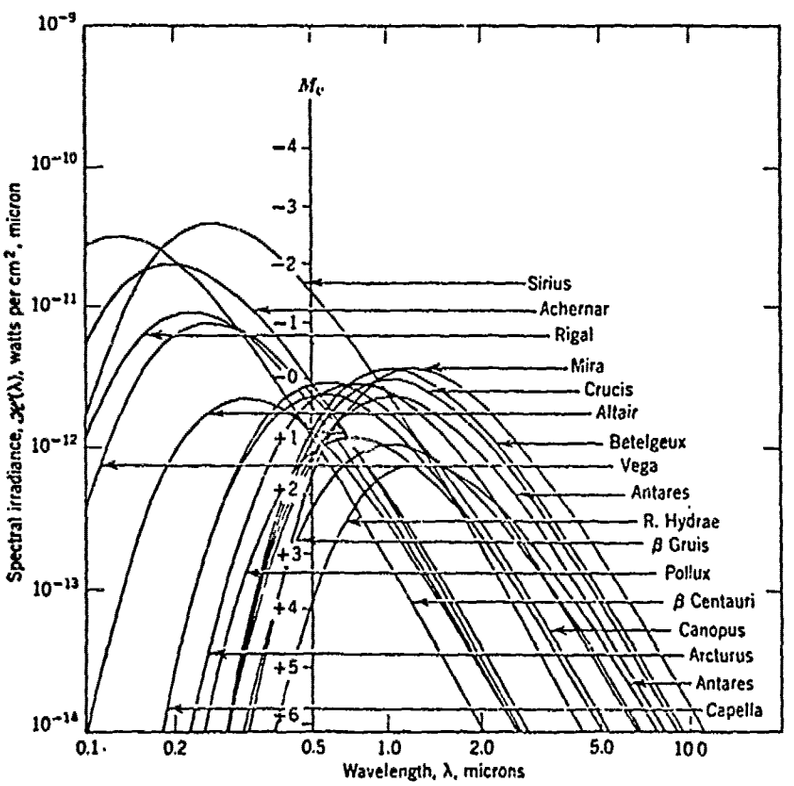

Fig. 6 — Spectral irradiance of brightest stars outside the terrestrial atmosphere

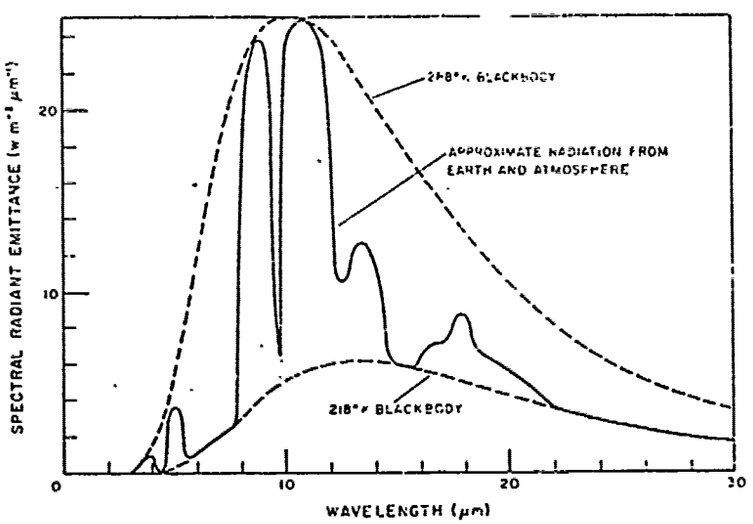

Fig. 7 — Earthshine: spectral radiant emittance from Earth and its atmosphere (after Wolfe [12])

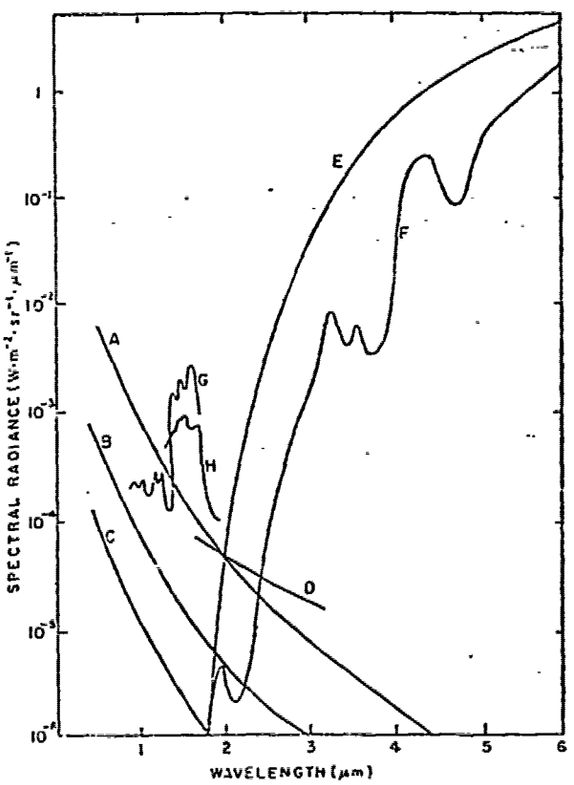

Night sky background data (absorption bands of Fig. 2 not included) Curve *A*: full Moon, 94 km visibility, $\theta = 10°$, $\Phi = 60°$. Curve *B*: full Moon, 94 km visibility, $\theta = 40°$, $\Phi = 60°$. Curve *C*: full Moon, 94 km visibility, $\theta = 90°$, $\Phi = 60°$. Curve *D*: maximum scatter from city lights. Curve *E*: blackbody radiation at 283°K. Curve *F*: water vapor and CO_2 atmospheric emission. Curve *G*: bright aurora. Curve *H*: airglow. θ is angle through which light is scattered into field of view and Φ is the zenith angle of field of view (after Stewart and Hopfield [8]).

Figure 8

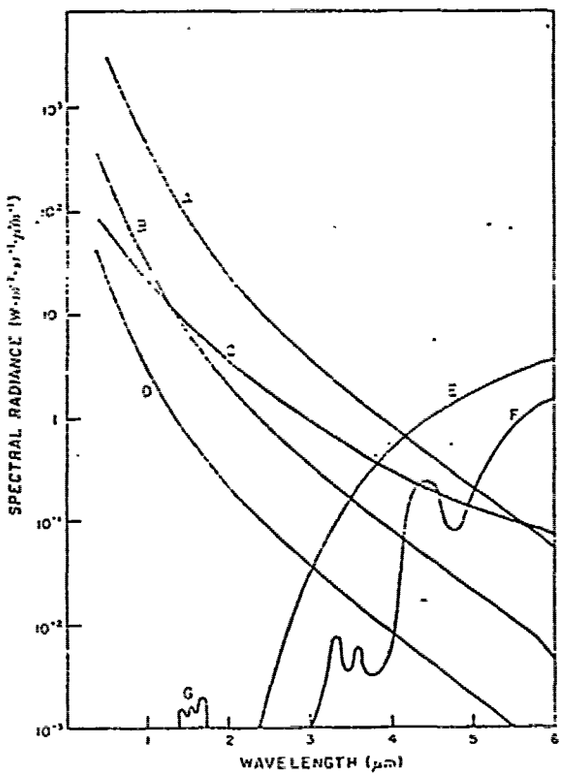

Day sky background data (absorption bands of Fig. 2 not included). Curve *A*: scattered sunlight, 94 km visibility, $\theta = 10°$, $\Phi = 60°$. Curve *B*: scattered sunlight, 94 km visibility, $\theta = 40°$, $\Phi = 60°$. Curve *C*: cloud or fog transmitting 50 percent, $\theta = 30°$, $\Phi = 30°$. Curve *D*: scattered sunlight, 94 km visibility, $\theta = 90°$, $\Phi = 60°$. Curve *E*: blackbody radiation at 283°K. Curve *F*: water vapor and CO_2 atmospheric emission. Curve *G*: bright aurora. θ is angle through which light is scattered into field of view and Φ is the zenith angle of field of view (after Stewart and Hesfield [8]).

Figure 9